FZD-460

# Joint Project: Migration of Actinides in the System Clay, Humic Substance, Aquifer

## Migration Behavior of Actinides (Uranium, Neptunium) in Clays: Characterization and Quantification of the Influence of Humic Substances

Susanne Sachs, Adéla Křepelová, Katja Schmeide,
Astrid Koban, Alix Günther, Jens Mibus, Vinzenz Brendler,
Gerhard Geipel, Gert Bernhard

Januar 2007

Wissenschaftlich-Technische Berichte
FZD-460 2007 · ISSN 1437-322X

WISSENSCHAFTLICH-TECHNISCHE BERICHTE

Forschungszentrum
Dresden Rossendorf

Wissenschaftlich-Technische Berichte
**FZD-460**
Januar 2007

Susanne Sachs, Adéla Křepelová, Katja Schmeide,
Astrid Koban, Alix Günther, Jens Mibus, Vinzenz Brendler,
Gerhard Geipel, Gert Bernhard

# JOINT PROJECT: MIGRATION OF ACTINIDES IN THE SYSTEM CLAY, HUMIC SUBSTANCE, AQUIFER

## MIGRATION BEHAVIOR OF ACTINIDES (URANIUM, NEPTUNIUM) IN CLAYS: CHARACTERIZATION AND QUANTIFICATION OF THE INFLUENCE OF HUMIC SUBSTANCES



Forschungszentrum
Dresden Rossendorf

# JOINT PROJECT: MIGRATION OF ACTINIDES IN THE SYSTEM CLAY, HUMIC SUBSTANCE, AQUIFER

# MIGRATION BEHAVIOR OF ACTINIDES (URANIUM, NEPTUNIUM) IN CLAYS: CHARACTERIZATION AND QUANTIFICATION OF THE INFLUENCE OF HUMIC SUBSTANCES

Susanne Sachs, Adéla Křepelová, Katja Schmeide, Astrid Koban, Alix Günther, Jens Mibus, Vinzenz Brendler, Gerhard Geipel, Gert Bernhard

Das diesem Bericht zugrunde liegende Vorhaben wurde mit Mitteln des Bundesministeriums für Wirtschaft unter dem Förderkennzeichen 02 E 9673 gefördert. Die Verantwortung für den Inhalt dieser Veröffentlichung liegt bei den Autoren.

Vorhaben:

VERBUNDPROJEKT: MIGRATION VON ACTINIDEN IM SYSTEM TON, HUMINSTOFF, AQUIFER

MIGRATIONSVERHALTEN VON ACTINIDEN (URAN, NEPTUNIUM) IN TONEN: QUANTIFIZIERUNG DES EINFLUSSES VON HUMINSTOFFEN

## Abstract

Objective of this project was the study of interaction processes between humic substances, U(VI), Np(V) and kaolinite KGa-1b. It contributed to the attainment of a better process understanding, the improvement of the knowledge on the interaction of humic substances and metal ions and the enhancement of the thermodynamic database.

With a synthetic humic acid (HA), N-containing functional groups of HA were characterized by $^{15}$N-NMR spectroscopy. Based on these results, model studies of the influence of amino groups on the complexation behavior of HA were performed. Spectroscopic studies with amino acids show that the amino group do not contribute to the U(VI) complexation at pH 4.

The impact of kaolinite on the formation of HA and humic substance-kaolinite-sorbates was studied in model syntheses. The results exhibit that the presence of kaolinite during the syntheses mainly influences the yields on HA and their elemental compositions. Synthetic humic substance-kaolinite-sorbates were isolated.

Under exclusion of $CO_2$, the U(VI) complexation by HA was investigated at pH 7 by means of the conventional time-resolved laser-induced fluorescence spectroscopy (TRLFS) and TRLFS with ultrafast pulses. Complexation parameters for the ternary complex $UO_2$(OH)HA(I) were determined ($\log\beta_{0.1M}$: 14.89 ± 0.54).

Studies of the Np(V) reduction in presence of HA with different functionalities under anaerobic conditions have shown that Np(V) is reduced to Np(IV) by HA. The redox capacity depends on the HA functionality. Applying a modified HA it was verified that phenolic/acidic OH groups play a dominating role in the Np(V) reduction.

The influence of HA on the U(VI) and Np(V) sorption onto kaolinite was investigated in batch experiments. In dependence on the experimental conditions, HA effects the sorption and consequently the mobility of U(VI) and Np(V). From studies of the U(VI) sorption onto synthetic humic substance-kaolinite-sorbates it was concluded that the structure and functionality of sorbed/associated humic substances considerably influence the sorption behavior of U(VI). The structure of U(VI)-kaolinite-surface complexes in presence of HA was studied by means of X-ray absorption spectroscopy and TRLFS and compared to those of U(VI)-kaolinite-complexes.

Investigations of the migration of HA and U(VI) in the laboratory system kaolinite-water were carried out in diffusion experiments. The migration of HA in compacted clay is governed by diffusion and influenced by its colloidal properties. Humic substances exert an immobilizing effect on the U(VI) transport in compacted kaolinite.

## Zusammenfassung

Ziel des Projektes war die Untersuchung von Wechselwirkungsprozessen zwischen Huminstoffen, U(VI), Np(V) und Kaolinit KGa-1b. Es diente der Erzielung eines besseren Prozessverständnisses, der Erweiterung des Wissens über das Wechselwirkungsverhalten von Huminstoffen mit Metallionen sowie der thermodynamischen Datenbasis.

Am Beispiel einer synthetischen Huminsäure (HS) wurden N-haltige funktionelle Gruppen in HS mittels $^{15}$N-NMR-Spektroskopie charakterisiert. Basierend auf diesen Ergebnissen wurden Modelluntersuchungen zum Einfluss von Aminogruppen auf das Komplexbildungsverhalten von HS durchgeführt. Spektroskopische Ergebnisse mit Aminosäuren zeigen, dass die Aminogruppe bei pH 4 nicht zur Komplexierung von U(VI) beiträgt.

Der Einfluss von Kaolinit auf die Bildung von HS und Huminstoff-Kaolinit-Sorbaten wurde in Modellsynthesen untersucht. Es wurde beobachtet, dass die Anwesenheit von Kaolinit bei der Synthese von HS vorwiegend deren Ausbeuten und Elementzusammensetzungen beeinflusst. Synthetische Huminstoff-Kaolinit-Sorbate wurden isoliert.

Unter Ausschluss von $CO_2$ wurde die U(VI)-Komplexierung mit HS bei pH 7 mittels konventioneller zeitaufgelöster laserinduzierter Fluoreszenzspektroskopie (TRLFS) und TRLFS mit ultrakurzen Pulsen untersucht und Komplexbildungsparameter für den ternären Komplex $UO_2$(OH)HA(I) bestimmt ($\log\beta_{0.1M}$: 14.89 ± 0.54).

Untersuchungen zur Np(V)-Reduktion in Gegenwart von HS unterschiedlicher Funktionalität unter anaeroben Bedingungen haben gezeigt, dass Np(V) durch HS zu Np(IV) reduziert wird. Die Redoxkapazität ist von der Funktionalität der HS abhängig. Durch Einsatz einer modifizierten HS konnte die dominierende Rolle phenolischer/acider OH-Gruppen für die Np(V)-Reduktion durch HS nachgewiesen werden.

Der Einfluss von HS auf die U(VI)- und Np(V)-Sorption am Kaolinit wurde in Batchexperimenten untersucht. In Abhängigkeit von den experimentellen Bedingungen beeinflusst HS die Sorption und folglich die Mobilität von U(VI) und Np(V). Untersuchungen zur U(VI)-Sorption an synthetisch hergestellten Huminstoff-Kaolinit-Sorbaten ergaben, dass Struktur und Funktionalität der sorbierten/assoziierten Huminstoffe einen wesentlichen Einfluss auf das Sorptionsverhalten von U(VI) ausüben. Mittels Röntgenabsorptionsspektroskopie und TRLFS wurde die Struktur von U(VI)-Kaolinit-Oberflächenkomplexen in Gegenwart von HS bestimmt und mit der von U(VI)-Kaolinit-Komplexen verglichen.

Studien zur Migration von HS und U(VI) im Laborsystem Kaolinit-Wasser erfolgten in Diffusionsexperimenten. Die Migration von HS im kompaktierten Ton wird durch Diffusion beherrscht und von ihren kolloidalen Eigenschaften beeinflusst. Huminstoffe üben eine immobilisierende Wirkung auf den Transport von U(VI) im kompaktierten Kaolinit aus.

## Contents

# 1 Introduction

The long-term risk assessment and conception of a future nuclear waste repository requires detailed knowledge of the migration behavior of actinides. The migration of actinides in a potential host rock formation as well as their transport after a possible release from the repository in the aquifer has to be known for the selection of a suitable host rock. For that a comprehensive and reliable thermodynamic database is necessary. A substantial database is already available for salt as possible host rock formation, whereas for clay formations and granite studies are still necessary.

The behavior of actinides in an aquifer system can be strongly determined by humic substances, organic macromolecules ubiquitous found in natural environments. Because of their solubility in the pH range of natural waters, their ability for complex and colloid formation as well as their redox properties, they can considerably influence the transport of actinides. Most natural clays are closely associated with natural organic matter, e.g., humic acid- and fulvic acid-like compounds, which can be mobilized from the clay. Both, organic compounds associated with the clay as well as released from the clay are able to influence the migration behavior of metal ions, such as actinides.

Aim of this project was to study basic interaction processes of actinides in the system clay-humic substance-aquifer. The performed works tend to a better processes understanding as well as to a completion of the thermodynamic database, which allows the formulation of more realistic geochemical models and consequently, a more realistic long-term risk assessment. The main focus was on the generation of thermodynamic data on the influence of humic acids (HA) on the migration of uranium and neptunium in clay formations. For these studies kaolinite was chosen as model mineral. The performed investigations can be divided in the synthesis and characterization of HA model substances as well as complexation, sorption and migration studies.

In order to amend the thermodynamic database under environmentally relevant conditions, interactions in the system actinide-HA-water were investigated. To that belong studies of the U(VI) complexation by HA in the neutral pH range and of the redox stability of Np(V) in presence of different humic substances. The impact of HA on the U(VI) and Np(V) sorption onto kaolinite as well as the U(VI) migration in compacted kaolinite was studied in batch and diffusion experiments, respectively. For the future modeling of the U(VI) sorption onto kaolinite, U(VI)-kaolinite-surface complexes in presence and absence of HA were spectroscopically investigated.

A further aim of this project was the improvement of the knowledge of the interaction behavior of HA with metal ions, which contribute to the specification of existing thermodynamic models for the HA metal ion complexation. The influence of HA functional groups, other than oxygen-containing, on the metal ion complexation by HA is widely unclear. Nitrogen-containing HA model substances were synthesized and spectroscopically analyzed to identify nitrogen functional groups in HA. Based on these results first model investigations were performed to study the influence of nitrogen-containing functional groups on the U(VI) complex formation by HA. Furthermore, the impact of clay minerals on the formation of humic substances and humic substance-kaolinite-sorbates and their properties was studied using synthetic HA.

This research project was performed in collaboration with the R&D projects of the Universities of Mainz (02 E 9653), Saarbrücken (02 E 9683), Potsdam (02 E 9924), München (02 E 9693), and Heidelberg (02 E 9703) and the Institute for Interdisciplinary Isotope Research Leipzig (02 E 9663) that were funded by Bundesministerium für Wirtschaft (BMWi). The project partners worked in cooperation with the Institute for Nuclear Waste Management (INE), Forschungszentrum Karlsruhe. Furthermore, the Institute of Radiochemistry (TU München) was an associated partner of the joint project.

## 2 Kaolinite

Within the framework of the joint project kaolinite KGa-1b (IN 47907-2054) from the Clay Minerals Society Source Clays Repository (Washington County, Georgia) was used as model mineral. Kaolinite KGa-1b is a well-crystallized kaolin, which was selected to replace the exhausted stock of kaolinite KGa-1. A comprehensive summary of the origin and analysis of kaolinite KGa-1b is given by Costanzo and Guggenheim (2001).

Kaolinite KGa-1b was characterized with regard to its structure, mineralogical and elemental composition, cation exchange capacity (CEC), and surface area within the project (Křepelová, 2006a) and the data were compared to literature. In the following some characteristics of kaolinite KGa-1b are summarized.

The grain size of KGa-1b amounts to 57.8% < 2 µm and 32.0% < 0.5 µm. The total organic carbon (TOC) content for unprocessed KGa-1b was determined to be 231 ppm (Pruett and Webb, 1993). Kaolinite KGa-1b is moderately hydrophilic and has a large negative $\xi$ potential

(-49.2 mV at pH 7.3-7.5, I: 0.015 M; Wu, 2001). The point of zero charge (p.z.c.) and point of zero net proton charge (p.z.n.p.c.) are reported to be 6.0 (Redden et al., 1998) and 5.1±0.2 (Sutheimer, et al., 1999) or 4.99 ± 0.03 (Schroth and Sposito, 1997), respectively.

Figure 2.1 shows the XRD spectrum of kaolinite KGa-1b which was measured with a Bruker-AXS D5005 powder diffractometer. The spectrum shows typical reflections for kaolinite. There is a peak at diffraction angle 25, which belongs to $TiO_2$ in the form of anatase. The spectrum is comparable with those reported in literature (e.g., Chipera and Bish, 2001). The measured FTIR spectrum of kaolinite KGa-1b (not shown) exhibits the typical spectrum for a well-crystallized kaolinite. The assignment of absorption bands (Křepelová, 2006a) matches the literature data very well (Madejová and Komadel, 2001).

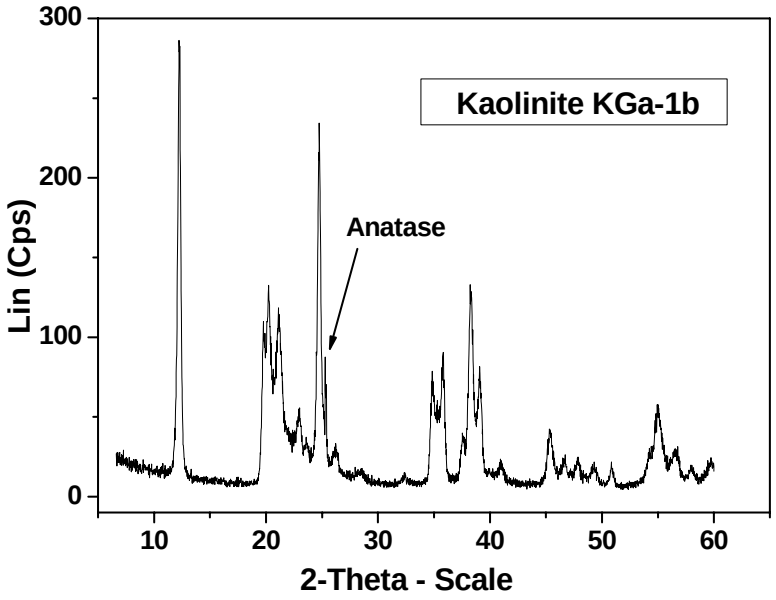


**Fig. 2.1:** XRD spectrum of kaolinite KGa-1b.

The chemical composition of KGa-1b was measured by ICP-MS (ELAN 6000, Perkin Elmer) after acidic digestion ($HNO_3$:HCl:HF = 3:1:1) in a microwave oven (Multiwave, Perkin Elmer). Table 2.1 summarizes selected data in comparison to literature values.

The cation exchange capacity (CEC) of kaolinite KGa-1b was determined by the compulsive exchange method (Sumner and Miller, 1996). The value determined in this work amounts to 1.8 meq/100 g. It is slightly lower than that reported with 3.0 meq/100 g by Borden and Giese (2001). This differences could be caused by the application of different method for the determination of CEC. Furthermore, due to the omnipresent impurities, it is generally difficult to determine true CEC values of clay minerals.

**Tab. 2.1:** Chemical composition of kaolinite KGa-1b (selected data) in comparison to literature.

| Compound/Element (wt%) | This work Untreated KGa-1b | Literature (Pruett and Webb, 1993) < 44 µm |
|---|---|---|
| $Al_2O_3$ | 47.85 | 39.2 |
| $SiO_2$ | 42.98 | 45.1 |
| $TiO_2$ | 1.45 | 1.66 |
| $Fe_2O_3$ | 0.27 | 0.21 |
| CaO | < 0.06 | 0.03 |
| $K_2O$ | 0.01 | 0.02 |
| U (ppm) | 3.69 | 1.96 (Kogel and Lewis, 2001) |

The surface area of kaolinite KGa-1b was determined by BET measurement (Oberflächenanalysator SA 3100, Beckman Coulter). It amounts to 11.8 $m^2/g$. This value agrees very well with the data reported by Pruett and Webb (1993).

Kaolinite KGa-1b was used without any pre-treatment for the experiments described in this report.

# 3 Natural and synthetic humic acid reference materials

As in the previous projects (Pompe et al. 2000a, Sachs et al., 2004), commercially available natural HA from Aldrich (AHA; Aldrich, Steinheim, Germany) was used as reference material for natural HA. Before use, the sodium salt of AHA (Batch H1, 675-2) was purified by repeated dissolution with 0.1 M NaOH (0.01 M NaF) and precipitation with HCl according to the purification method described by Kim and Buckau (1998). AHA batch A2/98 was applied, whose purification is described in detail in (Sachs et al., 2004).

In addition to AHA, synthetic HA type M42 (batch M145) and $^{14}C$-labeled HA type [$^{14}C$]M42 (batch M170 and M180) were used as synthetic HA reference materials (Pompe et al., 1998; Sachs et al., 2004). HA type M42 was synthesized starting from a mixture of xylose, glutamic acid and water. The $^{14}C$-labeled HA type M42 was prepared according to the unlabeled product, however, applying $^{14}C$-labeled glutamic acid as precursor substance. The synthesis of HA type M42 and [$^{14}C$]M42 is described in detail in (Sachs et al., 2004). Table 3.1 summarizes main properties of the applied HA. Further details on the HA characterization are given by Sachs et al. (2004).

**Tab. 3.1:** Main characteristics of the HA applied in this project according to Sachs et al. (2004).

| HA | Elemental composition | | | | | | |
|---|---|---|---|---|---|---|---|
| | C (%) | H [a] (%) | N (%) | S (%) | O [b] (%) | Ash (%) | Moisture (%) |
| **AHA (batch A2/98)** | 58.6 ± 0.1 | 3.0 ± 0.1 | 0.8 ± 0.1 | 3.8 ± 0.1 | 23.5 ± 0.1 | 2.39 | 7.9 |
| **M42 (batch M145)** | 56.1 ± 0.3 | 4.1 ± 0.1 | 4.4 ± 0.1 | - | 26.8 ± 0.3 | 0.11 | 8.4 |

| HA | Functional groups | | |
|---|---|---|---|
| | COOH [c] (meq/g) | PEC [d] (meq/g) | Phenolic/acidic OH [e] (meq/g) |
| **AHA (batch A2/98)** | 4.49 ± 0.14 | 4.60 ± 0.08 | 3.1 ± 0.1 |
| **M42 (batch M145)** | 3.76 ± 0.09 | 3.51 ± 0.07 | 2.0 ± 0.2 |
| **[$^{14}$C]M42 (batch M170)** | 3.63 ± 0.03 | 3.55 ± 0.05 | not measured |
| **[$^{14}$C]M42 (batch M180)** | 3.59 ± 0.01 | 3.36 ± 0.53 | not measured |

| HA | Specific Activity ($^{14}$C) |
|---|---|
| **[$^{14}$C]M42 (batch M170)** | 2.38 MBq/g |
| **[$^{14}$C]M42 (batch M180)** | 17.0 MBq/g |

[a] Corrected for the water content of the HA. [b] The oxygen content was calculated from the difference to 100% in consideration of the ash and moisture content of the HA. [c] Determined by calcium acetate exchange (Schnitzer and Khan, 1972). [d] PEC: Proton Exchange Capacity. Determined by potentiometric titration. [e] Radiometrically determined (Bubner and Heise, 1994).

In addition to AHA and M42, further natural and synthetic HA were used for the study of the Np(V) reduction in presence of HA as well as for some sorption studies. For the description of these humic materials see the corresponding chapters 9 and 11, respectively.

# 4 Nitrogen-containing humic acid model substances: synthesis and characterization by $^{15}$N-NMR spectroscopy

Humic substances contain nitrogen, although in very different and occasionally very small amounts (e.g., 0.8-4.3% N in HA; Stevenson, 1994). It is very probable that the nitrogen in humic substances is derived from amino acids or peptides as biochemically induced fragments of proteins. Its fixation takes place during humification and occurs in several ways (Ziechmann, 1994). One possible way is the condensation of reducing sugars and α-amino acids (melanoidin formation), which is used for the synthesis of HA-alike substances (e.g., Pompe

et al., 2000a). The nitrogen associated with humic and fulvic acids cannot be accounted for in known compounds. It occurs in different types of linkages such as in form of free amino groups (-$NH_2$), open chain groups (–NH-, =N-), and as part of heterocyclic rings (-NH- of indole and pyrrole, -N= of pyridine) (Stevenson, 1994).

To which extent nitrogen-containing functional groups contribute to the complexation process of HA with metal ions is widely unknown so far and not considered in thermodynamic models describing the HA-metal ion-complexation. Up to now the complexation behavior of humic substances is mainly attributed to their oxygen-containing functional groups. In order to elucidate the impact of nitrogen-containing functional groups on the HA complexation behavior, metal ion complexation studies with suitable nitrogen-containing model compounds has to be performed and the results of these studies have to be compared with those obtained with corresponding oxygen-containing substances. In order to get more detailed information on the kind of nitrogenous functionalities in HA, synthetic HA type M1 (Pompe et al., 1996; Pompe et al., 2000a) was $^{15}$N-labeled and characterized by solid-state $^{15}$N-NMR spectroscopy.

## 4.1 Synthesis of a $^{15}$N-labeled humic acid

$^{15}$N-labeled HA type M1 ([$^{15}$N]M1) was synthesized from 3.4 g xylose (Merck), 1.0 g $^{15}$N-L-phenylalanine (Berlin Chemie), 0.5 g glycine (Merck), and 8 mL water. This mixture was refluxed in a nitrogen stream for 10 h. The HA-like melanoidin fraction was separated from the reaction mixture as described in (Pompe et al., 1996), dialyzed against purified water (dialysis tubes Thomapor®, exclusion limit MWCO < 1000, Roth), and lyophilized. For comparison, an unlabeled HA type M1 was synthesized under identical conditions, however, using non-labeled L-phenylalanine (Merck) as starting material. Table 4.1 summarizes the elemental composition and the functional group content of the synthesized HA. The FTIR spectra (FTIR spectrometer Spectrum 2000 GX, Perkin Elmer; KBr method ) are shown in Fig. 4.1.

Both batches of HA M1 and [$^{15}$N]M1 show comparable elemental compositions, functional group contents and FTIR spectra indicating a high reproducibility of the synthesis when L-phenylalanine or $^{15}$N-L-phenylalanine are used as precursor substances.

**Tab. 4.1:** Characterization of HA M1 and [$^{15}$N]M1.

| | Elemental composition | | | | |
|---|---|---|---|---|---|
| | **C (%)** | **H (%)** | **N (%)** | **S (%)** | **O (%) [a]** |
| **M1 (batch S1/05)** | 63.07 ± 0.08 | 5.69 ± 0.18 | 5.44 ± 0.01 | - | 25.81 ± 0.10 |
| **[$^{15}$N]M1 (batch S2/05)** | 62.76 ± 0.13 | 5.67 ± 0.17 | 5.43 ± 0.01 | - | 26.15 ± 0.30 |
| | **Functional groups** | | | | |
| | **COOH (meq/g) [b]** | | **PEC (meq/g) [c]** | | |
| **M1 (batch S1/05)** | 1.50 ± 0.06 | | 1.74 ± 0.22 | | |
| **[$^{15}$N]M1 (batch S2/05)** | 1.49 ± 0.01 | | 1.84 ± 0.12 | | |

[a] The oxygen content was calculated from the difference to 100%. [b] Determined by calcium acetate exchange (Schnitzer and Khan, 1972). [c] PEC: Proton Exchange Capacity. Determined by potentiometric titration.

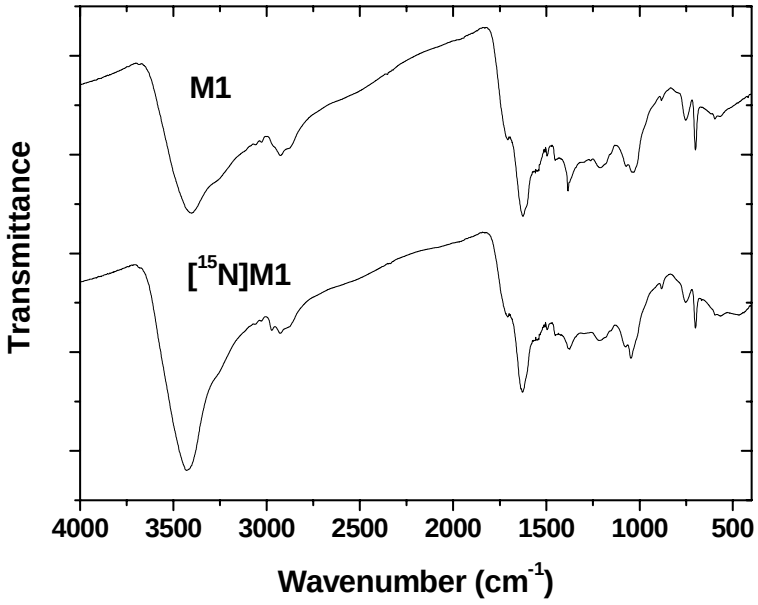


**Fig. 4.1:** FTIR spectra of synthetic HA type M1 and [$^{15}$N]M1.

## 4.2 NMR spectroscopic characterization of the $^{15}$N-labeled humic acid type M1

To identify nitrogen-containing functional groups, HA type [$^{15}$N]M1 was analyzed by $^{15}$N-NMR spectroscopy. Solid-state $^{15}$N-NMR measurements were carried out by Dr. E. Brendler (Institute of Analytical Chemistry, TU Bergakademie Freiberg) using the technique of cross polarization with magic-angle spinning (CP/MAS). The $^{15}$N-NMR spectra were recorded on a Bruker Avance 400 MHz WB spectrometer equipped with a 7 mm probehead. Contact times of 1 and 5 ms, repetition rates of 1 or 3 s, and rotation frequencies between 4 and 7 kHz were

applied. The samples were filled into 7 mm $ZrO_2$ rotors. Chemical shifts were measured relative to nitromethane (= 0 ppm). For comparison, spectra of [$^{15}$N]-L-phenylalanine and unlabeled HA type M1 were recorded. The peak assignment is based on data collections for $^{15}$N-NMR chemical shifts of organic compounds and humic substances (e.g., Berger et al., 1992; Bortiatynski et al., 1996).

Fig. 4.2 shows the $^{15}$N-NMR spectrum of $^{15}$N-L-phenylalanine. The spectrum shows one resonance signal at -336.3 ppm. This signal is attributed to the $NH_2$ group of phenylalanine. It agrees very well with literature data (neutral form of phenylalanine: -335.0 ppm; Berger et al., 1992).

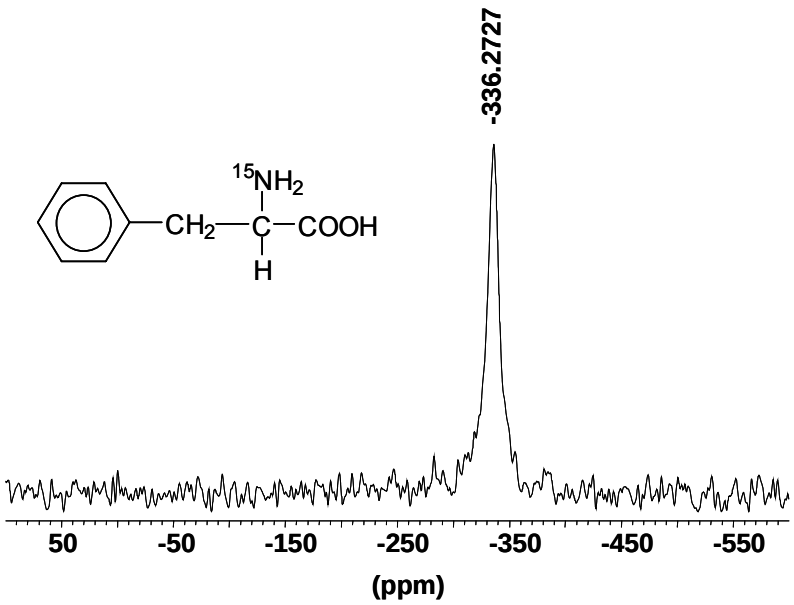


**Fig. 4.2:** $^{15}$N-NMR spectrum of [$^{15}$N]-L-phenylalanine (4 kHz; contact time: 1 ms; repetition time: 3 s).

A $^{15}$N-NMR spectrum of HA [$^{15}$N]M1 is depicted in Fig. 4.3. The spectrum shows different resonance signals between –150 and –350 ppm indicating the presence of various nitrogen-containing functionalities in the HA structure. It is dominated by signals at –223, –258, and -322 ppm.

In order to verify that the measured NMR signals are real resonance signals and no spinning side bands, the HA sample was measured at different rotation frequencies (Fig. 4.4). The main signals and shoulders in the spectra obtained with 5 and 7 kHz (contact time 5 ms) are nearly identical. Thus, it was concluded that the signals are real $^{15}$N chemical shifts of the synthetic HA.

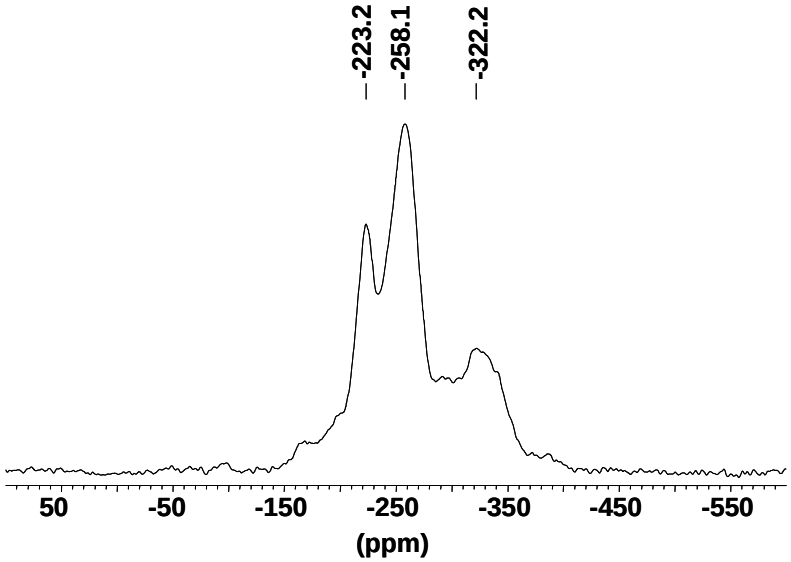


**Fig. 4.3:** $^{15}$N-NMR spectrum of HA [$^{15}$N]M1 (5 kHz, contact time: 1 ms; repetition rate: 3 s).

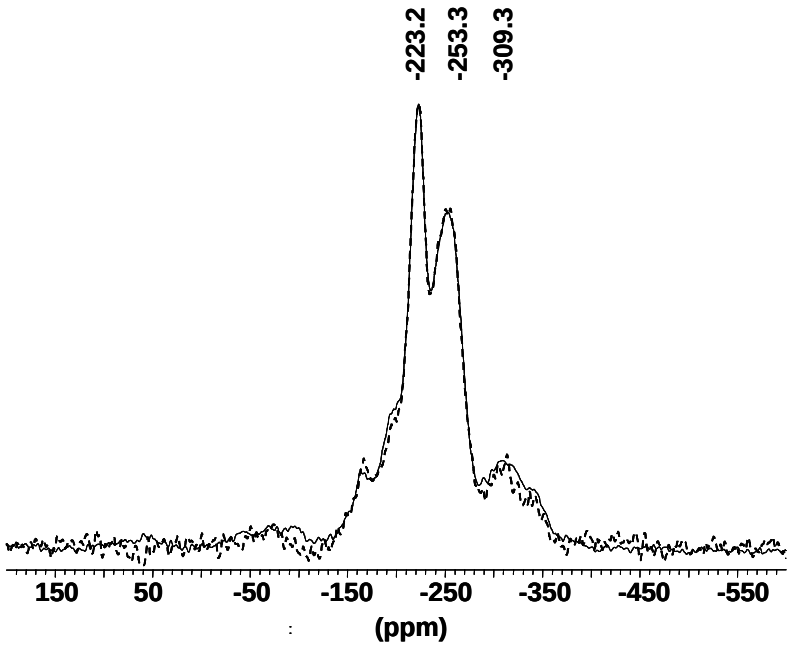


**Fig. 4.4:** $^{15}$N-NMR spectra of HA [$^{15}$N]M1 measured at different rotation frequencies (solid line: 5 kHz, dashed line: 7 kHz; contact time: 5 ms; repetition rate: 3 s).

The recording of $^{15}$N-NMR spectra is based on an indirect magnetization method. Thereby, the protons of a sample are excited and transfer their magnetization to the $^{15}$N nuclei by irradiating the resonance frequencies of $^{1}$H and $^{15}$N during a contact time $\tau_{CP}$, which results in an enhancement of the $^{15}$N signal. In general, the enhancement maximum for proton free environments is found at longer $\tau_{CP}$ than for proton carrying groups. To distinguish between pro-

ton-free, heterocyclic and proton-rich nitrogen in the HA, the sample was measured with different contact times. Figure 4.5 shows the spectra of HA [$^{15}$N]M1 recorded with 1 and 5 ms contact time. The increase in the contact time results in an intensity increase of the signals between -150 and –200 ppm. In contrast to that, the signals at –255 ppm and about –315 ppm have higher intensity at shorter contact time. From that it can be concluded, that the chemical shifts up to –200 ppm are due to hydrogen-free heterocyclic structural elements, whereas the others can be ascribed to amide and/or amino groups.

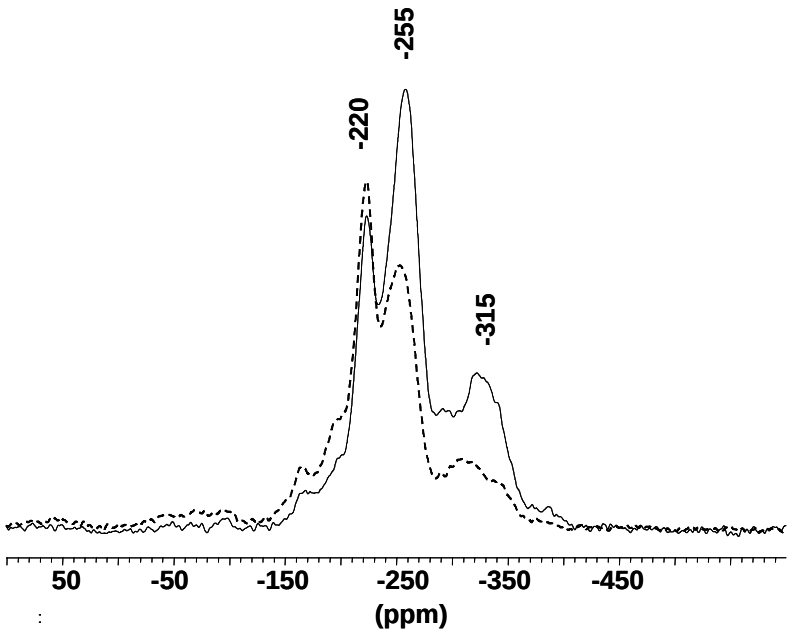


**Fig. 4.5:** $^{15}$N-NMR spectra of HA [$^{15}$N]M1 measured at different contact times (solid line: 1 ms, dashed line: 5 ms; 5 kHz; repetition rate: 3s).

Based on the peak assignments given in the literature (Bortiatynski et al., 1996), the main resonance signals in the spectra of HA [$^{15}$N]M1 can be attributed to NH in pyrroles, indoles and/or amides (-220 ppm), NH in amide structures (–255 ppm), and to primary and secondary amines (NH, $NH_2$, -315 ppm). The shoulders between –150 and –200 ppm can be ascribed to N-substituted pyrroles and/or indoles or heterocyclic -N= sites in these compounds. Comparable types of nitrogen were already found for condensation products of xylose, glycine and water synthesized with varying reaction times (Benzing-Purdie and Ratcliffe, 1986).

Free $NH_2$ groups of amino acids exhibit resonance signals between –325 and –350 ppm (Bortiatynski et al., 1996). The $^{15}$N-NMR spectra of [$^{15}$N]M1 show a broad unresolved signal in this spectral range, which is more intensive at lower contact time. This broad signal could be a result of overlapping chemical shifts of primary and/or secondary amines and terminal amino acid groups.

The $^{15}$N-NMR spectrum of unlabeled HA M1 is shown in Fig. 4.6. Due to the low natural abundance of $^{15}$N, the signal-to-noise ratio of this spectrum is very low, even after 36 h of measuring time. However, a resonance signal at –254 ppm with a shoulder at about -220 ppm was observed. These signals correspond to the main peaks in the spectrum of HA [$^{15}$N]M1 and can be attributed to NH in heterocyclic and amide structures.

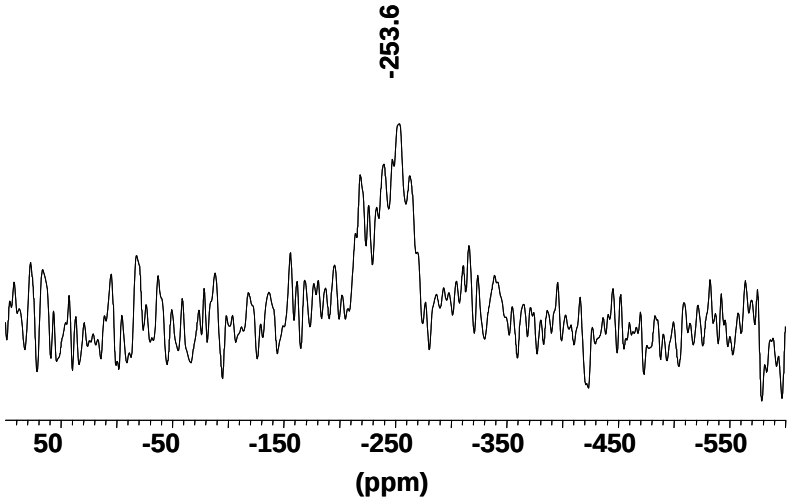


**Fig. 4.6:** $^{15}$N-NMR spectrum of HA M1 (4 kHz; contact time: 1 ms; repetition rate: 1 s; measuring time: 36 h).

The $^{15}$N-NMR spectra show that the amino groups of [$^{15}$N]phenylalanine are for the most part transformed into different heterocyclic and amide nitrogen functions. From the linewidth of the resonances can be concluded that no single, defined compound is formed but a heterogeneous, amorphous material.

Nevertheless the interpretation of the $^{15}$N-NMR spectra is difficult and not clear in each case. The resonance signals are broad due to a distribution of bond length and angles at nitrogen in the above mentioned chemical environments. In addition to that, signals in one resonance range can be assigned to different nitrogen-containing structures. However, from our studies it can be concluded that the nitrogen in synthetic HA type M1 can be attributed to pyrrole and/or indole like N, amide N, primary and/or secondary amine N, and possibly N in terminal amino acid groups. Our obtained data agree well with nitrogen structures for natural organic matter discussed in the literature (e.g., Stevenson, 1994).

In conjunction with literature data for natural organic matter, these NMR results represent a base for the suitable selection of model ligands to elucidate the impact of nitrogen functionalities on the metal ion complexation behavior of HA.

# 5 Synthesis of humic substances in presence of kaolinite and formation of humic substance-kaolinite-sorbates

Clay minerals are able to bind manifold organic compounds at their outer surfaces or within the interlayers. Depending on the clay type, organic compounds are bound by intercalation, complexation, solvation, and ion exchange (Lagaly, 1993).

Most natural clays are closely associated with natural organic matter. If organic compounds are mobilized from the clay rocks, they can influence the sorption behavior of metal ions, such as actinides. Claret et al. (2003) described the generation of humic and fulvic acid-like compounds from Callovo-Oxfordian clay under alkaline conditions, which could be an important source of complexing mobile organic matter, which probably influences the mobility of actinide ions. In addition, clay minerals can catalyze the formation of humic substances. Taguchi et al. (1986) found that montmorillonite is able to promote the formation of humic substance-like melanoidins from glucose and glycine or alanine.

The objective of our work was to study the influence of kaolinite KGa-1b on the formation of synthetic HA and their properties. Furthermore, we investigated the formation of humic substance-kaolinite-sorbates as model compounds for natural organic matter-containing clays.

## 5.1 Synthesis of humic acid type M1 and M42 in presence of kaolinite

HA type M1 (Pompe et al., 1996) and M42 (Pompe et al., 1998) were synthesized in presence of kaolinite KGa-1b based on their standard synthesis methods. For synthesis of HA type M1 the following two methods were applied.

**Method A):** 17 g xylose (Merck), 5 g phenylalanine (Fluka), 2.5 g glycine (Merck), 2 g kaolinite, and 40 mL water were refluxed in a nitrogen stream for 10 h. The solid reaction product was separated by centrifugation and ground with ethanol and ether. The HA-like melanoidin fraction was extracted from the solid product with 2 M NaOH under nitrogen atmosphere and precipitated by 2 M HCl. The HA precipitate was dialyzed against purified water (dialysis tubes Thomapor®, exclusion limit MWCO < 1000, Roth) and lyophilized. The remaining NaOH insoluble solid fraction containing kaolinite and an alkaline less or not soluble melanoidin fraction was repeatedly washed with Milli-Q water and then lyophilized. A

synthetic HA type M1-K(A) and a humic substance-kaolinite sorbate M1-KS(A) were obtained as synthesis products.

**Method B):** Method B starts with a diluted reaction mixture. 17 g xylose, 5 g phenylalanine, 2.5 g glycine, 2 g kaolinite, and 200 mL water were boiled under reflux in a nitrogen stream for 10 h. After separation, the solid reaction product was ground with ethanol and ether, washed with water, dialyzed (dialysis tubes Thomapor®, exclusion limit MWCO < 1000, Roth), and lyophilized. Then, synthetic HA M1-K(B) was isolated by alkaline extraction, however, using only 0.1 M NaOH, and acid precipitation with 2 M HCl. The remaining NaOH insoluble solid was neutralized, dialyzed, and lyophilized resulting in the humic substance-kaolinite-sorbate M1-KS(B).

The synthesis of HA type M42 in presence of kaolinite KGa-1b starts also from a diluted reaction mixture. 16.5 g xylose, 11 g glutamic acid monohydrate (Fluka), 2 g kaolinite, and 150 mL water were kept under reflux at 80 °C for 90 h. The isolation of HA type M42-K and of the synthetic humic substance-kaolinite-sorbate M42-KS was carried out according to method B.

Parallel syntheses were performed in absence of kaolinite resulting in HA type M1-A (method A), M1-B (method B), and M42.

The pH values of the reactions mixtures were measured at the start and the end of the syntheses. It was found that the presence of kaolinite exhibits no clear pH effect. This is in contrast to observations during the reaction of glucose with glycine or alanine in presence of montmorillonite (Taguchi et al., 1986). Due to reactions between exchangeable cations present in montmorillonite and the cation-exchange capacities of the melanoidins, montmorillonite caused an constant increased pH value in the reaction mixtures resulting in a promotion of the melanoidin formation. The different behavior of kaolinite and montmorillonite can be attributed to their different cation exchange capacities which amount to 1.8 and 70-120 meq/100 g for kaolinite KGa-1b (see chapter 2) and montmorillonite, respectively (Lagaly, 1993).

## 5.2 Characterization of humic acids synthesized in presence of kaolinite

The obtained HA were characterized with regard to their elemental composition (C, H, N, Al, Si), functionality (COOH) and structure (FTIR spectroscopy; FTIR spectrometer Spectrum 2000 GX, Perkin Elmer; KBr method). Results for three selected parallel syntheses in absence and presence of KG1a-1b are summarized in Tab. 5.1.

**Tab. 5.1.:** Characterization of selected HA type M1 and M42 synthesized in absence and presence of Kaolinite KGa-1b.

| | HA Type M1 | | | | HA Type M42 | |
|---|---|---|---|---|---|---|
| | Method A | | Method B | | | |
| | **M1(A)** | **M1-K(A)** | **M1(B)** | **M1-K(B)** | **M42** | **M42-K** |
| **Batch** | M183 | M182K | M191 | M189K | M194 | M192K |
| **Yield (mg)** | 2530 | 2290 | 356 | 77 | 196 | 137 |
| **C (%)** | 61.5 | 61.5 | 60.3 | 56.3 | 55.5 | 55.2 |
| **H (%)** | 5.6 | 5.5 | 6.0 | 5.8 | 4.9 | 5.4 |
| **N (%)** | 5.2 | 5.2 | 5.8 | 5.8 | 4.7 | 5.5 |
| **Si (ppm)[a]** | <40 | <32 | 8 | 2948 | <NWG | <600 |
| **Al (ppm)[a]** | 76 | 143 | 20 | 4688 | <80 | 4377 |
| **COOH [b] (meq/g)** | 1.39 ± 0.03 | 1.45 ± 0.01 | 1.21 ± 0.22 | 1.30 ± 0.21 | 2.94 ± 0.15 | 2.34 ± 0.13 |

[a] Measured by ICP-MS after digestion of the HA with $HNO_3$ in a microwave oven. [b] Determined by calcium acetate exchange method (Schnitzer and Khan, 1972).

From Tab. 5.1 it becomes obvious, that for all HA syntheses in presence of kaolinite the yields on HA-like substances are lower than those of syntheses in absence of kaolinite. These differences could be attributed to the sorption of humic substances onto kaolinite, which probably promotes the formation of higher polymerized substances which are less or not at all soluble in alkaline solutions compared to the extracted HA. The decrease of the initial precursor concentrations for the synthesis of HA type M1 (method A → method B) results in a significant decrease in the yield on HA-alike substances as expected.

HA type M1(A) and M1-K(A) exhibit comparable elemental compositions and COOH group contents. Furthermore, they show nearly identical FTIR spectra (not shown). Therefore, it can be concluded that the presence of kaolinite has no significant influence on the properties of HA type M1 synthesized according to method A. However, after dilution of the reaction mixture, an influence of kaolinite on the formation of HA M1 becomes obvious. HA M1(B) and M1-K(B) show differences in their elemental compositions, especially in their carbon contents. The lower carbon content of M1-K(B) can be explained by an increase of the Si and Al content in the HA due to the presence of kaolinite. Both HA show similar amounts of COOH

groups. Figure 5.1 presents the FTIR spectra of HA M1(B) and M1-K(B) in comparison to kaolinite KGa-1b.

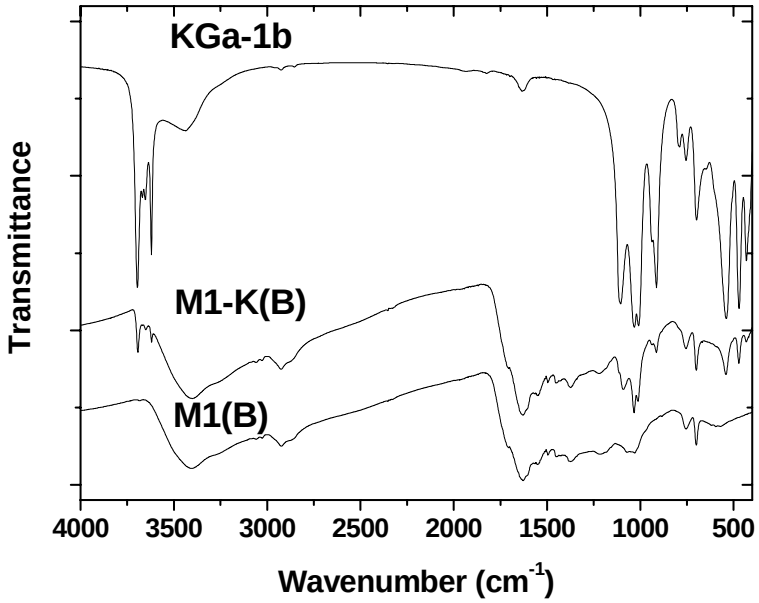


**Fig. 5.1:** FTIR spectra of HA type M1 synthesized in absence (M1(B)) and presence (M1-K(B)) of kaolinite KGa-1b according to method B in comparison to the spectrum of kaolinite KGa-1b.

Generally, FTIR bands of both HA are comparable. In the spectrum of HA M1-K(B), however, additional IR absorption bands were detected (e.g., at 3700, 3620, 1035, 1010, 905, 540, 470 $cm^{-1}$) that point to the occurrence of kaolinite residues in this HA. It can be concluded that the elemental composition of HA type M1 is influenced by kaolinite when the HA is synthesized according to method B.

HA M42 and M42-K possess no clear differences in their carbon, hydrogen and nitrogen contents. However, also HA M42-K shows an increased amount of Si and Al, pointing to an association of HA with kaolinite. Again, this is reflected in the FTIR spectrum of M42-K (Fig. 5.2), which exhibits absorption bands, as already found for HA M1-K(B), indicating the presence of kaolinite. The COOH group content of HA M42-K is slightly lower than that of HA M42 which is probably caused by the presence of kaolinite in HA M42-K.

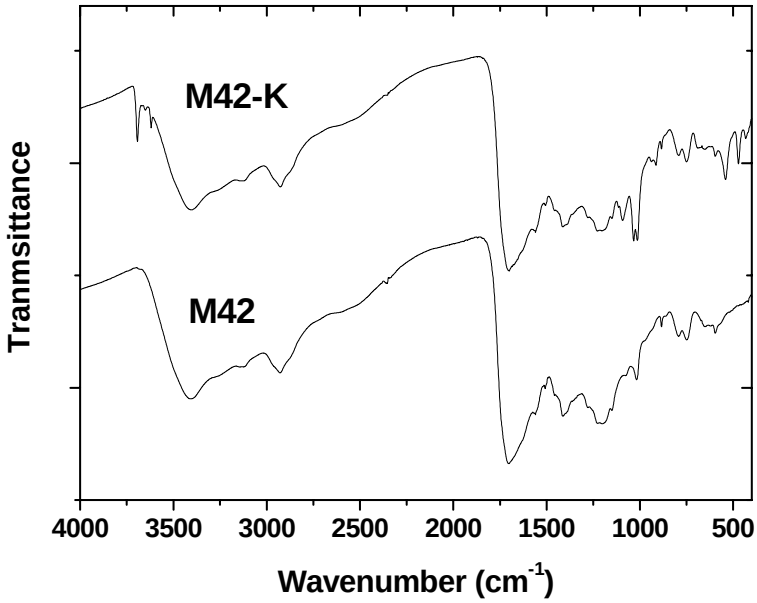


**Fig. 5.2:** FTIR spectra of HA type M42 synthesized in absence (M42) and presence (M42-K) of kaolinite KGa-1b.

The obtained results indicate that the presence of kaolinite during the HA synthesis mainly influences the yields on HA and their elemental compositions. Furthermore, a slight influence on the carboxyl group content of HA type M42 was observed.

In further syntheses, which are not subject of this report, comparable results were found. However, it was determined that the presence of kaolinite in the syntheses decreases the reproducibility of the product properties. A possible reason for that could be the heterogeneity of the reaction mixture.

## 5.3 Characterization of synthetic humic substance-kaolinite sorbates

The synthetic humic substance-kaolinite-sorbates were characterized with regard to their total organic carbon content (TOC) and structure as well as to the distribution of humic substances in the sorbate.

The TOC contents of the humic substance-kaolinite-sorbates were determined using a multi N/C analyzer with additional ELTRA high temperature oven (Analytik Jena). Table 5.2 summarizes the TOC contents of selected synthetic humic substance-kaolinite-sorbates and the derived amounts of humic substances. Comparing the TOC contents of M1-KS synthesized with method A and B (method B was started from a diluted reaction mixture), it can be seen

that it is decreased with decreasing precursor concentrations. Consequently, the amount of humic substances associated with kaolinite is decreased. It is assumed that higher polymerized and more hydrophobic substances are associated with kaolinite after the alkaline extraction of the HA-like substances. As expected, the amount of these substances should be increased when a higher starting concentration on precursor substances is used for the synthesis. The TOC contents of the synthetic humic substance-kaolinite sorbates M42-KS that were synthesized under comparable experimental conditions exhibit variations. Batch M192KS shows a significant higher TOC content than the other batches. The lower reproducibility of the synthesis in the heterogeneous reaction mixture could be a reason for that observation.

**Tab. 5.2:** TOC and humic substance concentrations of selected synthetic humic substance-kaolinite sorbates.

| | **M1-KS(A)** | **M1-KS(B)** | **M42-KS** [a] | | |
|---|---|---|---|---|---|
| **Batch** | M182KS | M189KS | M192KS | R11/04KS | R1/06KS |
| **TOC (mg/g)** | 10.4 | 3.9 | 24.1 | 4.9 | 5.1 |
| **HS** [b] **(mg/g)** | 17 | 7 | 44 | 9 | 9 |

[a] Different batches of synthetic humic substance-kaolinite-sorbates synthesized under comparable experimental conditions. [b] Estimated amount of humic substances (HS) in the sorbate. Calculated based on the carbon content of the corresponding HA.

The structure of the sorbates was analyzed by FTIR spectroscopy (FTIR spectrometer Spectrum 2000 GX, Perkin Elmer; KBr method). The FTIR spectra of the isolated synthetic humic substance-kaolinite-sorbates are dominated by the spectrum of kaolinite. Due to the low concentrations of humic substances in the sorbates (0.7-4 mass%), no or only very weak indications exist in the spectra that point to the occurrence of humic substances in the sorbates. For example, the FTIR spectrum of M42-KS (batch M192KS) in comparison to that of untreated kaolinite is plotted in Fig. 5.3. Both FTIR spectra are dominated by IR absorption bands of kaolinite. Only very small differences occur between 1700 and 1630 $cm^{-1}$. In this range, the intensity of the spectrum of M42-KS is slightly increased. This intensity increase is attributed to FTIR signals of aromatic structural elements and carbonyl groups of the humic substances associated with kaolinite. Generally, these bands are the most pronounced absorption bands in the spectra of humic substances (cf. Fig. 5.1 and 5.2). Therefore, it is not surprising that no other FTIR signals indicating the presence of humic substances in the sorbates could be detected. The FTIR signals of the original untreated kaolinite are identical to those of kaolinite in the sorbate. This indicates that no significant structural changes of kaolinite occur during the synthesis and the reprocessing procedure.

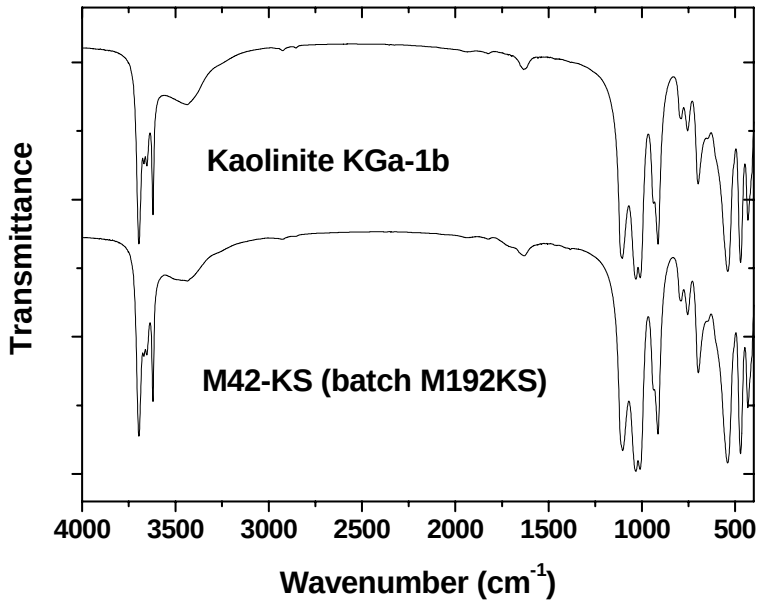


**Fig. 5.3:** FTIR spectrum of the synthetic humic substance-kaolinite-sorbate M42-KS (batch M192KS) in comparison to the spectrum of kaolinite KGa-1b.

The distribution of humic substances in a kaolinite sorbate type M42-KS (batch R11/04KS) was determined by X-ray photoelectron spectroscopy (XPS) in cooperation with the Institut für Kernchemie, Johannes-Gutenberg University Mainz (Reich et al., 2006a). The results were compared to those of untreated kaolinite KGa-1b as well as to two kaolinite samples with 1.2 and 2.4 mg/g of sorbed HA (Reich et al., 2006a). For the measurements, the powders were pressed into indium foil. Mg Kα radiation (1253.6 eV) was used for the excitation of XPS spectra. The measuring conditions are described in (Reich et al., 2006a). Figure 5.4 shows a section of the XPS spectrum. The main conclusions drawn from the XPS measurements of M42-KS are the following: At the untreated kaolinite surface relatively small amounts of adsorbed hydrocarbons (~1 atom%) were detected. The C1s/Al 2p intensity ratio of all humic samples with varying amounts of humic substances (1.2–9 mg/g) is nearly constant and does not show any correlation with the humic substance loading. Only approximately 5 atom% carbon were found on the surface of the samples. This shows that the surface of the clay particles is not covered by a homogenous layer of humic substances. A part of the humic substances must be distributed between the kaolinite particles. The surface composition of the synthetic humic substance-kaolinite-sorbate sample with respect to Si, Al, and O is comparable to the untreated kaolinite. This indicates that the chemical composition of the kaolinite surface was not altered during the synthesis and reprocessing procedure. A detailed summary of binding energies and XPS line intensities is given in (Reich et al., 2006a).

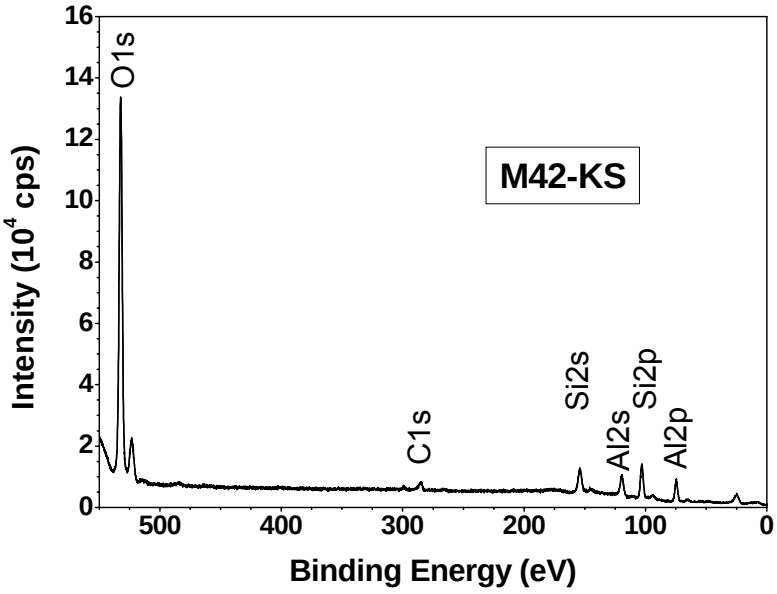


**Fig. 5.4:** XPS spectrum of a synthetic humic substance-kaolinite-sorbate M42-KS (batch R11/04KS, TOC: 4.9 mg/g).

It can be concluded that it is possible to synthesize humic substance-kaolinite-sorbates. Based on their synthesis this materials contain humic substances that are assumed to be more hydrophobic than synthetic HA-like substances extracted from the sorbates. Such sorbates are suitable model compounds for organic rich clays. Within the present project synthetic humic substance-kaolinite sorbates were used in batch sorption and diffusion experiments (see chapter 11 and 13). The results were compared to those obtained from untreated kaolinite and HA.

# 6 Studies of the influence of nitrogen-containing functional groups of humic substances of the complex behavior with model compounds

To receive an impression if nitrogen-containing functional groups can influence the interaction between humic substances and actinides even at acidic pH ranges, investigations with uranium(VI) (U(VI)) and some model compounds were done. As model substances were chosen L-phenylalanine (2-amino-3-phenylpropionic acid, $C_6H_5$-$CH_2$-$CH(NH_2)$-COOH), for comparison its equivalent without amino function 3-phenylpropionic acid ($C_6H_5$-$CH_2$-$CH_2$-COOH), and glycine (aminoacetic acid, $CH_2(NH_2)$-COOH). The complex behavior of these compounds toward U(VI) at acidic pH values has been studied by TRLFS (time-resolved laser-induced fluorescence spectroscopy) and ATR (attenuated total reflection) FTIR spectroscopy.

## 6.1 Experimental

### *Solutions and reagents*

The stock solutions of the ligands L-phenylalanine (Merck), 3-phenylpropionate (3-phenylpropionic acid, Aldrich) and glycine (Aldrich) were prepared freshly for each experiment. For TRLFS measurements the stock solution of $UO_2^{2+}$ were made from $UO_2(ClO_4)_2 \cdot 6H_2O$ (Merck). For ATR FTIR measurements a $UO_2Cl_2$ stock solution was used. It was obtained from $UO_2(NO_3)_2$ (provided from VKTA Rossendorf), which was heated to get $UO_3$, and the nitrate free oxide was dissolved in 1M HCl. The ionic strength was kept constant by adding a $NaClO_4$ stock solution ($NaClO_4 \cdot H_2O$, Merck) for TRLFS measurements or a NaCl stock solution for ATR FTIR measurements. All stock solutions were prepared with deionized water. Necessary pH adjustments were made with $HClO_4$ (TRLFS), HCl (ATR FTIR) or NaOH with an accuracy of 0.05 units.

### *TRLFS measurements*

The TRLFS measurements were performed at a total uranyl concentration of $10^{-5}$ M as a function of the ligand concentration (10 different concentrations between $1 \cdot 10^{-5}$ M to $2 \cdot 10^{-3}$ M each) at pH = 4.0 and an ionic strength of 0.1 M ($NaClO_4$).
The spectra were recorded at room temperature using a pulsed Nd:YAG laser system (minilite continuum Electro-Optics, Inc., Santa Clara, USA) with a digital delay/pulse generator (model DG535, Stanford Research systems, Inc., USA). The excitation wavelength of the uranyl fluorescence was 266 nm with pulse energy of 0.2 – 0.5 mJ. The TRLFS spectra were measured from 440 to 620 nm, averaging 3 spectra with 100 laser pulses each, and a gate time of 1 μs. The time-resolved fluorescence emission was detected using a digital triple grating spectrograph (EG&G Princeton Instruments, USA, model 1235). All functions of the laser spectrometer are computer controlled with the program WinSpec/32, version 2.5.19.6, Roper Scientific 2003 (Microsoft corporation).

### *ATR FTIR measurements*

The ATR FTIR measurements were performed with aqueous solutions containing a uranyl-to-ligand ratio of 1 : 1, a concentration of $10^{-2}$ M, an ionic strength of 1 M (NaCl), and pH = 3.2.

At higher pH values precipitation of a not yet defined uranyl compound (either hydroxide and/or complex) was observed.

The infrared spectra were recorded at room temperature with an FTIR spectrometer (Spectrum 2000 GX, Perkin Elmer) and a diamond ATR cell (crystal diameter: 4 mm, 9 reflections). For the experiments a flow cell (volume: 200 µL) with a constant flow rate of 200 µL/min was used. The spectra were calculated out of single beam spectra each co-added from 128 scans at a spectral resolution of 4 $cm^{-1}$ in the wavenumber range from 5200 to 580 $cm^{-1}$. The results are presented as difference spectra between an aqueous solution of the free ligand and the related uranyl complex in the range from 1800 to 800 $cm^{-1}$.

## 6.2 Results and discussion

### *TRLFS measurements*

Figure 6.1 shows the fluorescence spectra of the uranyl ion as a function of the ligand concentration of L-phenylalanine (left) and 3-phenylpropionate (right) at pH = 4.0. Both ligands caused a strong decrease of the fluorescence intensity with increasing concentration. We noticed no shift of the fluorescence peaks. This behavior is typical for static fluorescence quenching due to the complex formation.

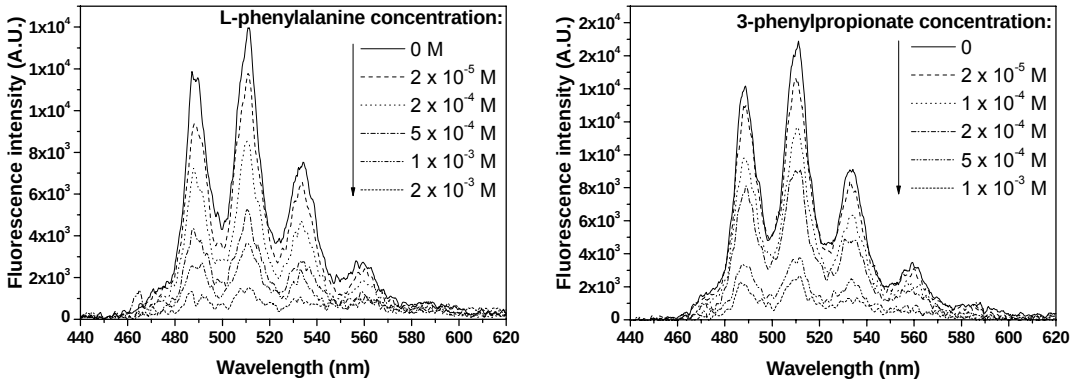


**Fig. 6.1:** Fluorescence spectra of U(VI) ($10^{-5}$ M) at pH = 4.0 as a function of the ligand concentration of L-phenylalanine (left) and 3-phenylpropionate (right).

The complex formation reaction can be written as:

$$UO_2^{2+} + n\ HL \rightleftarrows UO_2L_n^{(2-n)+} + n\ H^+ \qquad (6.1)$$

Provided that the fluorescence intensity is straight proportional to the concentration of the free uranyl ion, with the following modified logarithmic form of the mass action law

$$\log \frac{[\{UO_2(L)_n\}^{(2-n)+}]}{[UO_2^{2+}]} = n \log[HL] + \log K' + pH \qquad (6.2)$$

the stoichiometry and the complex stability constant can be graphical determined via slope analysis, as demonstrated in Fig. 6.2. For both complex systems a slope (n) near 1 was calculated, indicating a predominant 1 : 1 complex. The intersection offers the equilibrium constant log$K$', which can be converted under consideration of the pH and the p$K_a$ of the ligand into the stability constant log$K_{ML}$ (see Tab. 6.1).

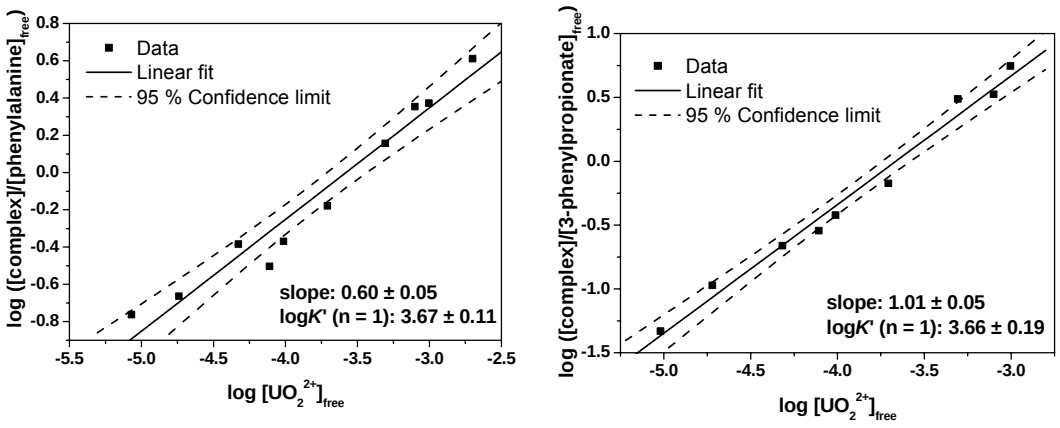


**Fig. 6.2:** Validation plot (slope analysis) of the complexation of U(VI) with L-phenylalanine (left) and 3-phenylpropionate (right) at pH = 4.0.

The fluorescence decay was mono-exponential in all samples. The lifetime, which belongs to the free uranyl ion, decreases with increasing ligand concentration, as to be seen in Fig. 6.3. This indicates additional dynamic fluorescence quenching, caused by the free ligand.
With the aid of the Stern-Volmer equation (Eq. (6.3)) the lifetimes likewise can be used to calculate the complex stability constants.

$$\frac{\tau_0}{\tau} = 1 + K_{SV} \cdot [Q] \qquad (6.3)$$

$\tau_0$ represents the fluorescence lifetime of the uranyl ion without quencher, and $\tau$ is the lifetime with quenching substance Q (free ligand). The Stern-Volmer plots gave straight lines with an

intersection of zero within the error limits. Their slope ($K_{SV}$) represents the complexation constant. Figure 6.4 shows the Stern-Volmer plots for both complex systems.

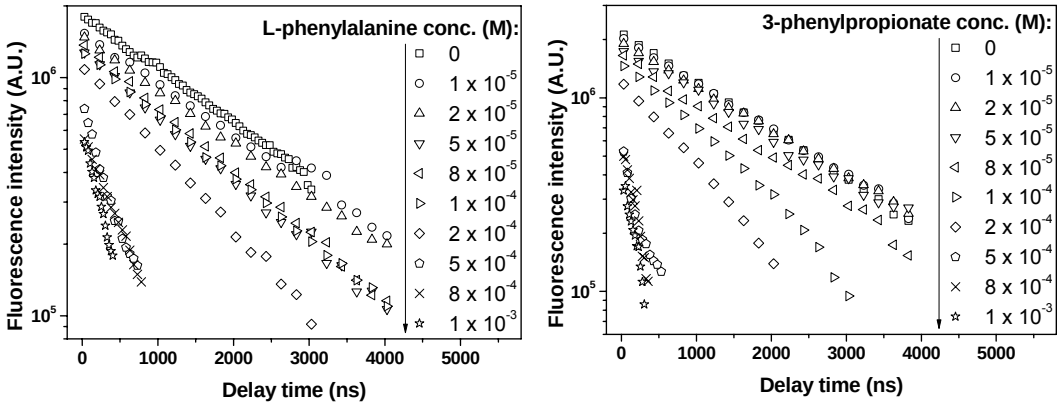


**Fig. 6.3:** Fluorescence decay of U(VI) as a function of the ligand concentration (dynamic quenching).

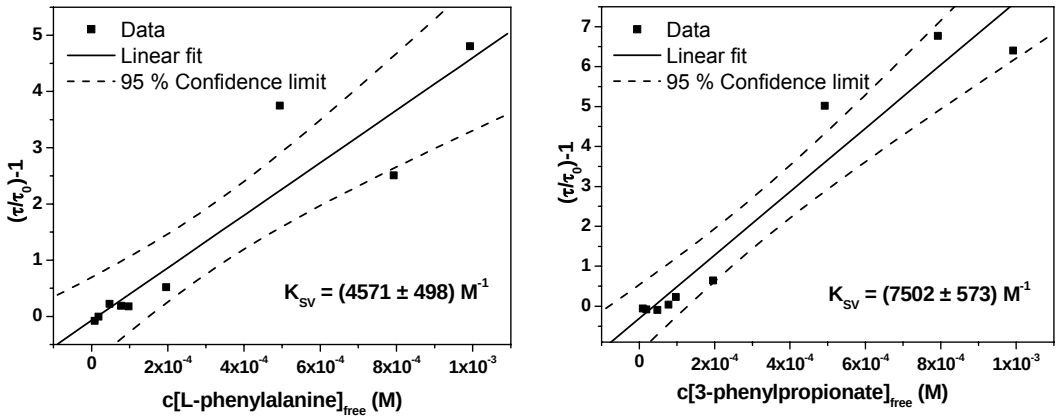


**Fig. 6.4:** Stern-Volmer plot (dynamic quenching) of U(VI) by L-phenylalanine (left) and 3-phenylpropionate (right).

The Stern-Volmer constant $K_{SV}$ likewise can be converted into the complex stability constant $\log K_{ML}$, taking into account the pH and the $pK_a$ values of the ligand (see Table 6.1).

Both methods to calculate the complex stability constants are well established and described detailed in the literature (e.g., Koban et al., 2003; Geipel et al., 2004; Vulpius, 2005). Table 6.1 summarizes the determined complex stability constants.

**Tab. 6.1:** Summary of the complex stability constants.

| Complex | $\log K_{ML}$ (slope analysis) | $\log K_{ML}$ (Stern-Volmer plot) | $\log K_{ML}$ (average) |
|---|---|---|---|
| L-phenylalanine[a]: $UO_2[C_6H_5\text{-}CH_2\text{-}CH(NH_3)\text{-}COO]^{2+}$ | 1.91 ± 0.18 | 1.90 ± 0.07 | 1.9 ± 0.2 |
| 3-phenylpropionate[b]: $UO_2[C_6H_5\text{-}CH_2\text{-}CH_2\text{-}COO]^{+}$ | 4.06 ± 0.19 | 4.28 ± 0.08 | 4.2 ± 0.2 |

[a] $pK_{a1}(COOH) = 2.24 \pm 0.07$; $pK_{a2}(NH_3^+) = 9.16 \pm 0.01$ ($pK_{a2}$ is not to be considered in the investigated pH range) (Ishimitsu et al., 1977).
[b] $pK_a(COOH) = 4.40 \pm 0.01$ ( Hasegawa et al., 1990).

The complex stability constant of the uranyl L-phenylalanine complex ($\log K = 1.9 \pm 0.2$) is remarkable smaller than that of the uranyl 3-phenylpropionate complex ($\log K = 4.2 \pm 0.2$). This indicates that the amino group, which appears in its protonated form $R\text{-}NH_3^+$ in acidic solution, is not involved in the complexation, but may rather destabilize the complex. This result is in accordance with other investigations (Fernandez-Botello et al., 2002; Moll et al., 2003; Koban and Bernhard, 2006).

***ATR FTIR measurements***

Figure 6.5 shows the difference IR spectra of the uranyl L-phenylalanine system (left panel) and of the uranyl 3-phenylpropionate system (right panel). The bands below 1000 $cm^{-1}$ represent the antisymmetric stretching vibration $\nu_{as}$ of the uranyl cation. The bands at 959 and 957 $cm^{-1}$ can be assigned to the free uranyl ion whereas the complexation of the uranyl cation causes a shift of the $\nu_{as}$ mode to 928 $cm^{-1}$ (L-phenylalanine) and 926 $cm^{-1}$ (3-phenylpropionate).

In the region between 1600 and 1400 $cm^{-1}$ stretching vibrations of the carboxylate groups are normally observed. Therefore, the absorption peaks at 1457 and 1531 $cm^{-1}$ (L-phenylalanine), and 1458 and 1533 $cm^{-1}$ (3-phenylpropionate) are assigned to the symmetrical ($\nu_s$) and antisymmetrical ($\nu_{as}$) stretching vibration of the uranyl coordinating carboxylate group, respectively. The spectral region above 1600 $cm^{-1}$ is characterized by the strong absorption band of the water solvent and therefore can not be interpreted accurately.

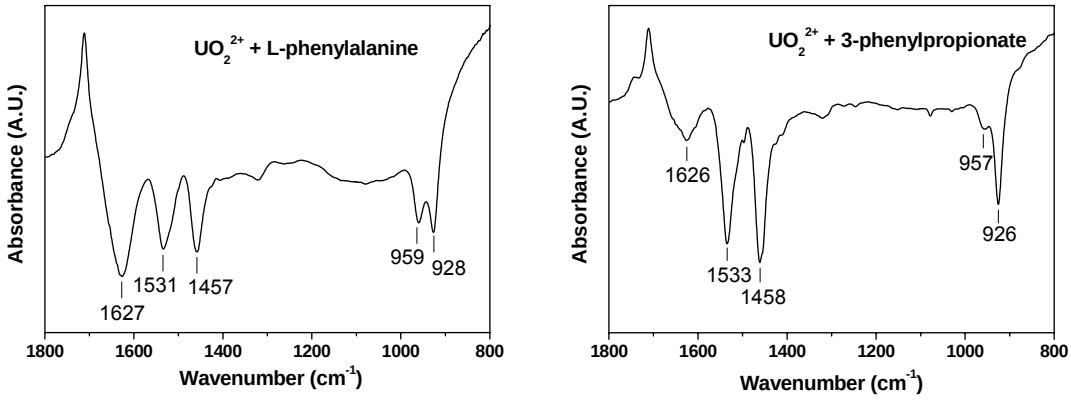


**Fig. 6.5:** FTIR difference spectra of solutions containing 10 mM $UO_2^{2+}$ and 10 mM ligand at pH 3.2.

The spectra clearly demonstrate that the $UO_2^{2+}$ cation is bound via the carboxylate groups to the ligands since the frequency of the uranyl band around 927 $cm^{-1}$ is typically found for aqueous $UO_2^{2+}$-carboxylate complexes (Kakihana et al., 1987). Additionally the degree splitting between the $\nu_{as}$ and $\nu_s$ mode of the carboxylate group indicates a bidentate binding to the actinide cation (Kakihana et al., 1987).

In the uranyl L-phenylalanine mixture the $\nu_{as}$ mode of the free (959 $cm^{-1}$) and of the complexed (928 $cm^{-1}$) uranyl ion show nearly the same intensities. In contrast, in the uranyl 3-phenylpropionate complex the $\nu_{as}$ mode of the complexed uranyl ion (926 $cm^{-1}$) shows a considerably higher intensity compared to the band of the free uranyl ion (957 $cm^{-1}$). This is in accordance with the findings by TRLFS, that the 3-phenylpropionate is the stronger complexing agent for the $UO_2^{2+}$ cation.

In the FTIR spectrum of the uranyl L-phenylalanine complex system no bands can be assigned to a coordinating amino group. This underlines the conclusion made from TRLFS measurements, that the amino group is not involved in uranyl complexation under these experimental conditions, especially at acidic pH ranges. However, contributions from amino groups to the spectra might be hidden under the strong difference band of the water solvent above 1600 $cm^{-1}$ and therefore can not be ruled out entirely.

In addition to fluorescence emission and UV-Vis absorbance studies (Günther et al., 2007) FTIR spectroscopic investigations of the U(VI) / glycine system were carried out.

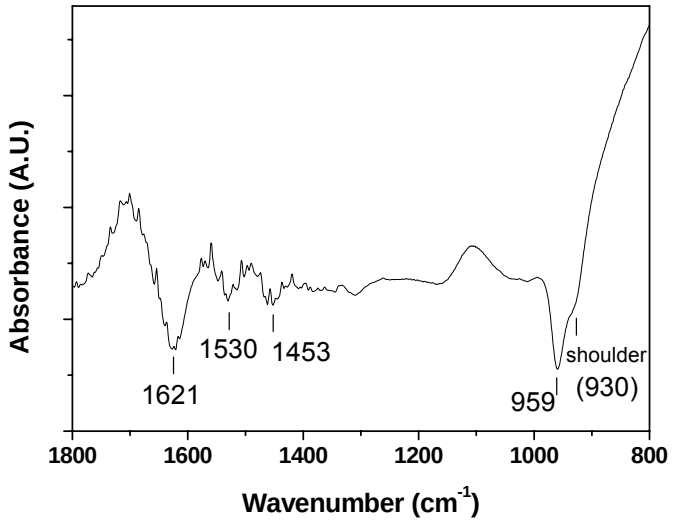


**Fig. 6.6:** FTIR difference spectra of U(VI) / glycine solution, initial solution contained 10 mM $UO_2^{2+}$ and 10 mM glycine at pH 3.2.

A spectrum of the U(VI)/glycine system is shown in Fig. 6.6. Again, the relative intensities of the uranyl bands at 959 and around 930 $cm^{-1}$ reflect the ratio of the $UO_2^{2+}{}_{aq.}/UO_2^{2+}$-ligand system. The detection of the shoulder indicates the formation of uranyl glycine species. The low intensity of the band of the $UO_2^{2+}$-glycine complex around 930 $cm^{-1}$ confirms the low complex formation constant and only a small amount of complex species in the solution at a uranyl to ligand concentration ratio of 1:1 as it was found by TRLFS measurements (Günther et al., 2007). Consequently the symmetric and antisymmetric stretching vibration of the carboxylate anion of 1453 and 1530 $cm^{-1}$ also show very low intensities (Fig. 6.6). In homology to the $UO_2^{2+}$-L-phenylalanine system no contributions of $NH_3^+$ or $NH_2$-groups can be identified in the spectra.

In conclusion, the complexation of uranyl with L-phenylalanine and 3-phenylpropionate was examined in acidic solution by TRLFS and FTIR spectroscopy to determine the influence of the amino function on the complexation. Both techniques showed very similar complex behavior of both ligands. The amino function seems not to be involved in the uranyl coordination, but it may rather destabilize the uranyl complex. The results of the investigated U(VI)/ glycine system using TRLFS, UV-Vis and FTIR spectroscopy supports the evidence that the uranyl cation is only bound on the carboxyl group of the amino acid in the acid pH range. To elucidate the impact of nitrogen functionalities on the metal ion complexation behavior of HA, further investigations with other model ligands, which represent alternative N-containing functional groups, should be done.

# 7 Uranium(VI) complexation by humic acid under neutral pH conditions

Thermodynamic complexation data for the interaction of U(VI) with HA have been determined applying different methods and complexation models (e.g., Shanbhag and Choppin, 1981; Czerwinski et al., 1994; Moulin and Moulin, 1995; Pompe et al., 2000b). These studies were predominantly performed under acidic pH conditions where competing reactions such as hydrolysis and carbonate complexation of the $UO_2^{2+}$ ion are negligible. However, this does not hold for the environmentally relevant pH range. Thus, the formation of ternary U(VI) complexes with HA has to be taken into account for any trustworthy geochemical modeling.

There are only few works investigating the formation of such ternary U(VI) complexes in the presence of HA. Zeh et al. (1997) studied the sorption of the $UO_2^{2+}$ ion onto humic colloids in Gorleben groundwater by ultrafiltration and anion exchange and fitted their data with a uranyl hydroxo humate complex $UO_2$(OH)HA(I). The solubility of $UO_2(OH)_2$ in presence and absence of HA was investigated by Pashalidis et al. (2006) resulting in complexation data for $UO_2$(OH)HA. Using the equilibrium dialysis-ligand exchange technique, Glaus et al. (1995) studied the formation of a mixed uranyl carbonato fulvate complex.

In order to improve the thermodynamic data base for the interaction of U(VI) with HA, we studied the complexation of U(VI) with HA at pH 7 in the absence of $CO_2$. These studies were performed in continuation of our previous work (Pompe et al., 2000a), however, the updated U(VI) complex formation constants compiled in Guillaumont et al. (2003) were used for calculation of the U(VI) speciation in solution. For the first time, two direct spectroscopic methods, the conventional time-resolved laser-induced fluorescence spectroscopy (TRLFS) and TRLFS with ultrafast pulses, were applied to study the formation of a ternary uranyl hydroxo humate complex (Sachs et al., 2006).

## 7.1 Experimental

### *Preparation of sample solutions*

U(VI) humate solutions were prepared from Aldrich HA (AHA). The experiments were performed under $N_2$ atmosphere, excluding $CO_2$. The HA concentration was kept constant at 2

mg/L and the U(VI) concentration was varied between $1 \cdot 10^{-7}$ and $1 \cdot 10^{-5}$ mol/L. The ionic strength was set to 0.1 M $NaClO_4$ and the pH values were adjusted to 7.01 ± 0.02.
Reference samples without HA (1: $8.6 \cdot 10^{-6}$ M U, pH 6.61; 2: $5.6 \cdot 10^{-6}$ M U(VI), pH 6.69) were prepared to characterize the fluorescence behavior of the aqueous U(VI) hydroxo species present in solution. These samples were measured under the same experimental conditions as the humate solutions. The total uranium concentration in each sample was checked by ICP-MS analyses (Elan 6000, Perkin Elmer) to account for container wall adsorption. A detailed description of the sample preparation is given in (Sachs et al., 2006).

***TRLFS measurements (U(VI) fluorescence)***

The U(VI) fluorescence in solution was measured with a time-resolving fluorescence spectrometer. For that a Nd:YAG laser (Spectron, Laser Systems, Rugby, UK) was used as light source. The fourth harmonic oscillation of the Nd:YAG laser (266 nm) with laser energies of about 500 µJ was applied to excite the U(VI) fluorescence. The emission signal was focused into a spectrograph (Acton Research, Acton, USA) by a fiber optic cable. The fluorescence spectra were measured with an intensified CCD camera system (ROPER-Scientific, Ottobrunn, Germany). Using the internal delay generator time-resolved spectra were recorded during a gate width of 2000 ns. The first time step started 30 ns after the excitation pulse. In 76 delay steps, the gate was then shifted to delay times of 30.03 µs (series 1) or 56.28 µs (series 2). At each delay time, five accumulations of a spectrum were collected over 95 laser shots per spectrum. Fluorescence spectra were recorded in the wavelength range between 446 and 618 nm at a resolution of 0.168 nm (for more details see Sachs et al., 2006).

***fs-TRLFS measurements (HA fluorescence)***

For the measurement of the HA fluorescence as a function of the U(VI) concentration, a femtosecond-laser-pulse-based TRLFS system was applied (Geipel et al., 2004). A Nd:$YVO_4$ laser seeded amplifier system (Spectra Physics, Mountain View, USA) used as light source. The excitation of the HA fluorescence was generated by the third harmonic of the Nd:$YVO_4$ laser (266 nm) with laser energies of about 200 µJ. The emitted fluorescence was focused into a spectrograph (Acton Research, 300i, Acton, USA) and collected by an intensified CCD camera system (PICOSTAR, LaVision Inc., Göttingen, Germany). Applying a delay generator, time-resolved fluorescence spectra were recorded at delay times between 0 and 9 ns after ap-

plication of the laser pulse, with time steps of 50 ps. The gate width for detection was set to 0.5 ns. Spectra were measured in the wavelength range between 330 and 524 nm at a resolution of 0.283 nm (for more details see Sachs et al., 2006).

## 7.2 Complexation model for neutral pH conditions

The U(VI) species distribution at pH 7 in absence of HA ($1 \cdot 10^{-7}$ – $1 \cdot 10^{-5}$ M U(VI), 0.1 M $NaClO_4$, no $CO_2$) was calculated with the code EQ3/6 (Wolery, 1992) based on the latest revision of the U(VI) complex formation constants (Guillaumont et al., 2003). Under the considered conditions, U(VI) occurs in form of various hydroxo species, mainly $(UO_2)_3(OH)_5^+$, $(UO_2)_4(OH)_7^+$, $UO_2OH^+$, and $UO_2(OH)_2(aq)$, with $(UO_2)_3(OH)_5^+$ dominating for U(VI) concentrations above 0.4 µmol/L (Fig. 7.1). In principle, HA can react with all the positively charged hydroxo species, whereas the neutral species $UO_2(OH)_2(aq)$ has a very low affinity to the negatively charged binding sites of HA at pH 7. Therefore, the presence of the different hydroxo species has to be taken into account in the spectra analyses and evaluation of the experimental data.

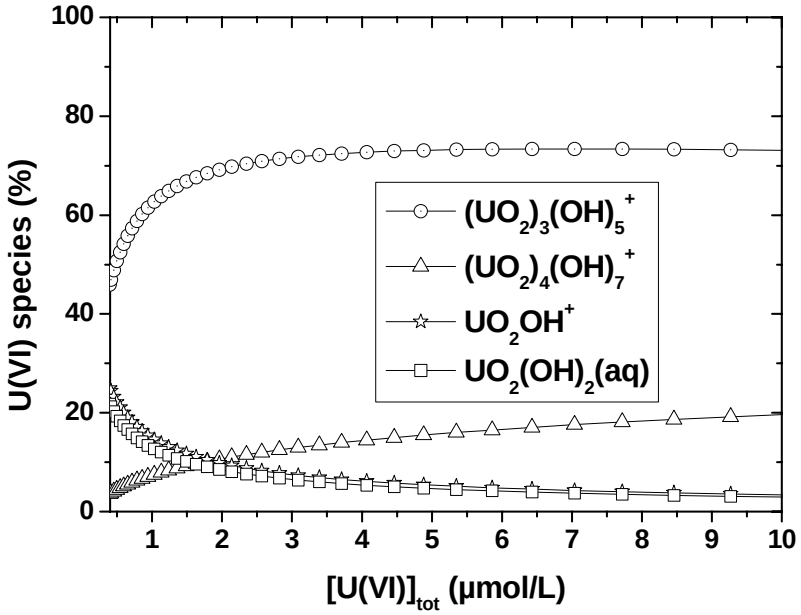


**Fig. 7.1:** U(VI) species distribution at pH 7 in absence of $CO_2$ and HA (I: 0.1 M $NaClO_4$). Species with a maximum concentration below 4% of the respective total U(VI) concentration are neglected.

Data analysis was based on the chemical model that $UO_2OH^+$ reacts with HA(I) as ligand forming a ternary uranyl mono hydroxo humate complex $UO_2(OH)HA(I)$ as shown in Eq. (7.1). HA(I) means that one proton exchanging functional group of the HA is taking part in the reaction.

$$UO_2OH^+ + HA(I)^- \rightleftarrows UO_2(OH)HA(I) \tag{7.1}$$

Other possible chemical models involving $(UO_2)_3(OH)_5^+$ or $(UO_2)_4(OH)_7^+$ could be ruled out. The stability constant is described by Eq. (7.2), with square brackets denoting concentrations of the respective species:

$$K = \frac{[UO_2(OH)HA(I)]}{[UO_2OH^+]_{free} \cdot [HA(I)]_{free}} \tag{7.2}$$

The free HA concentration in solution $[HA(I)]_{free}$ was determined based on two different models. Model A assumed that all proton exchanging functional groups of the HA are available for U(VI) complexation (subsequently identified by $[HA(I)]_{tot}$ = 100%; cf. Eq. (7.3)). In model B, $[HA(I)]_{free}$ was estimated according to the metal ion charge neutralization model (CNM, cf. Eq. (7.4); Kim and Czerwinski, 1996). CNM introduces the loading capacity (LC, Eq. (7.5)). There, $[UO_2(OH)HA(I)]_{max}$ is the maximum concentration of U(VI) mono hydroxo humate that can be formed under the same conditions.

A) $[HA(I)]_{tot}$ = 100%: $$[HA(I)]_{free} = [HA(I)]_{tot} - [UO_2(OH)HA(I)] \tag{7.3}$$

B) CNM: $$[HA(I)]_{free} = [HA(I)]_{tot} \cdot LC - [UO_2(OH)HA(I)] \tag{7.4}$$

$$LC = \frac{[UO_2(OH)HA(I)]_{max}}{[HA(I)]_{tot}} \tag{7.5}$$

In both models, $[HA(I)]_{tot}$ was determined according to Eq. (7.6) (Kim and Czerwinski, 1996).

$$[HA(I)]_{tot} = \frac{[HA] \cdot PEC}{z} \tag{7.6}$$

[HA] stands for the weight concentration of HA in g/L, PEC for the proton exchange capacity of HA in meq/g, and z for the nominal charge of the complexing metal ion, which is one in case of $UO_2OH^+$.

## 7.3 Results and discussion

### 7.3.1 Results of TRLFS measurements

***U(VI) fluorescence in absence of humic acid***

From the analysis of the fluorescence decay behavior of the reference samples (following Brendler et al., 1997), two decay constants (lifetimes) of $\tau_1 = 4.2 \pm 0.4$ µs and $\tau_2 = 19.8 \pm 1.8$ µs were obtained, pointing to at least two distinct fluorescent species. For the long-living fluorescence species a single emission spectrum was derived with peak maxima at 484, 498, 514, 534, 557, and 583 nm. Comparing lifetime and peak maxima of this species with those obtained for further reference samples containing various U(VI) hydroxo species (Brendler and Sachs, 2006) the long-living fluorescence species can be ascribed to the $(UO_2)_3(OH)_5^+$ complex which dominates the U(VI) speciation in the reference system. This assignment is supported by literature data of Moulin et al. (1998), who reported a fluorescence lifetime of 23 ± 3 µs and peak maxima at 479, 496, 514, 535, 556, and 584 nm for the $(UO_2)_3(OH)_5^+$ complex. The species with the shorter lifetime is assigned to $(UO_2)_4(OH)_7^+$ (Brendler and Sachs, 2006), the second largest contributor to the U(VI) speciation at pH 7. For more details see (Sachs et al., 2006)

***U(VI) fluorescence in presence of humic acid***

TRLFS spectra were measured at constant HA and varied U(VI) concentration. An example for a time-resolved fluorescence spectrum is shown in Fig. 7.2.

By analysis of the fluorescence decay behavior of the samples it was found that the fluorescence spectra of the uranyl humate solutions are clearly dominated by the HA-non-complexed $(UO_2)_3(OH)_5^+$ species. The proposed ternary U(VI) humate complex formed in solution obviously does not contribute to the fluorescence signal during the time window of the measurements. Therefore, the first step in data processing was to calculate $[(UO_2)_3(OH)_5^+]_{free}$ for each sample as described in (Sachs et al., 2006). In a second step, the corresponding concentrations

of free $UO_2OH^+$ ($[UO_2OH^+]_{free}$) and the total HA-uncomplexed U(VI) concentration ($[U(VI)]_{non\text{-}HA}$) were computed for each sample, assuming equilibrium conditions in solution and using the geochemical speciation code EQ3/6. In a third step, $[UO_2(OH)HA(I)]$ was determined according to Eq. (7.8).

$$[UO_2(OH)HA(I)] = [U(VI)]_{tot} - [U(VI)]_{non-HA} \tag{7.8}$$

Finally, $[HA(I)]_{free}$ followed directly from Eq. (7.3) or Eqs. (7.4) and (7.5), and $\log K$ was calculated based on Eq. (7.2).

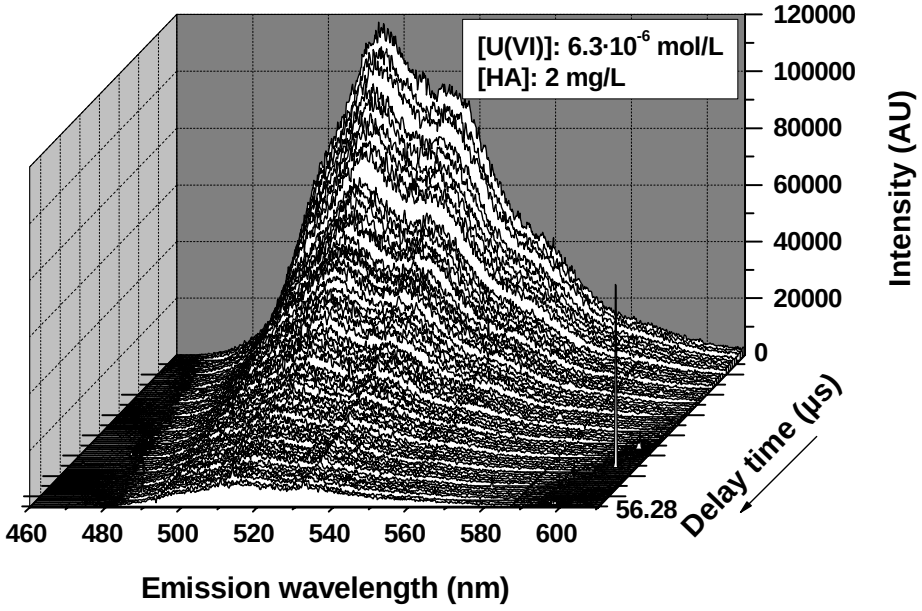


**Fig. 7.2:** Time-resolved fluorescence spectrum of a uranyl humate solution ([U(VI)]: $6.3 \cdot 10^{-6}$ mol/L, [HA]: 2 mg/L, pH 7, I: 0.1 M $NaClO_4$).

The complexation data resulting from the TRLFS measurements of series 1 and 2 as well as their weighted averages are summarized in Tab. 7.1. The two different definitions of $[HA(I)]_{free}$ give complexation constants that agree within their experimental errors for both series. In model B, applying the CNM, a LC value of 0.76 ± 0.28 was obtained. It indicates that at pH 7 about 80% of the HA proton exchanging sites are accessible for complexation of $UO_2OH^+$, which is quite close to the 100% assumed in model A. All other data processing steps are identical for both models. Thus, as expected, the $\log K$ values obtained by CNM are slightly higher than the ones for model A.

### 7.3.2 Results of fs-TRLFS measurements

Time-resolved fluorescence spectra of AHA were measured at varying U(VI) and constant HA concentration. Figure 7.3 shows a time-resolved fluorescence spectrum of AHA.

In all studied samples, AHA shows a comparable fluorescence decay behavior. It was best modeled by a bi-exponential decay function yielding two fluorescence decay times: $\tau_1 = 0.56 \pm 0.16$ ns and $\tau_2 = 2.52 \pm 0.30$ ns. These two lifetimes indicate the existence of a short and a long-living fluorescence species contributing to the HA fluorescence. The obtained lifetimes have the same order of magnitude as those reported by Kumke et al. (1998, 1999) for aqueous solutions of fulvic acid and natural organic matter. There, the authors reported further the occurrence of a third fluorescence contribution with a longer fluorescence lifetime $\tau_3$ in the range from 11 to 24 ns. Our evaluation of the fluorescence decays of the AHA samples with a three-exponential decay yielded unacceptable strongly varying lifetimes with large errors, most likely due to the limited overall measurement duration of only 9 ns. An assignment of the two fluorescence lifetimes to distinct HA species or structural components of HA is not possible at the moment.

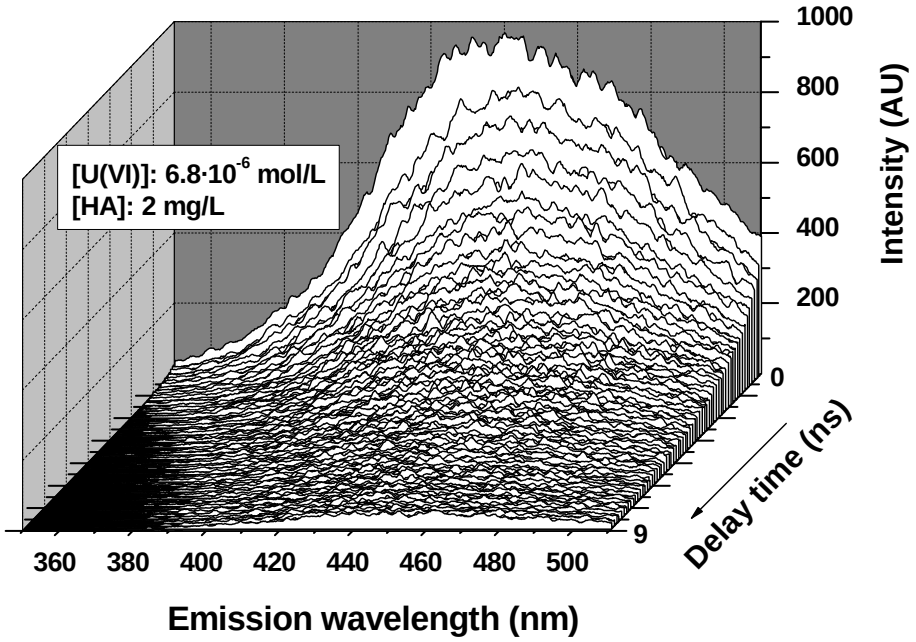


**Fig. 7.3:** Fs-time-resolved fluorescence spectrum of a uranyl humate solution ([U(VI)]: $6.8 \cdot 10^{-6}$ mol/L, [HA]: 2 mg/L, pH 7, I: 0.1 M $NaClO_4$).

The observed fluorescence intensities decrease with increasing U(VI) concentration. This static fluorescence quenching results from the uranium binding by the HA, which was already

observed in synchronous fluorescence spectroscopic studies with fulvic acid in presence of $UO_2^{2+}$ (Shin et al., 2001). From this quenching the amount of non-complexed HA in the U(VI) humate solutions could be derived as described in (Sachs et al., 2006).

The fs-TRLFS data were evaluated assuming that all proton exchanging functional groups of the HA contribute to the complex formation (cf. Model A: $[HA(I)]_{tot}$ = 100%). A direct evaluation of the fs-TRLFS data based on the CNM is not possible. Knowing the free and the total HA concentrations in solution, the difference gives the concentrations of $UO_2(OH)HA(I)$. Using Eq. (7.8), the total non-HA-complexed U(VI) concentrations $[U(VI)]_{non\text{-}HA}$ were calculated. Supposing chemical equilibrium in solution, the respective concentrations of uncomplexed $UO_2OH^+$ were then computed from $[U(VI)]_{non\text{-}HA}$ using EQ3/6.

Assuming $(UO_2)_3(OH)_5^+$ or $(UO_2)_4(OH)_7^+$ as reaction partner for HA would result in negative concentrations for non-HA-complexed U(VI), hence both can be excluded from further considerations. Finally, based on Eq. (7.2), the complexation constant was determined (Tab. 7.1).

**Tab. 7.1.** Parameters for the U(VI) complexation by Aldrich HA at pH 7 (I: 0.1 M $NaClO_4$).

| Model | $[HA(I)]_{tot}$ = 100% | Metal Ion Charge Neutralization Model | |
|---|---|---|---|
| | log*K* [a] | LC [a] | log*K* [a] |
| | **TRLFS measurements** | | |
| **Series 1** | 6.69 ± 0.52 | 0.77 ± 0.36 | 7.14 ± 0.22 |
| **Series 2** | 6.47 ± 0.18 | 0.74 ± 0.40 | 6.76 ± 0.04 |
| ***Weighted Average*** | *6.58 ± 0.24* | *0.76 ± 0.28* | *6.95 ± 0.10* |
| | **fs-TRLFS measurements** | | |
| | 6.33 ± 0.20 | n.a. [b] | n.a. [b] |

[a] ± 2σ. [b] n.a.: not applicable.

## 7.4 Discussion

Table 7.1 summarizes all parameters for the U(VI) complexation by AHA that were independently obtained by direct measurements of the U(VI) and HA speciation by TRLFS and fs-TRLFS, respectively. Based on the assumption that all HA functional groups contribute to the U(VI) complexation ($[HA(I)]_{tot}$ = 100%), TRLFS and fs-TRLFS yield log*K* values that are comparable within their experimental errors. The agreement of the results of these two independent methods allows us to conclude that a U(VI) mono hydroxo humate complex is formed in the neutral pH range. Furthermore, the obtained data agree also with that from $UO_2(OH)_2$ solubility studies in presence of HA (Pashalidis, 2006), where a complex stability

constant of 6.8 is reported for the formation of $UO_2(OH)HA$ starting from $UO_2OH^+$ (Eq. (7.1)).

Considering the first hydrolysis of $UO_2^{2+}$, the autoprotolysis of water (Cox, 1989) and the HA complexation by $UO_2OH^+$, an overall complex stability constant $\log\beta_{0.1M}$ of 14.89 ± 0.54 was calculated for the complexation process:

$$UO_2^{2+} + OH^- + HA(I)^- \rightleftarrows UO_2(OH)HA(I) \qquad (7.9).$$

This value is in very good agreement with $\log\beta_{0.1M}$ values of 14.7 ± 0.5 and 15.2 that were derived by Zeh et al. (1997) and Pashalidis et al. (2006), respectively, for the formation of $UO_2(OH)HA(I)$.

Comparing the data of $UO_2(OH)HA(I)$ with those of the binary complex $UO_2HA(II)$ (e.g., Aldrich HA $\log\beta_{0.1M}$ = 6.20 ± 0.56, evaluated based on the CNM (Pompe et al., 2000b) it becomes obvious that they are in the same order of magnitude. The complexation constant for $UO_2(OH)HA(I)$ determined based on the CNM in this work is about 0.8 log units higher than that of $UO_2HA(II)$ indicating a slightly stronger HA complexation by $UO_2OH^+$ than by $UO_2^{2+}$.

The formation of mixed actinide hydroxo humate complexes in the neutral pH range was also investigated for Am(III) and Cm(III) (Panak et al., 1996; Morgenstern et al., 2000). The formation of $An(OH)HA(II)$ and $An(OH)_2HA(I)$ complexes (An: $Cm^{3+}$and $Am^{3+}$) with Gorleben HA was reported in (Morgenstern et al., 2000) with stability constants evaluated to be $\log\beta_{111}$ = 12.82 ± 0.11 and $\log\beta_{121}$ = 17.53 ± 0.13 for Cm(III) and $\log\beta_{111}$ = 12.71 ± 0.17 and $\log\beta_{121}$ = 17.40 ± 0.21 for Am(III) in 0.1 M $NaClO_4$. Based on these overall stability constants, the first hydrolysis constants for Cm(III) (Wimmer et al., 1992) and Am(III) (Silva et al., 1995) as well as the autoprotolysis constant of water, the individual stability constants for the reaction of $CmOH^{2+}$ and $AmOH^{2+}$ with HA (cf. Eq. (7.10)) were recalculated and compared to that obtained for $UO_2OH^+$ in the present work.

$$AnOH^{2+} + HA(II)^{2-} \rightleftarrows An(OH)HA(II) \quad \text{with An: } Cm^{3+}, Am^{3+} \qquad (7.10)$$

The resulting stability constants amount to 6.37 and 5.78 for Cm(OH)HA(II) and Am(OH)HA(II), respectively. The data of Cm(III) and U(VI) agree very well. In contrast to that, $AmOH^{2+}$ shows a slightly lower tendency for HA complex formation. This dissimilarity

in the Am(III) and Cm(III) complexation behavior may point to limitations of oxidation state analogues often used for trivalent actinides and lanthanides.

Above pH 8, Cm(III) and Am(III) form dihydroxo humate complexes ($An(OH)_2HA(I)$) by a charge neutralization process (Panak et al., 1996; Morgenstern et al., 2000). The formation of a comparable U(VI) complex is unlikely because of its lower charge and its tendency to form polynuclear hydroxo species at higher pH values.

To assess the impact of the binary and ternary U(VI) humate complex on the U(VI) speciation, the U(VI) distribution in the presence of HA was calculated for two U(VI) concentrations as a function of pH (Fig. 7.4). The calculations were performed based on U(VI) complex formation constants (Guillaumont et al., 2003), literature data for $UO_2HA(II)$ (Pompe et al., 2000a and 2000b; Montavon et al., 2000) and the data for $UO_2(OH)HA(I)$ from this work using the modified geochemcial speciation code EQ3/6 with integrated CNM (Sachs et al., 2004). At a U(VI) concentration of $1 \cdot 10^{-6}$ M in absence of $CO_2$, the U(VI) speciation is dominated by $UO_2HA(II)$ and $UO_2(OH)HA(I)$ between pH 4 and 8. $UO_2HA(II)$ exists in the acidic pH range between pH 3 and 6 with a maximum concentration around pH 4. Above pH 4.5 the U(VI) speciation is dominated by $UO_2(OH)HA(I)$, which occurs nearly quantitative in the pH range from 6.0 to 7.5, that is relevant for natural waters. This species distribution can significantly influence the mobility of U(VI). From U(VI) migration experiments in a laboratory quartz sand system, it is known that humic colloid-borne U(VI) is transported through the system and mobilized compared to U(VI) in a HA-free system (Mibus et al., 2007). The increase of the U(VI) concentration from $1 \cdot 10^{-6}$ to $1 \cdot 10^{-5}$ M at constant HA concentration causes a change in the species distribution. The hydrolysis of U(VI) and the formation of polynuclear U(VI) hydroxo species becomes more important. Nevertheless, in the pH region from about 6 to 8 the ternary $UO_2(OH)HA(I)$ complex is still dominating. An increase in the HA concentration promotes the formation of U(VI) humate complexes and consequently, a suppression of the U(VI) hydrolysis. It can be concluded that in the presence of HA the formation of the ternary $UO_2(OH)HA(I)$ complex significantly influences the U(VI) speciation under environmental conditions. Due to this the mobility of U(VI) can be enhanced.

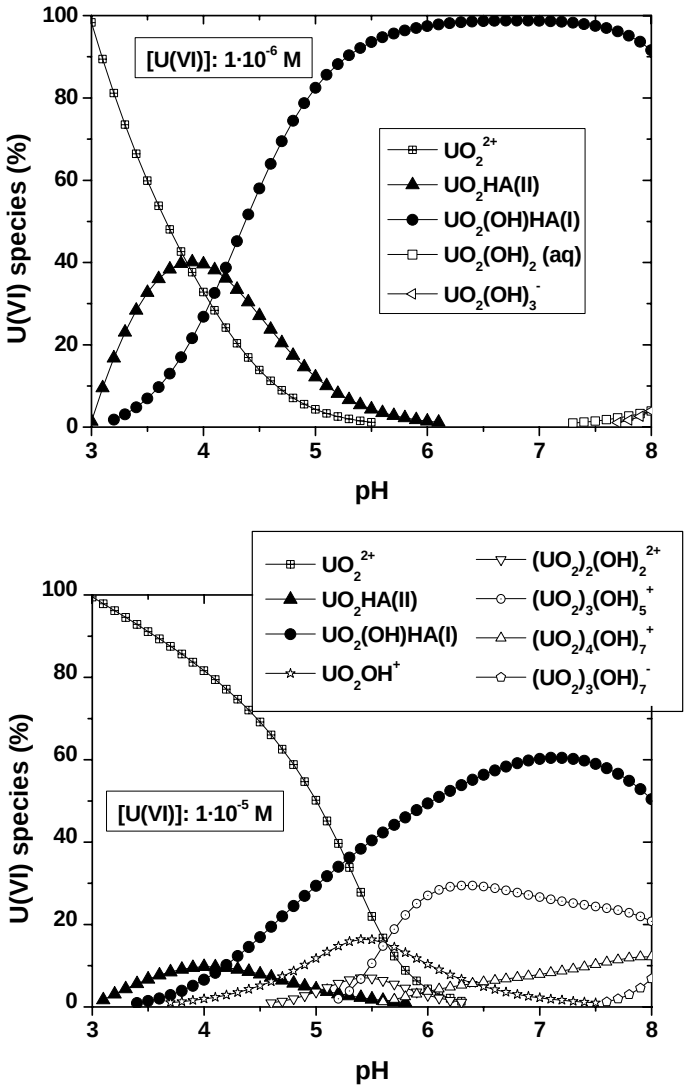


**Fig. 7.4:** Speciation of U(VI) in presence of HA as a function of the pH calculated with EQ3/6 ([U(VI)]: $1 \cdot 10^{-6}$ and $1 \cdot 10^{-5}$ mol/L, [HA]: 2 mg/L, I: 0.1 M $NaClO_4$, 0% $CO_2$). Data points below 1% are not plotted.

# 8 Update of the database for humics complexation

Within the previous project a digital "Database for Humics Complexation – DHC" was developed covering so far published HA complexation data based on the metal ion charge neutralization model (Kim and Czerwinski, 1996) including the reported experimental conditions and data processing details (Sachs et al., 2004). This database provides an overview concerning investigated HA types, ligands, and parameter ranges (e.g., concentration of reaction

partners, ionic strength, pH, …). In addition, it offers an extensive bibliography. Every stored data item is linked to both original citations and secondary literature references.
In the present project the database was updated. Data of ternary actinide hydroxo humate complexes from this study (see chapter 7) as well as from literature were added. In addition, actually complexation data generated based on the metal ion charge neutralization at the Institute of Interdisciplinary Isotope Research Leipzig were amended.
As of December 2006, the DHC database covers 12 different types of HA, contains 20 data records for proton exchange capacities and 92 complex formation constants with LC values.

# 9 Neptunium(V) reduction by various natural and synthetic humic substances

The migration behavior of actinide contaminants in natural aquatic systems can be effected by humic substances due to their strong complexing and redox properties and their ability for colloid formation. Therefore, risk assessments, predicting the fate and transport of actinides in the environment, require basic knowledge of the interaction of humic substances with metal ions. The complexation of Np(V) by humic substances has been studied in a number of publications (e.g., Marquardt, et al., 1996; Marquardt and Kim, 1998; Seibert et al., 2001; Sachs et al., 2005a). In a study of Np(IV) complexation by fulvic acid at pH 1 and 1.5, first values for conditional complexation constants were estimated (Marquardt et al., 2000). The redox behavior of humic substances of different origin towards Np and Pu in higher oxidation states (mostly hexa- or pentavalent) was reported in (André and Choppin, 2000; Artinger et al., 2000; Chen et al., 1993; Choppin, 1988; Marquardt et al., 1999 and 2004; Nash et al., 1981; Tan et al., 1993; Zeh et al., 1999).
Due to reduction of Np(V) to Np(IV), the migration behavior of the actinide changes strongly. Compared to Np(V), which shows a relatively weak interaction with HA, Np(IV) is generally stronger complexed by HA (Artinger et al., 2000). The humic colloid-borne Np(IV) species is known to remain stable in groundwater and to be easily mobile in porous aquifer systems (Artinger et al., 2000; Zeh et al., 1999).
Recently, synthetic HA with distinct redox properties were synthesized by oxidation of diphenolic compounds in the presence of amino acids in alkaline solution by Sachs et al. (2004). The most promising synthetic HA were the HA type Cat-Gly, which is an oxidation product of catechol and glycine, and the HA type Hyd-Glu, which is an oxidation product of

hydroquinone and glutamic acid. These synthetic HA have shown significantly higher Fe(III) redox capacities (Sachs et al., 2004) and also higher U(VI) redox capacities than the natural Aldrich HA (Sachs et al., 2005b).

In this work, the stability of Np(V) in contact with various natural and synthetic aqueous humic substances was studied under anaerobic conditions between pH 3.5 and pH 9. For Np speciation in solution liquid-liquid extraction, NIR absorption spectroscopy and ultrafiltration were applied.

## 9.1 Experimental

### *Humic substances*

Two natural humic substances and three synthetic HA were used in this study: The natural Kranichsee fulvic acid (KFA) was isolated from surface water of the mountain bog 'Kleiner Kranichsee' (Saxony, Germany) (Schmeide et al., 1998). The commercial Aldrich HA (AHA, charge A2/98) was purified before use (see chapter 3). The synthetic products were the HA type Cat-Gly (charge R1/03) and type Hyd-Glu (charge R13/02), as well as the HA with blocked phenolic/acidic OH groups type Hyd-Glu-PB (charge R20/02). Details to synthesis and characterization of the synthetic HA are given in (Sachs et al., 2004). The functional group contents of the humic substances are compiled in Tab. 9.1.

**Tab. 9.1:** Functional group contents of humic substances.

| Humic substance | COOH [a] (meq/g) | Phenolic/acidic OH [b] (meq/g) |
|---|---|---|
| Cat-Gly (batch R1/03) | 4.39 ± 0.13 | 6.6 ± 0.9 |
| Hyd-Glu (batch R13/02) | 3.65 ± 0.14 | 5.8 ± 0.2 |
| Hyd-Glu-PB (batch R20/02) | 2.67 ± 0.03 | 1.4 ± 0.1 |
| KFA | 6.05 ± 0.31 | 4.8 ± 0.7 |
| AHA (batch A2/98) | 4.49 ± 0.14 | 3.1 ± 0.1 |

[a] Determined by calcium acetate exchange (Schnitzer and Khan, 1972). [b] Radiometrically determined (Bubner and Heise, 1994).

### *Sample preparation*

The Np(V) stock solution was obtained by dissolving solid $^{237}NpO_2NO_3$ in 0.1 M $HNO_3$. The pentavalent oxidation state of Np in the stock solution was verified by NIR absorption spec-

troscopy and liquid-liquid extraction. Prior to the preparation of the various humic substance stock solutions, the humic material (50 mg each) was suspended in about 4 mL 0.1 M $NaClO_4$ and degassed under vacuum. The Np(V) humate samples were prepared in a glove box under nitrogen atmosphere using carbonate-free solutions. The initial Np(V) and humic substance concentration was $1 \cdot 10^{-4}$ M and 100 mg/L, respectively. The ionic strength of the solutions was 0.1 M $NaClO_4$. The pH value of the samples (pH 3.5, 5, 7, 9) was adjusted applying diluted NaOH and $HClO_4$ solutions, no buffers were added. During the experiment, the pH value of the solutions was checked and readjusted repeatedly. Blanks without Np were prepared from each humic substance at pH 3.5 to pH 9. All samples were stored in the dark to minimize degradation of the organic material.

***Methods for Np speciation***

The Np(V) reduction was determined by monitoring the Np(V) and Np(IV) concentrations in solution over time. For this, samples were taken after different time intervals and characterized by the redox speciation methods described in the following.

*Liquid-liquid extraction*

The separation of Np(V) and Np(IV) was performed by liquid-liquid extraction using 2-thenoyltrifluoroacetone (TTA) as complexing agent (Bertrand and Choppin, 1982). For this, 1.5 mL of the Np(V,IV) sample solution (pH 1) were shaken vigorously with 2 mL of 0.5 M TTA solution in xylene for 15 min. Under these conditions, Np(IV) is extracted into the organic phase, while Np(V) remains in the aqueous phase. After centrifugation, the Np content in the aqueous and organic phase was determined by liquid scintillation counting (Wallac system 1414, Perkin Elmer) using $\alpha$-$\beta$ discrimination. For this, 200 µL aliquots were mixed with 15 mL of a Ultima Gold$^{TM}$ scintillation cocktail (Packard BioScience Company).

*NIR absorption spectroscopy*

NIR absorption spectroscopy (CARY-5G, Varian) was applied for the direct spectroscopic detection of Np species in the sample solutions. Quartz cuvettes (Hellma) with 1 cm pathlength were used and thermostated at 20°C. The sample solutions were measured directly, without any further preparations, in the spectral range from 920 nm to 1050 nm. For quantitative determination of uncomplexed $Np^{4+}$ and $NpO_2^+$ aquo ions, the absorption bands at 960 nm and 980.4 nm with molar absorption coefficients of 162 L $mol^{-1}$ $cm^{-1}$ (Keller, 1971) and

395 ± 5 L $mol^{-1}$ $cm^{-1}$ (Marquardt et al., 1998), respectively, were used. For Np(IV) and Np(V) humate complexes, the absorption bands at 967.5 nm and 990 nm with molar absorption coefficients of 63 ± 8 L $mol^{-1}$ $cm^{-1}$ (Marquardt et al., 2000) and 230 ± 8 L $mol^{-1}$ $cm^{-1}$ (Marquardt et al., 1998), respectively, were used.

*Ultrafiltration*

For ultrafiltration experiments, MicroSep™ centrifugal concentrators (PallGelman Laboratory) of different pore sizes were used: 1 kDa, 10 kDa, 30 kDa, 100 kDa, 300 kDa, 1000 kDa.

## 9.2 Results and discussion

In Fig. 9.1, the Np(V) speciation in the starting solutions is shown for the experimental conditions applied in this study. It was calculated with the geochemical computer code EQ3/6 (Wolery, 1992) applying the Np(V) hydrolysis constants compiled in the NEA data base (Guillaumont et al., 2003), the Np(V) humate complexation constant $\log\beta = 3.6$ and the pH function of the loading capacity (LC) with LC = -0.589 + 0.101 · pH (Sachs et al., 2004). The results show that the free neptunyl ion predominates the Np speciation in aqueous solution. The $NpO_2HA(I)$ species is formed increasingly in solution between pH 6 and pH 10. For the pH region higher than 9, the formation of the mixed complex $(NpO_2(OH)HA)_{coll.}$ is suggested by Marquardt et al. (1998). However, presently, this complex cannot be quantified thermodynamically. The formation of the neptunyl hydroxyl species $NpO_2OH_{(aq)}$ can be neglected in the considered pH range.

In contrast to Np(V), Np(IV) has a strong tendency to hydrolyze. In the absence of complexing ligands, at an Np(IV) concentration of $1 \cdot 10^{-4}$ M, amorphous $NpO_2$ can precipitate at pH values higher than pH 3.3. In the presence of complexing ligands such as humic substances, a strong complexation of Np(IV) already at low pH values is observed. The formation of mixed hydroxo fulvate complex species ($Np(OH)_2FA(II)$ and Np(OH)FA(III)) at pH 1 and 1.5 was proposed by Marquardt et al. (2000). Thus, it is assumed that the Np(IV) which is produced in the course of our reduction experiments occurs mainly as mixed Np(IV) hydroxo fulvate/humate complex species.

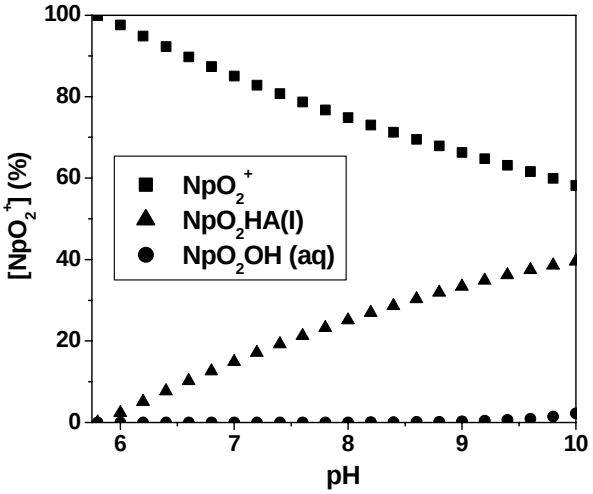


**Fig. 9.1:** Np(V) speciation at start of equilibration of the Np humic substance solutions. ($[NpO_2^+]$: $1 \cdot 10^{-4}$ M; [HA]: 100 mg/L; I: 0.1 M $NaClO_4$; $N_2$ atmosphere).

The reduction of Np(V), determined by TTA extraction, is shown in Figs. 9.2 and 9.3 as plot of the ratio of pentavalent Np to total Np versus equilibration time. It is obvious, that the Np(V) reduction is dependent on equilibration time, on the type of humic substances as well as on pH value of the sample solutions. In the initial phase of the equilibration of the Np humic substance solutions, the formation of Np(IV) is fast. With increasing equilibration time the rate of Np(IV) formation slows down. The synthetic HA type Cat-Gly and Hyd-Glu show a stronger Np(V) reduction in comparison to the natural humic substances AHA and KFA.

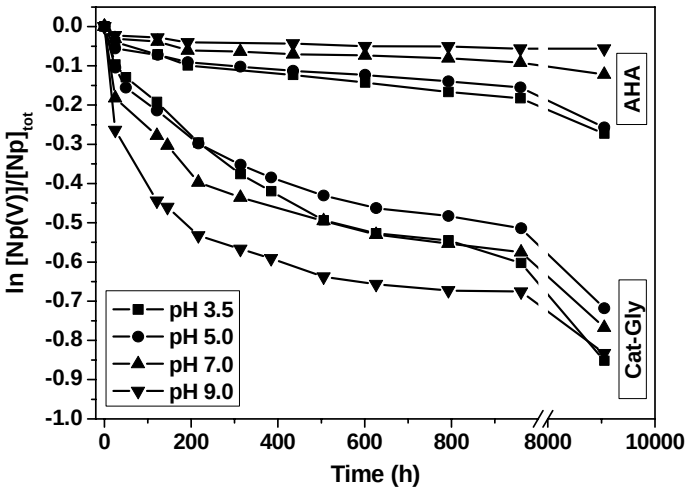


**Fig. 9.2:** Reduction of Np(V) to Np(IV) by HA type Cat-Gly and AHA between pH 3.5 to pH 9.0. Determination of Np(V) by TTA extraction.

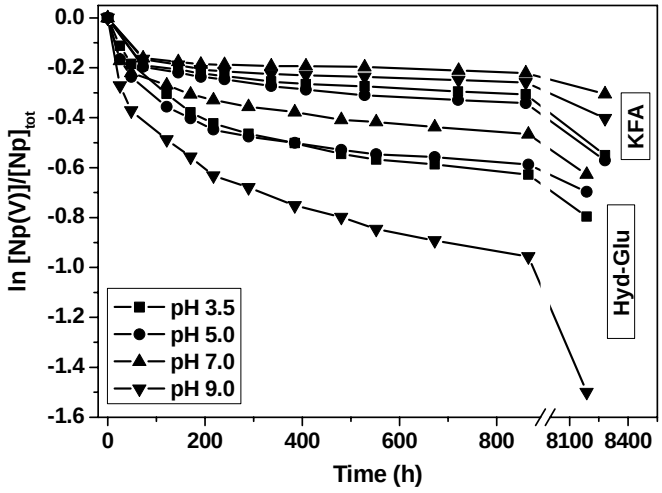


**Fig. 9.3:** Reduction of Np(V) to Np(IV) by HA type Hyd-Glu and KFA between pH 3.5 to pH 9.0. Determination of Np(V) by TTA extraction.

The strongest Np(V) reduction is found for the HA type Hyd-Glu at pH 9. After 865 h (36 d) 62% of the Np(V) is converted to Np(IV). Also in case of HA type Cat-Gly, the strongest Np(V) reduction is found at pH 9 (961 h (40 d), 49% Np(IV)). The pH dependency determined for the Np(V) reduction by AHA correlates with that found by Marquardt et al. (1996) for the same HA. Generally, however, no trend is observable for the pH dependency of the Np(V) reduction for the various humic substances. The samples taken about one year after starting the experiments (between 8200 h to 9050 h after start) show that Np(IV) is formed continually but with a comparatively slow rate.

The redox capacity, which decreases in the sequence synthetic HA > KFA > AHA, can be correlated to the phenolic/acidic OH group contents of the humic substances (cf. Tab. 9.1). A comparable correlation between the phenolic/acidic OH group content of various synthetic and natural HA and their Fe(III) and U(VI) redox capacities was observed in (Sachs et al., 2004 and 2005b).

Contrary to the partial reduction of Np(V) under the experimental conditions applied in this work, a nearly complete reduction of Np(V) was found in experiments applying the same Np concentration but the fourfold HA concentration (400 mg/L HA type Cat-Gly). After 1000 h only 4% Np(V) were detected.

As already mentioned, by liquid-liquid extraction with TTA as complexing agent, Np(IV) is extracted into the organic phase, while Np(V) remains in the aqueous phase. However, in case of the humic substance solutions studied here, the Np(IV) could not be extracted

quantitatively into the organic phase but partly remained bound in the humic substance precipitate. Exemplary this is shown for HA type Hyd-Glu in Fig. 9.4. With increasing equilibration time, the amount of Np(V) determined in the aqueous phase decreases but the amount of Np(IV) determined in the organic phase does not increase to the same extent. This results in a decreasing Np recovery during TTA extraction. The part of Np that cannot be extracted represents a fraction of tetravalent Np which is strongly bound to the HA and which is not released from the HA even at pH 1. Np(V), however, would decomplex from the HA under these pH conditions and remain in aqueous solution as $NpO_2^+$ ion. This effect was even more pronounced in experiments applying the fourfold HA concentration (not shown here) which confirms again the strong complexation of Np(IV) by HA. Too low activity recoveries were also reported for liquid-liquid extraction of Pu species (Artinger at al., 2004).

To verify that no Np(IV) had precipitated during the reduction reaction the total Np content was also checked. Figure 9.4 shows, that the total amount of Np in the sample solutions remains constant in the course of the experiments. This also means, that the Np adsorption onto the vial walls is negligible, even at pH 9.0.

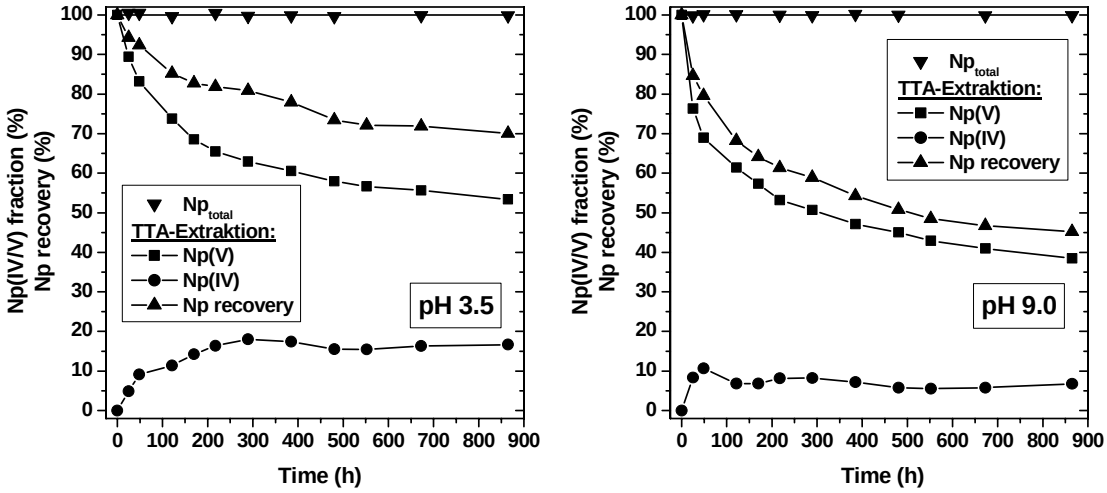


**Fig. 9.4:** Recovery of Np during TTA extractions in comparison to the total Np content for HA type Hyd-Glu equilibrated at pH 3.5 and pH 9.0.

To study influence of phenolic/acidic OH groups on the redox behavior of humic substances further, the synthetic HA with blocked phenolic/acidic OH groups of type Hyd-Glu-PB was equilibrated with Np(V) under the same experimental conditions as described above. Due to methylation with diazomethane (Pompe et al., 2000a; Schmeide et al., 2003), the phenolic/acidic OH group content of HA type Hyd-Glu-PB is 76% lower than that of HA type Hyd-Glu (cf. Tab. 9.1), which was used as starting material. The carboxylic group content of HA

type Hyd-Glu-PB is also somewhat lower than that of HA type Hyd-Glu. Possible reasons are a partial decomposition of HA molecules in acid-soluble components and/or leaching of smaller HA molecules with a higher carboxylic group content from the HA mixture (Pompe at al., 2000a) or an incomplete hydrolysis of the methyl ester groups that were previously formed during methylation with diazomethane. Nevertheless, Tab. 9.1 shows that the molar ratio of phenolic OH to carboxylic groups becomes significantly smaller due to the modification process.

The amount of Np(IV) formed by the modified HA with blocked phenolic/acidic OH groups type Hyd-Glu-PB is very small compared to the strong Np reduction by the unmodified HA type Hyd-Glu (Fig. 9.5). After 865 h (36 d) the amount of Np(IV) formed by HA type Hyd-Glu-PB is about 55% lower than the amount of Np(IV) formed by HA type Hyd-Glu (pH 9). This again shows that the phenolic/acidic OH groups play a major role for the redox behavior of humic substances. The slight Np reduction in the initial phase of the experiment can be attributed to the small amount of phenolic/acidic OH groups that could not be blocked by methylation (1.4 ± 0.1 meq/g).

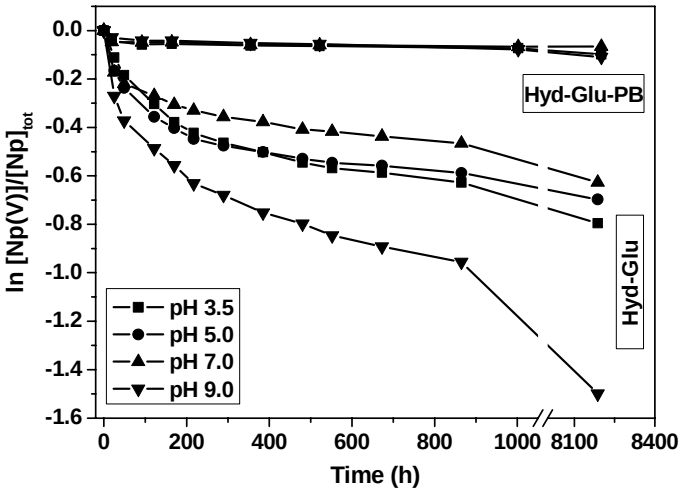


**Fig. 9.5:** Reduction of Np(V) to Np(IV) by HA type Hyd-Glu and HA type Hyd-Glu-PB between pH 3.5 to pH 9.0. Determination of Np(V) by TTA extraction.

By NIR absorption spectroscopy the gradual decrease of the Np(V) absorption peaks is observed, while the total Np concentration in the sample solutions remains constant in the course of the experiments (cf. Fig. 9.4). The formation of Np(IV) hydrolysis products besides the formation of Np(IV) humate cannot be excluded completely by this method since the various Np(IV) hydrolysis species and their mixed hydroxo fulvate or humate complex spe-

cies cannot be distinguished by NIR absorption spectroscopy (Marquardt et al., 2000) or EXAFS (Schmeide et al., 2005).

The results of ultrafiltration of the Np(IV,V)/HA type Hyd-Glu sample solutions with membrane filters of pore sizes between 1 kDa and 1000 kDa are shown in Fig. 9.6. At pH 7 and pH 9, where 36.1% and 64.3% Np(IV) are detected by TTA extraction (after 1513 h), a Np fraction of 43.1% and 86.6%, respectively, is found to be retained on a 1 kDa filter, whereas at 1000 kDa, Np passes quantitatively through the filter. That means, that a fraction of about 43.1% or 86.6% of the Np is bound onto HA colloids, mostly as Np(IV) and but also as Np(V) (especially at pH 9, cf. Np(V) speciation given in Fig. 9.1). At pH 3.5 and pH 5, where 47.4% and 44.2% Np(IV) are detected by TTA extraction, a Np fraction of 49.2% and 45.8%, respectively, is found to be retained on a 1 kDa filter, showing the fraction of humic colloid-bound Np(IV). In this pH range, no Np(V) humate is formed (cf. Fig. 9.1), and the $NpO_2^+$ ion, detected by NIR absorption spectroscopy, passes through the filter. The Np humate solution at pH 3.5 shows the peculiarity that the amount of Np retained on the filters of pore sizes between 1 kDa and 1000 kDa is nearly constant. This is attributed to the precipitate and/or large aggregates that are formed by the humic colloid-bound Np(IV) in the sample solution at pH 3.5.

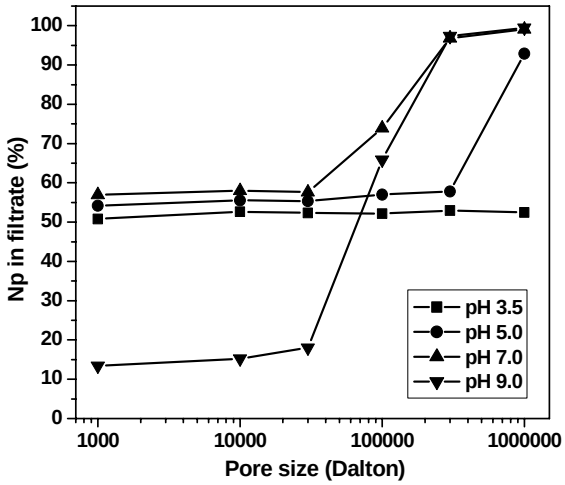


**Fig. 9.6:** Ultrafiltration of Np(IV,V)/HA type Hyd-Glu equilibrated at pH 3.5 to pH 9.0 for 1543 h (~64 d).

The results have shown that in comparison to the natural humic substances (AHA, KFA), the synthetic HA (type Hyd-Glu and Cat-Gly) lead to a stronger reduction of Np(V) to Np(IV). The Np(IV) formed in the course of the experiments is stabilized in form of Np(IV) humate complexes, whereas the remaining Np(V) occurs as $NpO_2^+$ ion or Np(V) humate depending on pH. The higher reduction potential of the synthetic HA can be attributed to their higher phenolic/acidic OH group contents compared

to natural humic substances. This correlation could be verified applying a synthetic HA with blocked phenolic/acidic OH groups.

# 10 Influence of humic acid on the U(VI) sorption onto kaolinite

An important mechanism for retarding radionuclide migration in natural environment is sorption onto minerals present along the groundwater flow path. Due to their complexation, redox and colloidal properties, HA affects the speciation of actinide ions, and therefore, their sorption and migration in the environment. In the present study, we investigated the influence of HA on the U(VI) sorption onto kaolinite KGa-1b. Kaolinite is a main mineral component of clay-rich host rock formations considered as potential nuclear waste repositories. Batch sorption experiments were performed to study the U(VI) sorption onto kaolinite in absence and presence of HA under different experimental conditions. Furthermore, the HA sorption onto kaolinite was studied. Spectroscopic investigations were performed in order to identify U(VI)-kaolinite surface complexes in absence and presence of HA. These information are necessary for a future modeling of the U(VI) sorption onto kaolinite. The obtained results help to improve the understanding of the geochemical interactions of hexavalent actinides in the environment. The outcome of these studies is published in (Křepelová, 2006a and Křepelová et al., 2006b).

## 10.1 Batch sorption experiments

### 10.1.1 Experimental

***Materials***

Kaolinite KGa-1b (see chapter 2) was used without any pretreatment in all experiments. For the experiments, the $^{14}C$-labeled synthetic HA type M42 (Batch M170, see chapter 3) was used. A HA stock solution of 5 g/L was prepared by weighting of 50 mg of HA, adding of 1720 µL of 0.1 M NaOH and filling the volume with 0.1 M $NaClO_4$ (Merck) up to 10 mL. A $1 \cdot 10^{-3}$ M $UO_2(ClO_4)_2$ was used as U(VI) stock solution for all experiments.

***Batch experiments***

The sorption experiments were performed under ambient atmosphere ($pCO_2$: $10^{-3.5}$ atm) or inert gas conditions ($N_2$-box). 40 mg of kaolinite were weighed into 15 mL polypropylene centrifuge tubes (Cellstar, Greiner Bio-One), 10 mL of 0.1 or 0.01 M $NaClO_4$ were added subsequently. The desired pH values were adjusted between pH 3 and 10. For studies at pH >7 in the presence of $CO_2$, a calculated amount of $NaHCO_3$ was added to accelerate the equilibrium process with atmospheric $CO_2$. For pre-equilibration the samples were continuously shaken on a horizontal shaker (mod. Promax 2020, Heidolph Instruments) and the pH values were controlled and readjusted. The conditioning time was 72 h and 4 – 5 weeks in the presence and absence of $CO_2$, respectively. After pre-equilibration, 9.26 or 92.6 µL U(VI) stock solution were added to the kaolinite suspension for the investigation of the U(VI) sorption onto kaolinite. The final concentration of U(VI) in the solution was $1 \cdot 10^{-6}$ M or $1 \cdot 10^{-5}$ M. To determine HA sorption onto kaolinite, 20 or 100 µL of the HA stock solution were added to the kaolinite suspension. The final concentration of HA in the solution was 10 or 50 mg/L. For the investigation of U(VI) sorption onto kaolinite in the presence of HA, pre-equilibrated U(VI)-HA solution (equilibration time: 24 h, pH ~ 7) was added. The final concentrations of U(VI) and HA in the solution were $1 \cdot 10^{-5}$ M or $1 \cdot 10^{-6}$ M and 10 or 50 mg/L, respectively. After addition of U(VI), HA or U(VI)/HA solutions, the pH values were readjusted immediately. The samples were shaken on the horizontal shaker for 60 h to equilibrate. After shaking, the final pH values of the samples were measured and the samples were centrifuged (30 min, 4000 rpm, mod. Megafuge 1.0, Heraeus Sepatech). The supernatants of single samples were filtered (450 nm, Minisart N, Sartorius). Prior to filtering, the filters were rinsed with 1 mL of sample solution. The filtrates were analyzed for the final U(VI) and HA concentration. The U(VI) concentration in solution was determined by ICP-MS (ELAN 6000, Perkin Elmer) and the HA concentration in solution was measured by liquid scintillation counting (LSC, mod. LS 6000 LL, Beckman Coulter). A quantity of 1 mL of the filtered solution was mixed with 5 mL Ultima Gold (Perkin Elmer). Prior to the measurement of the U(VI) concentrations in the samples in presence of HA, HA was removed by digestion in a microwave oven (mod. mls 1200 mega, MLS) with $HNO_3$ (Riedel de-Haën) in order to avoid any disturbing effects of HA during ICP-MS measurements.

Finally, the U(VI) or HA sorption onto vial walls was investigated. The vials were washed with water and dried. Then, 7 mL 1 M $HNO_3$ or 1 M NaOH were added and the vials were shaken for 2 days. The maximal vial wall sorption of U(VI) was observed between pH 6 and

7.5 and reached values up to 5%. In the acidic pH range the vial wall sorption was maximal 3%, above pH 8 the vial wall sorption was negligible. HA vial wall sorption was negligible in the entire pH range.
The amount of U/HA adsorbed on the mineral surface was calculated as the difference between the initial U(VI)/HA concentration and the sum of the amounts of U(VI)/HA remaining in solution and U(VI)/HA adsorbed onto the vial walls.

***Kinetic experiments***

Kinetic experiments were conducted to evaluate the time required for the sorption equilibrium. The effect of equilibration of the suspensions as well as the influence of the sequence of the U(VI) and HA addition to the kaolinite suspension (a: addition of a 24 h pre-equilibrated U(VI)-HA solution, b: simultaneous addition of U(VI) and HA without pre-equilibration, c: U(VI) addition after 60 h contact time of HA with kaolinite) were studied. The experimental conditions were similar to those in the batch experiments (see above). The kinetic curves were obtained at two pH values: pH 5 and pH 7.5. Samples were shaken and taken after different contact times. The final U(VI)/HA concentrations were measured and the vial wall adsorption was determined. For more details see (Křepelová, 2006a; Křepelová et al., 2006b)

### 10.1.2 Results and discussion

#### 10.1.2.1 Kinetic experiments

Figure 10.1 shows the results of the kinetic experiments for U(VI) and HA adsorbed onto kaolinite from the solution. It becomes obvious that both systems reach the sorption equilibrium quite fast. At pH 5 and pH 7.5, the amount of the adsorbed HA does not change significantly after 50 h; thus, 60 h are sufficient to establish the sorption equilibrium in the system. The kinetics of the U(VI) sorption onto kaolinite in the absence of HA is very similar. The amount of U(VI) adsorbed onto kaolinite is stable after 50 h at pH 5 and even earlier at pH 7.5.
Comparing the different sequences of U(VI) and HA addition to the kaolinite suspensions (not shown), no significant differences in the U(VI) sorption behavior were observed. Therefore, it can be concluded that the pre-equilibration of the U(VI)-HA solution before the addition to the kaolinite has no significant influence on the U(VI) sorption kinetic in the studied time scale, for more details see (Křepelová, 2006a; Křepelová et al., 2006b).

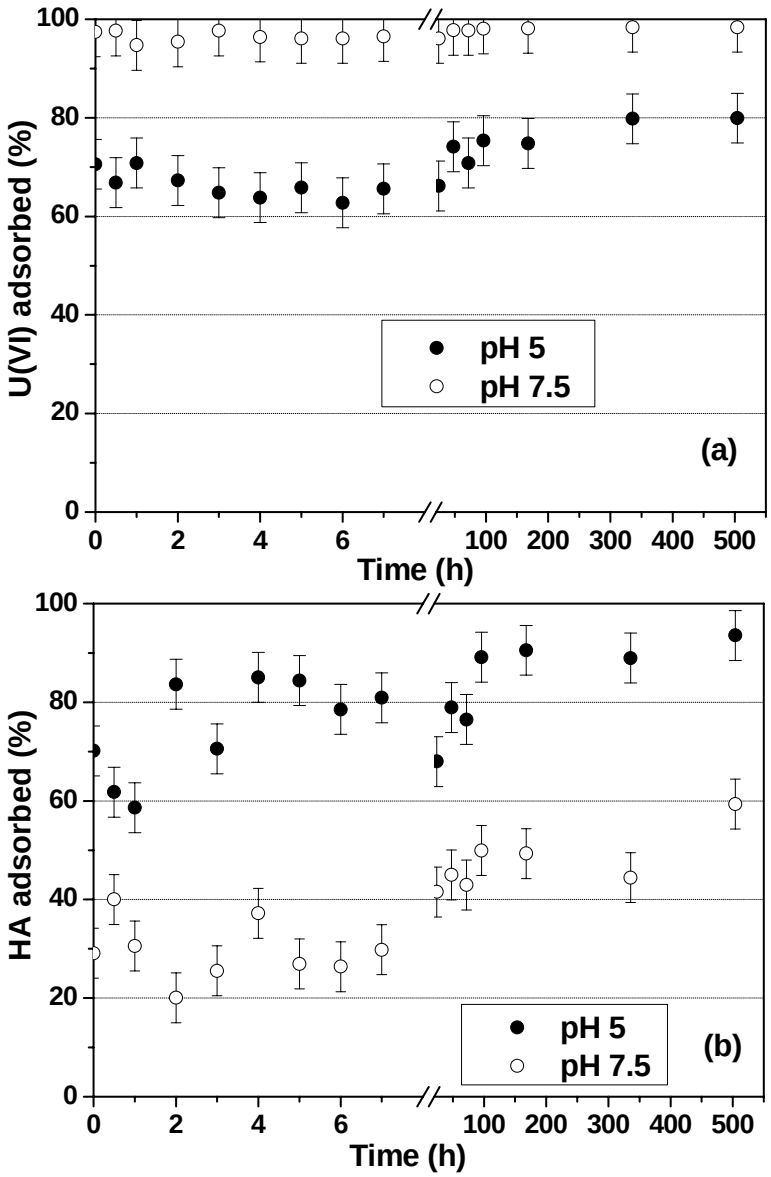


**Fig. 10.1:** Percentage of (a) U(VI) and (b) HA adsorbed from solution during kinetic experiments at pH 5 (filled symbols) and pH 7.5 (open symbols) ([U(VI)]: $1 \cdot 10^{-6}$ M, [HA]: 10 mg/L, I: 0.01 M $NaClO_4$, $pCO_2$: $10^{-3.5}$ atm).

### 10.1.2.2 Humic acid sorption onto kaolinite

HA uptake onto kaolinite is shown in Fig. 10.2 as a function of pH and HA concentration. The observed results are comparable to those of natural HA described in the literature (e. g., Murphy et al., 1992; Kretzschmar et al., 1997; Samadfam et al., 2000). The sorption of HA

decreases with increasing initial HA concentration and pH. More than 90% of 10 mg/L HA is adsorbed onto kaolinite at pH 3. However, there is a possibility that a part of HA precipitates at pH 3. There could be an overlapping of both processes, HA sorption and precipitation. The percentage of HA adsorbed decreases with increasing HA concentration due to a saturation of kaolinite binding sites. The observed decrease of the HA sorption with increasing pH is regarded as a result of the electrostatic repulsions between negatively charged deprotonated carboxyl groups of HA and negatively charged kaolinite surface (cf. p.z.c. and p.z.n.p.c. values in chapter 2).

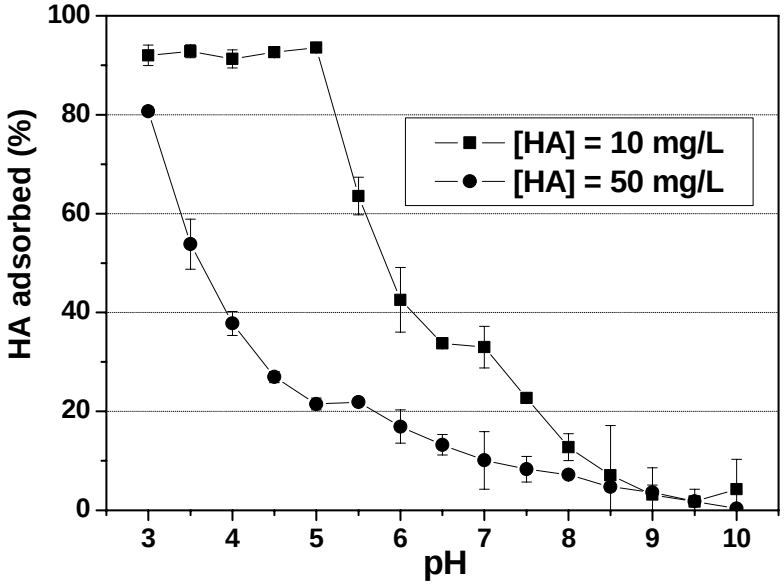


**Fig. 10.2:** HA sorption onto kaolinite as a function of pH and HA concentration (I: 0.01 M $NaClO_4$, $pCO_2$: $10^{-3.5}$ atm).

Figure 10.3 depicts the sorption of HA in 0.01 M and 0.1 M $NaClO_4$ solutions. Between pH 3 and pH 5, the HA adsorption at both ionic strengths reaches almost 95%. Strong differences in the amount of adsorbed HA occur at pH >5. The sorption of HA increased at higher ionic strength. The maximal difference in the adsorbed amount of HA between both ionic strengths (almost 60%) was achieved at pH 6.5. The changes in the macromolecular configuration of HA with the ionic strength can explain the observed phenomenon. At high ionic strength, the negative charges of HA macromolecules are well screened and consequently the HA wind up like random coils. Therefore, more HA can be adsorbed to the mineral surface (Kretzschmar et al., 1997). At low ionic strength, HA adopts a more linear and open configuration, therefore HA occupies a higher amount of kaolinite surface area (Murphy et al., 1992) resulting in lower HA adsorption on the surface.

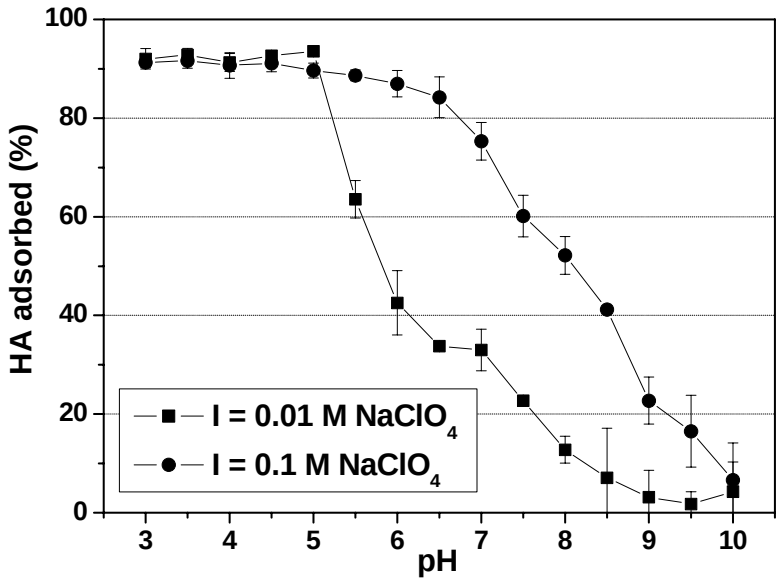


**Fig. 10.3:** Influence of the ionic strength on the HA sorption onto kaolinite ([HA]: 10 mg/L, $pCO_2$: $10^{-3.5}$ atm).

In the 0.01 M solution, the presence of U(VI) enhances the sorption of HA compared to the system without U(VI) at pH >5.5 (Fig. 10.4). This can be explained by the possible association between $UO_2^{2+}$ and HA on the kaolinite surface, which is expected to be strongest in the pH range of increased U(VI) adsorption onto kaolinite (see chapter 10.1.2.4). Redden et al. (1998) reported that U(VI) enhances adsorption of citrate onto kaolinite, when the citrate concentrations are comparable to those of U(VI). Schmeide et al. (2000) explained a high HA sorption onto albite due to specific interactions of cations, released into the aqueous phase due to mineral weathering and cation exchange processes with carboxylate groups of HA. These cations are able to form bridges between negatively charged surface species and HA carboxylate groups thus increasing the number of sorption sites for HA.

XPS measurements were performed to study how HA is distributed on the kaolinite surface (Reich et al., 2006a). These XPS measurements in the system HA/kaolinite showed that the surface of the kaolinite particle is not covered by a homogenous HA layer. Part of the HA must be distributed between the particles. This implies that in the ternary system, U(VI) can interact with significant parts of the kaolinite surface that are not covered by HA.

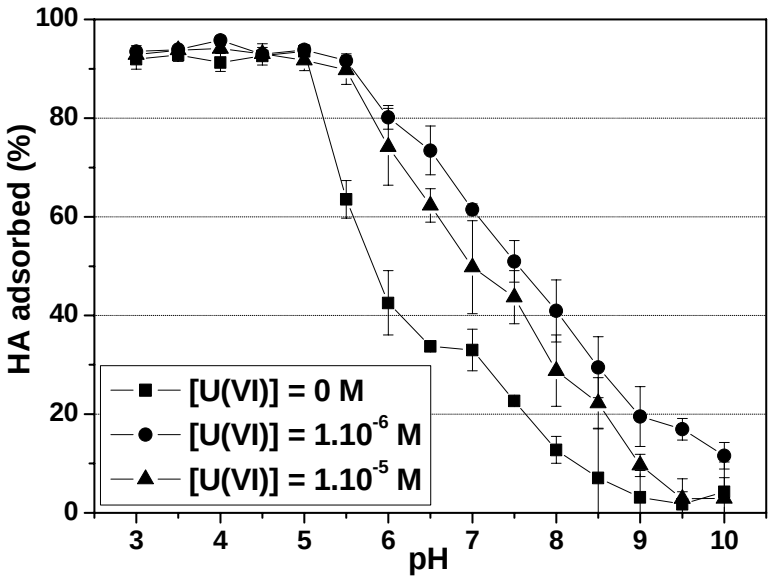


**Fig. 10.4:** Influence of the presence of U(VI) on the HA sorption onto kaolinite (I: 0.01 M $NaClO_4$, [HA]: 10 mg/L, $pCO_2$: $10^{-3.5}$ atm).

### 10.1.2.3 U(VI) speciation in solution

The sorption behavior of actinides is affected by their speciation in solution. Therefore, the aqueous distributions of U(VI) species for solutions in equilibrium with atmospheric $CO_2$ ($pCO_2$: $10^{-3.5}$ atm) and in the absence of $CO_2$ ($N_2$-atmosphere) were calculated using the code EQ3/6 (Wolery, 1992) based on the most recent compilation of U(VI) complex formation constants (Guillaumont et al., 2003). The results of speciation calculations for I: 0.1 M and [U(VI)]: $1 \cdot 10^{-6}$ M in the (a) absence and (b) presence of $CO_2$ shows Fig 10.5. Other calculations at I: 0.01 M are not shown because they do not differ significantly.

At pH <5, U(VI) prevails in solution as the free $UO_2^{2+}$ cation. At pH >5 the U(VI) speciation is dominated by a series of hydrolyzed U(VI) species, e.g., $UO_2OH^+$, $(UO_2)_3(OH)_5^+$ and $UO_2(OH)_3^-$. In the presence of $CO_2$, uranyl carbonato complexes $(UO_2)_2CO_3(OH)_3^-$, $UO_2(CO_3)_3^{4-}$ and $UO_2(CO_3)_2^{2-}$ dominate at higher pH values (pH >6.5).

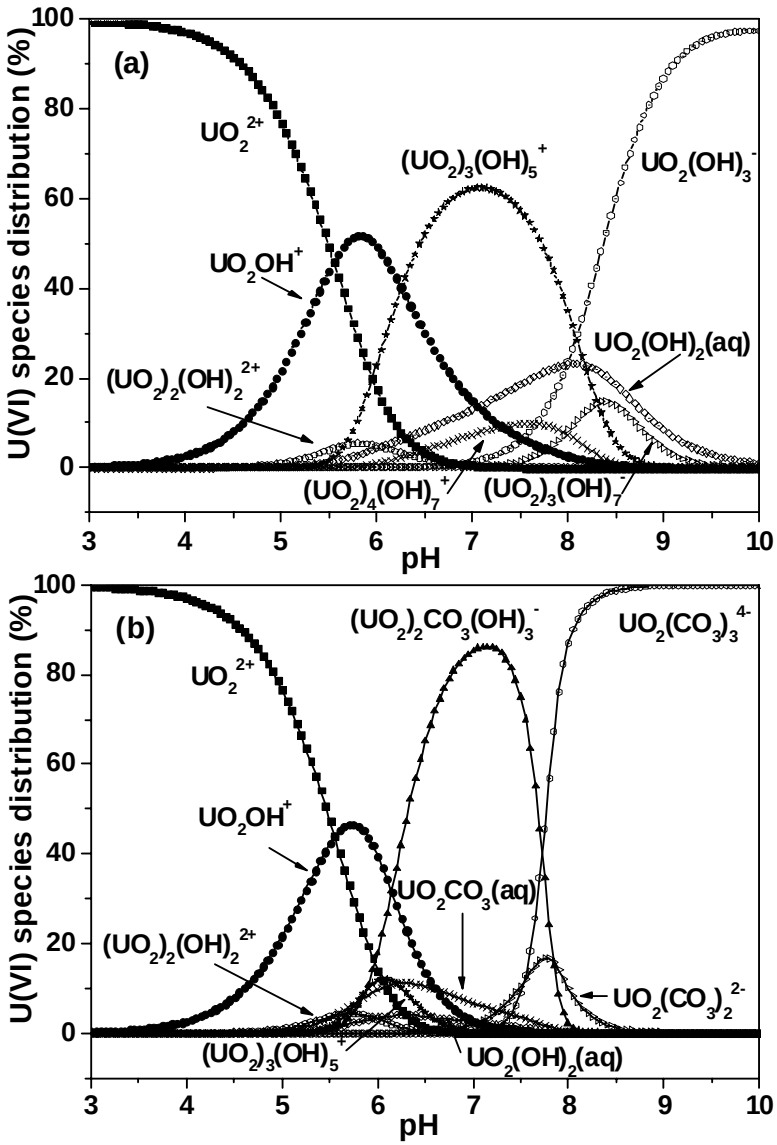


**Fig. 10.5:** U(VI) speciation in the (a) absence and (b) presence of $CO_2$ (I: 0.1 M $NaClO_4$, [U(VI)]: $1 \cdot 10^{-6}$ M).

HA affects the U(VI) speciation significantly. Figure 10.6 illustrates the U(VI) speciation in solution in the presence of HA. The computations were performed for solutions in equilibrium with atmospheric $CO_2$ and in its absence by means of EQ3/6 considering the metal ion charge neutralization model for the description of the HA complexation (Sachs et al., 2004). Within the calculations complexation data for two different U(VI)-humate complexes were considered: the binary $UO_2$HA(II) complex (e.g., Pompe et al., 2000a and 2000b; Montavon et al., 2000) and the ternary complex $UO_2$(OH)HA(I) (Sachs et al., 2006).

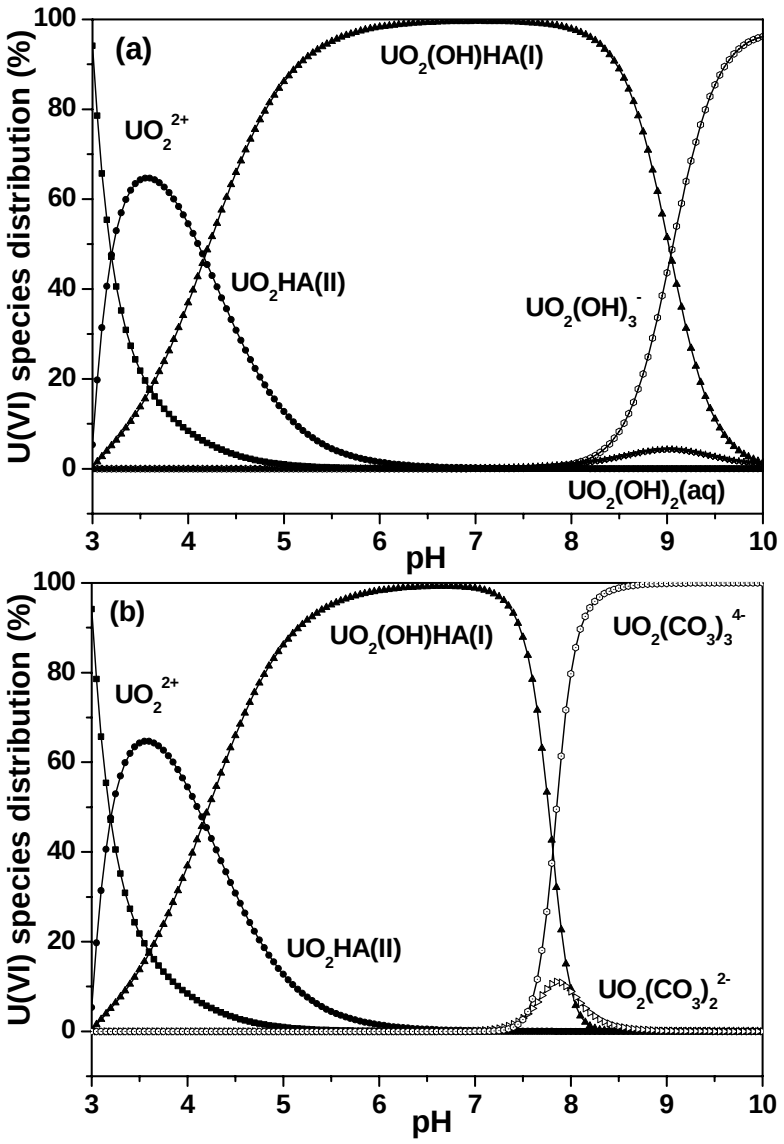


**Fig. 10.6:** U(VI) speciation in the presence of HA in the (a) absence and (b) presence of $CO_2$ (I: 0.1 M $NaClO_4$, [U(VI)]: $1 \cdot 10^{-6}$ M, [HA]: 10 mg/L).

In the presence of HA the free uranyl cation $UO_2^{2+}$ predominates in the solution only at very low pH values. The $UO_2HA(II)$ complex dominates the speciation in solution below pH 4. Both uranyl humate species determine the speciation in solution in the pH range between pH 4.5 and pH 9 (absence of $CO_2$) and pH 4.5 and 7.5 (presence of $CO_2$). Then, the prevailing species in solution is the $UO_2(OH)HA(I)$ complex. At higher pH values uranyl carbonato and uranyl hydroxo complexes become dominant in the presence and absence of $CO_2$, respectively.

#### 10.1.2.4 U(VI) sorption onto kaolinite in absence of humic acid

Results of batch experiments for kaolinite and U(VI) are depicted in Fig. 10.7. They are consistent with those data previously reported in the literature (e.g., Arnold et al., 1998; Kilislioglu and Bilgin, 2002; Payne et al., 2004). In the presence of $CO_2$, the percentage of the total U(VI) adsorbed onto kaolinite increases from nearly zero at pH 3 to 97% between pH 6 and pH 8. Above pH 8, the U(VI) sorption decreases. The highest U(VI) adsorption occurs in the pH range, where the U(VI) hydroxyl complexes are important. The positioning of the sorption edges at low pH values suggests the formation of relative strong actinide/surface site complexes. The U(VI) sorption behavior is comparable in the systems with and without $CO_2$ in the pH range between pH 3 and pH 8. At pH >8, however, no sorption decrease was observed in the absence of $CO_2$. This behavior is a result of the U(VI) speciation in the solution. In the presence of $CO_2$, U(VI) forms negatively charged uranyl carbonato complexes $UO_2(CO_3)_3^{4-}$ ($\log\beta = 21.0 \pm 0.3$, Pashalidis et al., 1997) and $(UO_2)_2CO_3(OH)_3^-$ ($\log\beta \approx 41$, Guillaumont et al., 2003). Under these conditions the kaolinite surface is also negatively charged. Therefore, the electrostatic repulsions between uranyl carbonato complexes and kaolinite result in the low U(VI) adsorption in this pH range.

An increase of the initial U(VI) concentration from $1 \cdot 10^{-6}$ M to $1 \cdot 10^{-5}$ M causes a shift of the sorption pH edge by one pH unit to higher pH values. The mass of adsorbed U(VI) in the maximum of sorption curves is higher in the case of $1 \cdot 10^{-5}$ M U(VI) concentration (e.g., pH 7: 532 µg U(VI)/ 1 g kaolinite is adsorbed) than in $1 \cdot 10^{-6}$ M U(VI) concentration (pH 7: 59 µg U(VI)/1 g kaolinite is adsorbed). However, the percentage of U(VI) adsorbed onto kaolinite decreases due to the higher initial U(VI) concentration. Varying the ionic strength from 0.01 M to 0.1 M has no (pH >6) or only a small (pH 3–5.5) influence on the U(VI) sorption (data not shown).

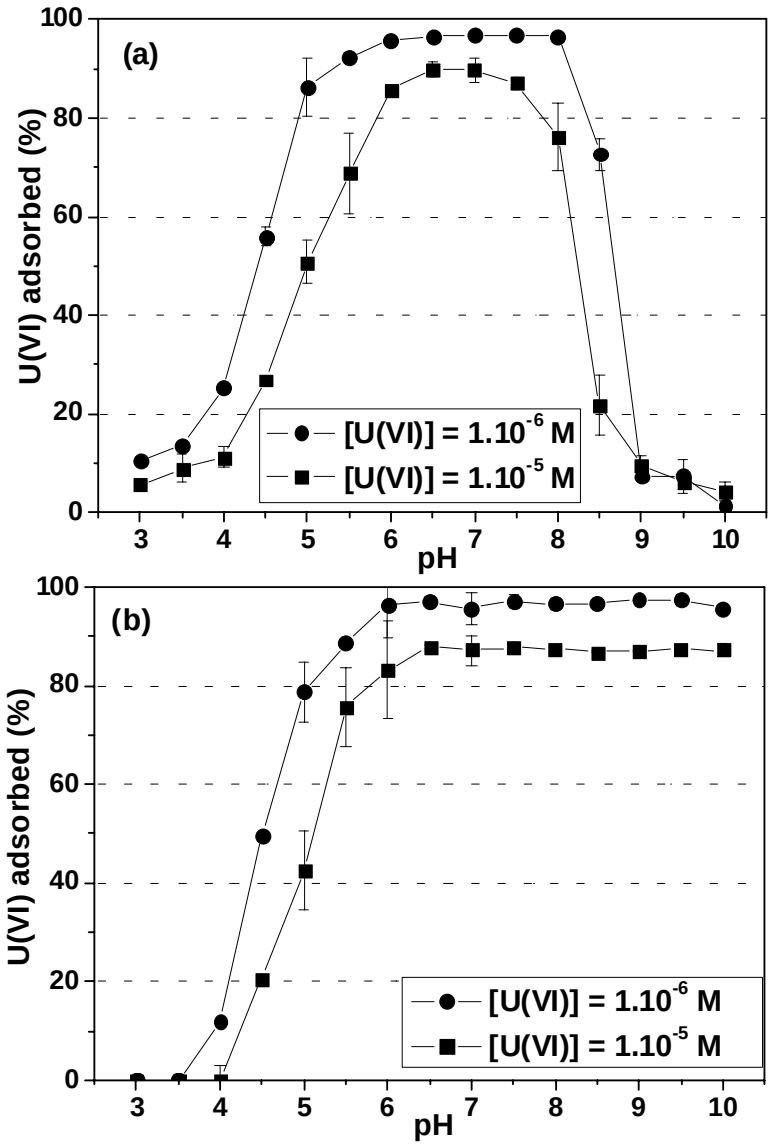


**Fig. 10.7:** U(VI) adsorption onto kaolinite as a function of pH and U(VI) concentration in the (a) presence and (b) absence of $CO_2$ (I: 0.01 M $NaClO_4$).

### 10.1.2.5 U(VI) sorption onto kaolinite in presence of humic acid

HA influences significantly the adsorption of U(VI) onto kaolinite in the entire studied pH range, see Fig. 10.8. The sorption curve can be divided into three parts. At pH <5, an enhancement in the U(VI) sorption was observed compared to the HA-free system. HA is almost 100% (10 mg/L) or 80% (50 mg/L) adsorbed on the kaolinite surface in this pH range (see Fig. 10.2), therefore reduction in the U(VI) uptake was expected due to the competition

between HA and U(VI) for available binding sites on the kaolinite surface. However, the adsorbed HA features additional binding sites for U(VI), hence the U(VI) adsorption can increase in its presence.

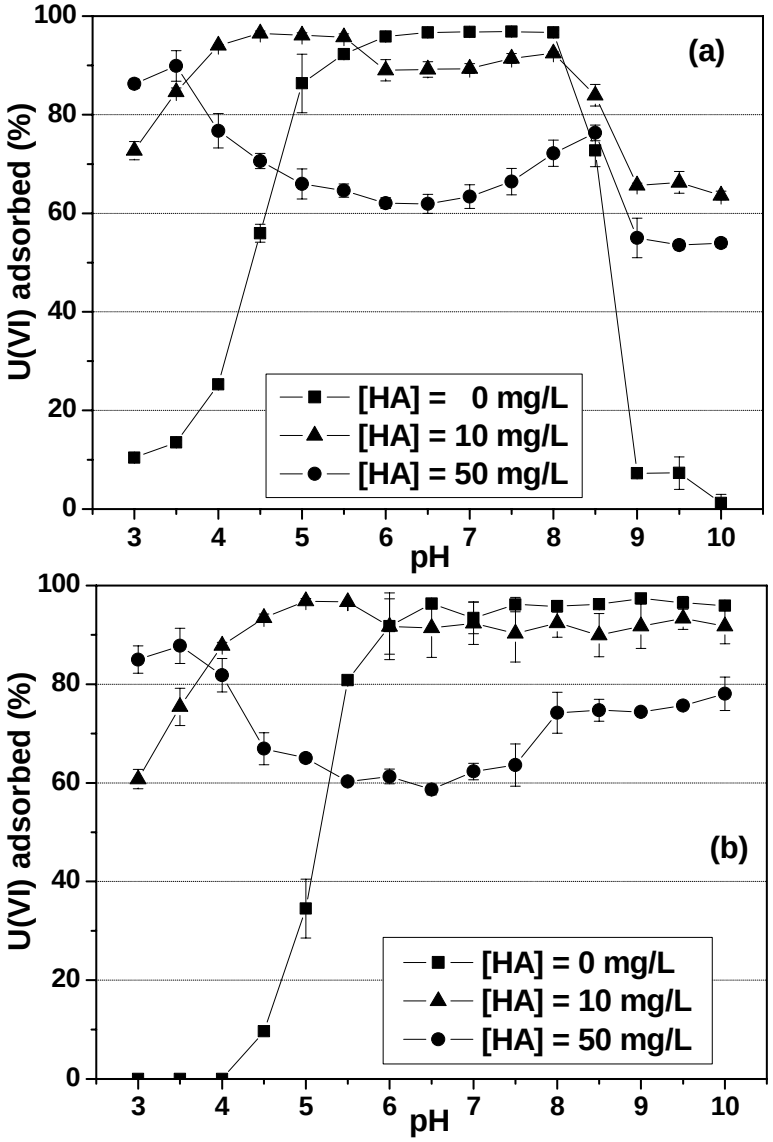


**Fig. 10.8:** U(VI) adsorption onto kaolinite as a function of pH and HA concentration in the (a) presence and (b) absence of $CO_2$ ([U(VI)]: $1 \cdot 10^{-6}$ M, I: 0.01 M $NaClO_4$).

In the near-neutral pH region, between pH 5 and pH 8.5, the U(VI) adsorption is lower in the presence of HA compared to the HA-free system. At pH 5, desorption of HA from the kaolinite surface starts (Fig.10.2). It leads to a decrease of the U(VI) adsorption onto kaolinite due to the formation of dissolved uranyl humate complexes. Binary complexes $UO_2HA(II)$ as well as mixed ternary uranyl hydroxo humate complexes $UO_2(OH)HA(I)$ can occur (see Fig.10.6).

Although the HA concentration (10 mg/L ≈ $1.8 \cdot 10^{-5}$ mol/L HA(II), calculated according to Eq. (7.6)) exceeds the U(VI) concentration ($1 \cdot 10^{-6}$ M) in the solution, U(VI) uptake in the presence of HA is reduced only very slightly (about 10%) compared to the system free of HA. It seems, that in spite of HA presence, U(VI) prefers sorption onto kaolinite than the complexation with HA in the solution. However, in the experiments carried out with higher HA concentration (50 mg/L) the U(VI) sorption is significantly lower than in the experiments conducted with only 10 mg/L. The lower U(VI) sorption at higher initial HA concentration results from a higher amount of dissolved HA forming aqueous complexes with U(VI). It can lead to an enhanced mobility of U(VI) in the environment. At pH >8.5, in the presence of $CO_2$, the sorption of U(VI) again increases in the presence of HA. As HA is nearly completely desorbed from the kaolinite surface (10% of HA remain adsorbed at pH 8.5), one should expect reduced adsorption of U(VI) onto kaolinite in the HA presence. However, the U(VI) sorption is enhanced. From the comparison with the corresponding system without $CO_2$, where no decrease of U(VI) sorption was observed in the presence of 10 mg/L HA, one can conclude that carbonate must play a role in the U(VI) sorption onto kaolinite also in the presence of HA. It is possible that uranyl carbonato humate complexes are formed, which can interact with the kaolinite surface and, therefore, enhance the U(VI) sorption onto kaolinite in the presence of HA in the alkaline pH region. Glaus et al. (1995) reported the possible existence of the ternary uranyl carbonato humate complex $(UO_2CO_3)HA$ in waters containing humic substances, however its stability constant is low ($\log\beta \approx 5$). Such sorption behavior in the alkaline pH range seems to be specific for our system and experimental conditions used.

In conclusions, effects of different parameters on U(VI) sorption onto kaolinite were studied. U(VI) sorption onto kaolinite is influenced by pH, presence of $CO_2$, U(VI) concentration and HA presence. In the absence of $CO_2$, the U(VI) sorption increases up to pH ~ 6.5. Then, it remains unchanged. Formation of negatively charged uranyl carbonato complexes causes a decrease of the U(VI) sorption onto the negatively charged surface of kaolinite above pH 8 in the presence of $CO_2$. Increase of U(VI) concentration results in a shift of the sorption pH edge by one pH unit to higher pH, whereas the ionic strength has only a slight influence on the U(VI) sorption onto kaolinite. The adsorption of U(VI) closely follows the adsorption of HA. HA enhances the U(VI) uptake in the acidic pH range compared to the system without HA due to the formation of additional binding sites for U(VI) coming from HA adsorbed onto kaolinite. Formation of dissolved uranyl humate complexes reduces U(VI) sorption in the near-neutral pH range.

Finally, we conclude that the presence of HA can enhance the U(VI) migration under environmentally relevant conditions. Therefore, HA has to be involved in model calculations for the assessment of the long-term stability of nuclear waste repositories.

## 10.2 Structure of U(VI)-HA-kaolinite surface complexes studied by EXAFS

The structure of U(VI)-kaolinite-surface complexes in presence of HA was studied by extended X-ray absorption fine structure analysis (EXAFS). The influence of HA, pH and $CO_2$ presence was determined. Results of the system U(VI)-HA-kaolinite were interpreted and compared with the binary systems U(VI)-kaolinite (Reich et al., 2006b; Thompson et al., 1998) to obtain information on the influence of HA on the near-neighbor surrounding of U(VI) in kaolinite surface complexes.

### 10.2.1 Experimental

EXAFS samples were prepared in form of wet pastes. U(VI) and HA (unlabeled HA type M42, batch M145, see chapter 3) were adsorbed onto 200 mg of kaolinite, as described in chapter 10.1, under the following conditions: [U(VI)]: $1 \cdot 10^{-5}$ M, [HA]: 10 mg/L, S/L ratio: 4 g/L, pH: 5-8.5, p($CO_2$): $10^{-3.5}$ atm, I: 0.1 M $NaClO_4$. The supernatants were removed and measured by ICP-MS. The wet pastes (kaolinite with adsorbed U(VI) and HA) were immediately filled into special polyethylene sample holders. These sample holders were then sealed with Kapton polyamide tape and heat-sealed in two layers of polyethylene foil to avoid moisture loss during analysis and to provide several layers of containment of the radioactive sample.

EXAFS data were collected at the Rossendorf Beamline (ROBL) at the European Synchrotron Radiation Facility (ESRF) Grenoble, France. Uranium $L_{III}$-edge absorption spectra were recorded in fluorescence mode at room temperature. The ionization potential of the uranium $L_{III}$-edge was defined as 17 185 eV. Multiple scans (5–8) were measured for all samples. The EXAFS spectra were analyzed according to standard procedures including statistical weighting of the 13 fluorescence channels and their dead-time correction using the suite of programs EXAFSPAK (George and Pickering, 1995). Theoretical scattering phases and amplitudes were calculated with the scattering code FEFF 8.20 (Ankudinov et al., 2002).

The structural model for fitting the EXAFS oscillations was derived from the EXAFS investigations of the binary system U(VI)-kaolinite KGa-1b (Reich et al., 2006b). The best fits of the measured EXAFS oscillations in the studied ternary system were obtained considering two oxygen atoms in the axial ($O_{ax}$) and five oxygen atoms in the equatorial ($O_{eq}$) coordination shells coordinated to the uranyl ion, multiple scattering (MS) along the uranyl unit, and two coordination shells each with one Al/Si atom (for more details see Křepelová, 2006a).

### 10.2.2 Influence of different experimental conditions on the near-neighbor surrounding of U(VI) in kaolinite surface complexes

In this paragraph the influence of different parameters – pH, $CO_2$ and HA-presence – on the U(VI) surface complexation will be discussed (for details see Křepelová, 2006a) .

#### 10.2.2.1 Effect of pH

Figure 10.9 shows the obtained U $L_{III}$-edge $k^3$-weighted EXAFS oscillations and the corresponding Fourier transforms (FTs) of the samples prepared at different pH values in the presence of HA.

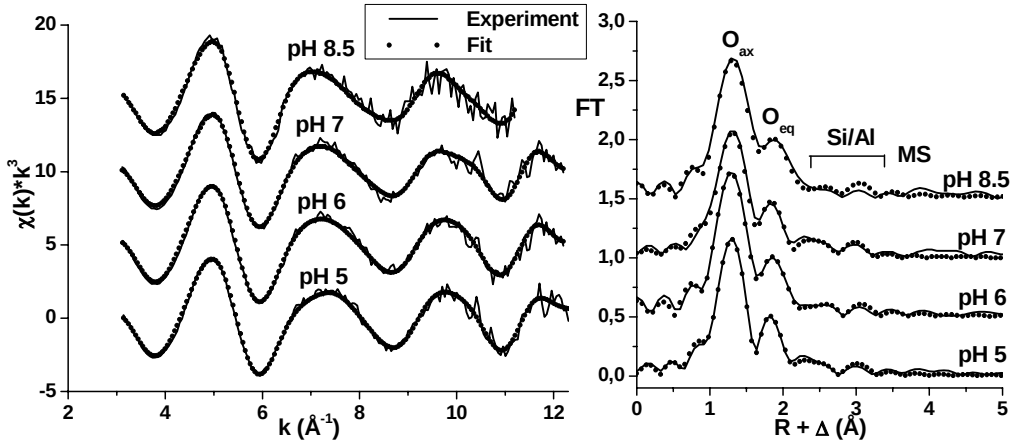


**Fig. 10.9:** EXAFS oscillations and FTs of the samples prepared at different pH values.

As it can be seen from the figure, all examined samples exhibit comparable EXAFS oscillations and FTs with no remarkable differences at different pH values. The results of the fitting procedure are summarized in Tab. 10.1.

**Tab. 10.1:** Obtained structural parameters for the samples prepared at different pH values.

| | | 2 x $O_{ax}$ | | 5 x $O_{eq}$ | | 1 x $Si_1/Al_1$ | | 1x $Si_2/Al_2$ | | | |
|---|---|---|---|---|---|---|---|---|---|---|---|
| **Sample** | **pH** | **R (Å)** | **$\sigma^2$ (Å)** | **R (Å)** | **$\sigma^2$ (Å)** | **R (Å)** | **$\sigma^2$ (Å)** | **R (Å)** | **$\sigma^2$ (Å)** | **ΔE (eV)** | **Red. error** |
| U4-134 | **5** | **1.76** | 0.0031 | **2.34** | 0.0144 | 3.10 | 0.0035 | 3.30 | 0.0036 | -12.6 | 0.114 |
| U4-135 | **6** | **1.77** | 0.0033 | **2.34** | 0.0140 | 3.10 | 0.0048 | 3.31 | 0.0056 | -12.3 | 0.071 |
| U4-136 | **7** | **1.77** | 0.0041 | **2.33** | 0.0145 | 3.08 | 0.0030 | 3.29 | 0.0032 | -13.0 | 0.113 |
| U4-137 | **8.5** | **1.78** | 0.0037 | **2.35** | 0.0130 | 3.08 | 0.0027 | 3.27 | 0.0036 | -11.3 | 0.230 |

$\Delta R$: ± 0.02 Å, $\Delta\sigma^2$: ± 0.001 Å

The obtained structural parameters show no significant differences. In the binary system, Reich et al. (2006b) observed an increase of U-$O_{eq}$ bond distances with increasing pH value from 2.36 Å to 2.41 Å probably due to the formation of ternary surface uranyl complexes with carbonate. This effect was not found in the ternary system studied in this work, presumably because U(VI) forms uranyl hydroxyl humate complexes and the effect of carbonate on the U-$O_{eq}$ atom distance is suppressed in the presence of HA.

#### 10.2.2.2 Influence of $CO_2$

Two samples were prepared to study the effect of $CO_2$ at pH 8.5 on the U(VI) coordination environment in the surface complexes in the presence of HA. Also in this case the obtained U $L_{III}$-edge $k^3$-weighted EXAFS oscillations and corresponding FTs are comparable for both samples, see Fig. 10.10. It is obvious that the fit of the sample prepared on air is more problematic than that for the sample prepared in nitrogen atmosphere. It is due to the lower signal-to-noise ratio, which caused that the *k*-range had to be reduced to 11.2 $Å^{-1}$.

The resulted structural parameters for these two samples are given in Tab. 10.2. There is a small observable drop from 2.35 Å to 2.33 Å of the U-$O_{eq}$ distance in the $CO_2$-free system. From this it could be derived that U(VI) adsorbed on the kaolinite surface interacts with carbonate, but the obtained difference is too small. Under consideration of the standard deviation it is not significant. However, Reich et al. (2006b) also observed such effect in the binary system U(VI)-kaolinite, where the decrease of the U-$O_{eq}$ distance was more significant, from 2.41 Å to 2.36 Å. However, the U-$O_{eq}$ distance in $[UO_2(CO_3)_3]^{4-}$ amounts to 2.44 Å, so it can not be concluded definitely that there is an influence of carbonate on the near-neighbor surrounding of U(VI) in the kaolinite surface complexes.

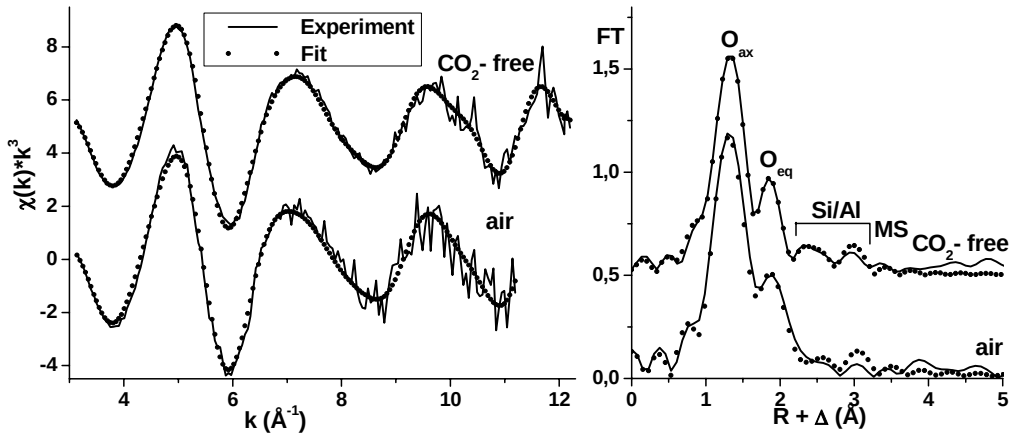


**Fig. 10.10:** EXAFS oscillations and FTs of the samples with different $CO_2$ concentration.

**Tab. 10.2:** Obtained structural parameters for the samples prepared in absence and presence of $CO_2$.

| | | 2 x $O_{ax}$ | | 5 x $O_{eq}$ | | 1 x $Si_1/Al_1$ | | 1x $Si_2/Al_2$ | | | |
|---|---|---|---|---|---|---|---|---|---|---|---|
| **Sample** | **pH: 8.5** | **R (Å)** | **$\sigma^2$ (Å)** | **R (Å)** | **$\sigma^2$ (Å)** | **R (Å)** | **$\sigma^2$ (Å)** | **R (Å)** | **$\sigma^2$ (Å)** | **ΔE (eV)** | **Red. error** |
| U4-137 | **Air** | **1.78** | 0.0037 | **2.35** | 0.0130 | 3.08 | 0.0027 | 3.27 | 0.0036 | -11.3 | 0.230 |
| U4-138 | **no $CO_2$** | **1.78** | 0.0040 | **2.33** | 0.0147 | 3.09 | 0.0035 | 3.30 | 0.0033 | -11.8 | 0.097 |

ΔR: ± 0.02 Å, $\Delta\sigma^2$: ± 0.001 Å

### 10.2.2.3 Effect of humic acid presence

Figure 10.11 illustrates U $L_{III}$-edge $k^3$-weighted EXAFS oscillations and their corresponding FTs for the samples prepared at the same pH value (pH ~ 7) in absence and presence of HA. Again, the samples exhibit comparable EXAFS oscillations and FTs with no significant differences.

Also in this case, the obtained structural parameters (see Tab. 10.3) are very similar. The U-$O_{ax}$ distances amount to 1.77 Å for both samples. The U-Si/Al distances are slightly shortened from 3.08 Å and 3.29 Å in the presence of HA to 3.06 Å and 3.26 Å in the absence of HA. The U-$O_{eq}$ distances are almost identical: 2.33 Å for the sample with HA and 2.34 Å for the sample without HA. It leads to the conclusion that HA has no influence on the EXAFS structural parameters of U(VI)-kaolinite surface complexes.

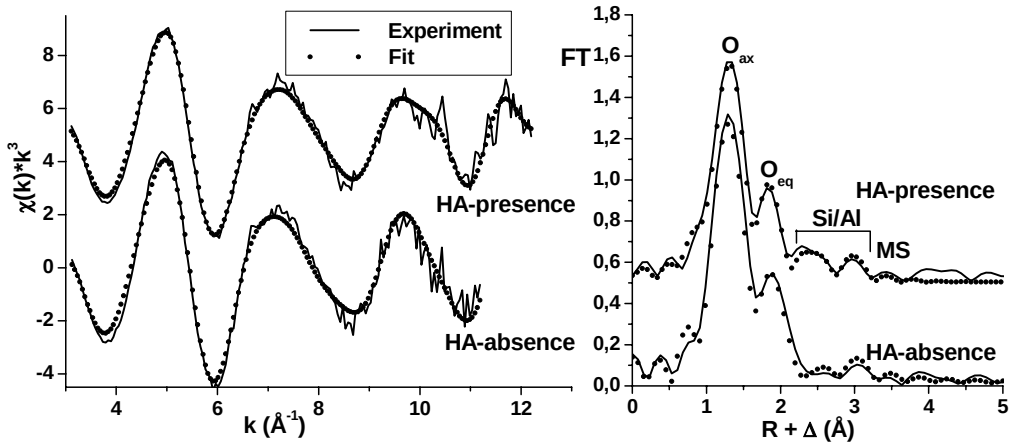


**Fig. 10.11:** EXAFS oscillations and FTs of the samples with and without HA.

**Tab. 10.3:** Obtained structural parameters for the samples prepared with and without HA.

| | | 2 x $O_{ax}$ | | 5 x $O_{eq}$ | | 1 x $Si_1/Al_1$ | | 1x $Si_2/Al_2$ | | | |
|---|---|---|---|---|---|---|---|---|---|---|---|
| **Sample** | **pH ~ 7** | **R (Å)** | **$\sigma^2$ (Å)** | **R (Å)** | **$\sigma^2$ (Å)** | **R (Å)** | **$\sigma^2$ (Å)** | **R (Å)** | **$\sigma^2$ (Å)** | **ΔE (eV)** | **Red. error** |
| U4-136 | **HA-** | **1.77** | 0.0041 | **2.33** | 0.0145 | 3.08 | 0.0030 | 3.29 | 0.0032 | -13.0 | 0.113 |
| U4-140 | **HA-absence** | **1.77** | 0.0030 | **2.34** | 0.0123 | 3.06 | 0.0040 | 3.26 | 0.0042 | -12.6 | 0.155 |

ΔR: ± 0.02 Å, $\Delta\sigma^2$: ± 0.001 Å

### 10.2.3 Comparison of EXAFS results of the binary and ternary systems

The EXAFS analysis of the ternary system was compared to the EXAFS analysis of the binary system U(VI)-kaolinite performed by Reich et al. (2006b). They studied the effect of pH, $CO_2$-presence and U(VI)-concentration on the U(VI) sorption onto kaolinite by means of combination of batch-type sorption experiments and EXAFS measurements.

For the EXAFS analysis they used two different tools. Firstly, the EXAFS analysis was performed using EXAFSPAK (George and Pickering, 1995). The following conclusions have resulted: No U-U interactions were observed, therefore U(VI) forms only mononuclear surface complexes. The U-$O_{eq}$ distances increased with increasing pH values. U-Si/Al interactions at 3.1 Å and 3.3 Å were found, which points out to inner-sphere sorption of $UO_2^{2+}$ by edge-sharing with $SiO_4$-tetrahedra and/or $AlO_6$-octahedra.

Secondly, the Tikhonov regularization method (Babanov et al., 1981) was used, which has been proposed for EXAFS analysis as an alternative to the analysis of EXAFS spectra by

conventional shell fitting. An improved algorithm was developed and applied to the analysis of U $L_{III}$-edge EXFAFS spectra of U(VI) adsorbed onto kaolinite (Reich et al., 2006b). The U $L_{III}$-edge EXAFS spectrum calculated agreed well with experimental data. Two peaks at 1.79 Å and 2.35 Å with N equal 1.9 ($O_{ax}$) and 5.1 ($O_{eq}$), respectively, were obtained. Approximately 0.7 Si/Al atoms at 3.06 Å and 0.4 Å atoms at 3.26 Å were found to surround the U(VI) atom.

Table 10.4 shows the comparison of the structural parameters that were obtained from EXAFS analysis of the ternary and binary systems U(VI)-kaolinite (Reich, et al., 2006b; Thompson et al., 1998).

**Tab. 10.4:** Comparison of the obtained structural parameters for the systems U(VI)-kaolinite and U(VI)-HA-kaolinite.

| System | R(U-$O_{ax}$) (Å) N = 2 | R(U-$O_{eq}$) (Å) N = 5 | R(U-Si/Al) (Å) N = 1 or 2 | Reference |
|---|---|---|---|---|
| **Kaolinite KGa-1b** | 1.80 | 2.36 – 2.41 | 3.1/3.3 | Reich et al., 2006 |
| **Kaolinite KGa-2** | 1.80 | 2.40 | 3.3 | Thompson et al., 1998 |
| **Kaolinite KGa-1b-HA** | 1.77 | 2.34 | 3.1/3.3 | this work |

The U-$O_{ax}$ distances obtained for both binary kaolinite systems KGa-1b and KGa-2 are the same, while in the presence of HA this distance was shortened. Reich et al. (2006b) observed an increase of U-$O_{eq}$ with increasing pH from 2.36 to 2.41 Å, which did not occur in the ternary system. The system with kaolinite KGa-2 gave a value for the U-$O_{eq}$ distance, which is comparable with that obtained for the binary system with kaolinite KGa-1b. The value obtained for the ternary system is slightly lower. Thompson et al. (1998) obtained only one U-Si/Al distance, but this distance is the same as the longer U-Si/Al distance found for the systems with kaolinite KGa-1b.

The obtained EAXFS structural parameters for the system U(VI)-HA-kaolinite studied are similar or they lie in the range of values that were obtained for the binary system U(VI)-kaolinite. Therefore, it can be concluded that HA has no effect on the EXAFS structural parameters in the system U(VI)-HA-kaolinite. Moreover, it seems that in spite of HA presence, U(VI) prefers to adsorb rather directly onto kaolinite than via HA, otherwise no U-Si/Al interactions could be observed. For more details about the EXAFS analysis and discussion see (Křepelová, 2006a).

## 10.3 TRLFS study of U(VI)-kaolinite surface complexes in absence and presence of humic acid

As additional method, time-resolved laser-induced fluorescence spectroscopy (TRLFS) was applied to study the kind of U(VI) surface complexes onto kaolinite. These investigations were performed at different pH values in the absence and presence of HA.

### 10.3.1 Experimental

The TRLFS data were collected for two systems. The binary system consists of U(VI) adsorbed onto kaolinite, whereas in the ternary system also HA was present. U(VI) or U(VI)/HA were adsorbed as described in chapter 10.1 under the following experimental conditions: [U(VI)]: $1 \cdot 10^{-5}$ M, [HA]: 10 mg/L (unlabeled HA type M42, batch M145, see chapter 3), I: 0.1 M $NaClO_4$, pH: 5-8, S/L: 4 g/L, $p(CO_2)$: $10^{-3.5}$ atm. After phases separation, the supernatants were analyzed by ICP-MS for U(VI) final concentrations. For the spectroscopic investigation, kaolinite samples from the batch experiments were first re-suspended in 10 mL of a solution with pH and ionic strength being identical to the original solution (without U(VI) and HA). This ascertained that only fluorescence signals caused from originally adsorbed U(VI) would be detectable, eliminating the dissolved U(VI) fraction. Time-resolved spectra of these kaolinite suspensions were then recorded at permanent stirring.

The TRLFS system consisted of a Nd:YAG diode laser with subsequent $4^{th}$ harmonic generation. The wavelength of 266 nm was used for the excitation of the samples with laser energies of about 0.3 mJ, providing a maximized signal-to-noise ratio. The delay time after the excitation laser pulse ranges from 0.03 μs to 10.03 μs (for details see Křepelová, 2006a).

The lifetimes of U(VI) fluorescence species were determined from bi-exponential fit analysis of obtained data indicating at least two surface species. An example for the sample of U(VI) adsorbed onto kaolinite at pH ~ 7 is shown in Fig. 10.12.

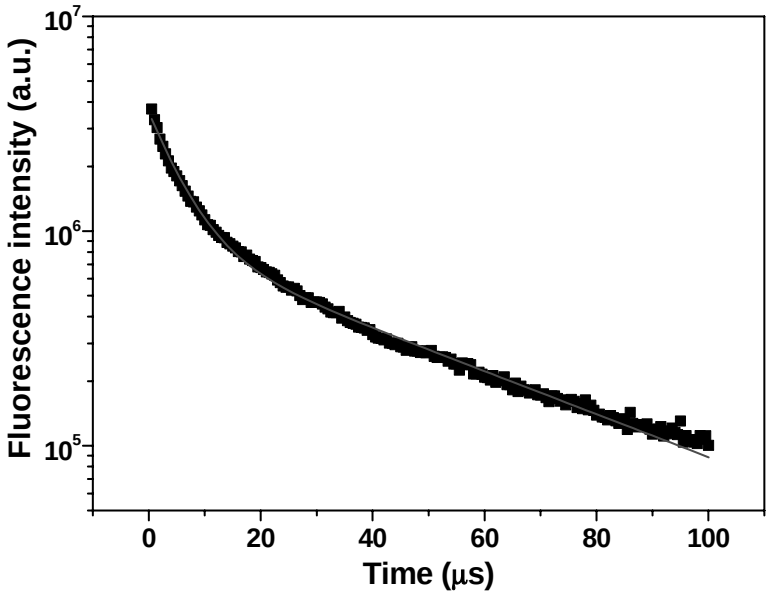


**Fig. 10.12:** Bi-exponential fluorescence decay behavior of a U(VI)-kaolinite (pH ~ 7).

The fluorescence lifetimes of two U(VI) surface species were calculated from Eq. 10.1:

$$y = y_0 + A_1 e^{-(x-x_0)/t_1} + A_2 e^{-(x-x_0)/t_2} \qquad (10.1)$$

The lifetime analysis and the generation of the graphics utilized OriginPro 7.5G software (OriginLab Corp., Northampton, MA). For more details about the lifetime analysis and the spectra deconvolution see (Křepelová, 2006a).

### 10.3.2 Measurements in the binary system U(VI)-kaolinite

TRLFS measurements provide two kinds of characteristic information: the position of fluorescence emission bands and the fluorescence lifetimes. The positions of fluorescence bands are primary attributes of the TRLFS spectrum, whereas the fluorescence lifetime is a secondary feature, because of its dependence on the sample preparation and temperature of the experiment. The fluorescence lifetime varies depending on the number of neighboring water molecules surrounding the U(VI) atom (Geipel, et al., 2000). Such characteristic spectral information is useful for the identification of fluorescent aqueous uranium species, as well as U(VI) surface species adsorbed onto kaolinite.

Fig. 10.13 shows the dependence of the relative fluorescence intensity on the delay time. The original spectra of all samples with U(VI) adsorbed onto kaolinite at different pH values are comparable, thus only the TRLFS spectrum of U(VI) adsorbed onto kaolinite at pH ~ 7 is shown as an example.

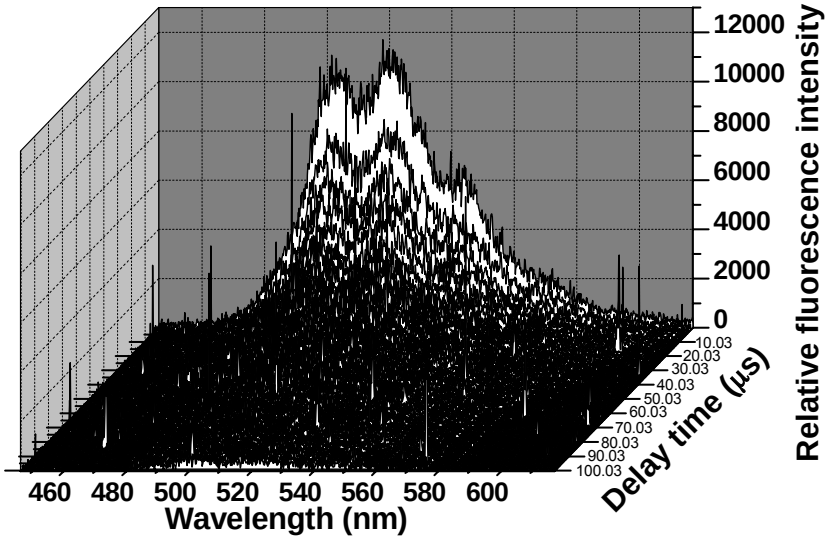


**Fig. 10.13:** TRLFS spectrum of U(VI) adsorbed onto kaolinite (pH ~ 7).

The TRLFS spectra of the adsorbed U(VI) surface species on kaolinite indicate at least two surface species with two different fluorescence lifetimes, i.e., one short- and one long-lived species. The results of the fluorescence lifetime determinations for all measured samples are summarized in Tab. 10.5. The values of the fluorescence lifetimes of both species demonstrate no dependence on pH value.

**Tab. 10.5:** Fluorescence lifetimes of the U(VI) species adsorbed onto kaolinite, errors represent 1σ.

| Sample | pH | $\tau_1$ (ns) | $\tau_2$ (ns) |
|---|---|---|---|
| U5 | **5** | 5640 ± 150 | 40800 ± 440 |
| U6 | **6** | 6880 ± 150 | 41300 ± 470 |
| U7 | **7** | 5610 ± 120 | 44100 ± 630 |
| U8 | **8** | 5330 ±160 | 43700 ± 730 |
| **Mean lifetime** | | **5870 ± 690** | **42480 ± 1670** |

Six fluorescence emission bands were obtained for the fluorescence spectra of all measured samples, which can be described by a set of six absorption peaks similarly to the work of Bell and Biggers (1968). The deconvoluted fluorescence spectra revealed six characteristic fluorescence emission bands that are almost identical for both U(VI) surface species. The peak

maxima are situated at 486.9 ± 0.9, 501.8 ± 0.6, 520.6 ± 0.9, 541.7 ± 0.7, 567. 8 ± 1.5, and 583.3 ± 0.6 nm. The positions of peak maxima are shifted significantly relative to the values for free uranyl ion in perchlorate medium (see Bell and Bigers, 1968). The shifts range from 16.8 nm for the first peak to 9.7 nm for the fifth one.

Due to coincidence of all the fluorescence peaks, the two adsorbed U(VI) surface species are assumed to be similar in coordination environment throughout the investigated pH range. Thus, they should have identical numbers of hydroxyl groups in their first coordination sphere, as different numbers of hydroxyl group cause changes in the spectral features (Baumann et al., 2005). Shorter fluorescence lifetimes indicate more water molecules in the coordination environment of the respective adsorbed U(VI) surface species, because water molecules quench the fluorescence lifetime (Arnold et al., 2006). On this basis, it can be concluded that U(VI) forms two surface species on kaolinite, which differ in the amount of water molecules in their coordination environment.

### 10.3.3 Measurements in the ternary system U(VI)-humic acid-kaolinite

The original TRLFS spectrum of U(VI) adsorbed on kaolinite in the presence of HA at pH ~ 7 is shown in Fig. 10.14 as representative of the original spectra of all samples with U(VI) adsorbed onto kaolinite in the presence of HA at different pH values.

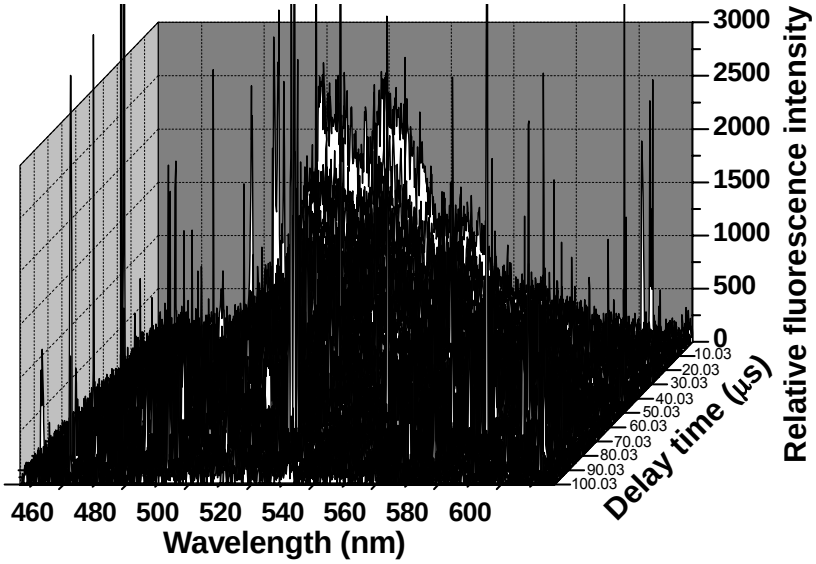


**Fig. 10.14:** TRLFS spectrum of U(VI) adsorbed onto kaolinite in the presence of HA (pH ~ 7).

It is obvious that, compared to the original TRLFS spectrum of U(VI) adsorbed onto kaolinite in the absence of HA at the same pH value, the spectrum has a lower quality due to the high signal noise because of the presence of HA. Therefore, the lifetime analysis and also the detection of the emission bands were more complicated and resulted in higher standard deviations.

The lifetimes of U(VI)-HA fluorescence species were determined from bi-exponential fit analysis of the obtained data. Comparable to the binary system, two different surface species with two different fluorescence lifetimes were indicated. Due to the high signal noise in the spectra the analysis was performed in the shortened wavelength range: 480 nm – 600 nm. The average fluorescence lifetimes were calculated from Eq. (10.1). The results of fluorescence lifetime determinations are summarized in 10.6. The obtained fluorescence lifetimes are not as consistent as in the binary system.

**Tab. 10.6:** Fluorescence lifetimes of the U(VI) species sorbed onto kaolinite in the presence of HA.

| Sample | pH | $\tau_1$ (ns) | $\tau_2$ (ns) |
|---|---|---|---|
| U-HA5 | **5** | 3540 ± 490 | 26300 ± 410 |
| U-HA6 | **6** | 4770 ± 370 | 31400 ± 1400 |
| U-HA7 | **7** | 4540 ± 220 | 32700 ± 450 |
| U-HA8 | **8** | 4680 ± 450 | 34700 ± 2980 |
| **Mean lifetime** | | **4380 ± 570** | **31300 ± 3580** |

Due to the lower quality of the spectra and the shortening of the evaluated wavelength range, the detection of the fluorescence emission bands was limited. As in the binary system, six peaks were assumed to describe satisfactorily the measured spectra. However, the position of the last peak was very uncertain and thus, only the positions of the first five peaks were found. The peaks maxima are situated at 486.6 ± 1.1, 501.1 ± 2.2, 520.5 ± 1.5, 542.2 ± 2.6, and 566.7 ± 3.6. Two different obtained lifetimes indicate, as in the binary system, the formation of at least two different surface complexes. The interpretation of these two complexes is, however, more complicated due to the presence of HA. Uranyl humate itself does not show fluorescence under the applied experimental conditions (Sachs et al., 2006). So if U(VI) would be bound on kaolinite via HA, no U(VI) fluorescence should be measured for the prepared U(VI)-HA-kaolinite samples. This leads to the conclusion that U(VI) is not bound to kaolinite via HA.

### 10.3.4 Comparison of TRLFS measurements in the binary and ternary systems

Table 10.7 shows the comparison of the fluorescence intensities and the amounts of U(VI) adsorbed onto kaolinite of the samples prepared at pH ~ 7 in the presence and absence of HA. It can be seen that the U(VI) adsorption onto kaolinite is comparable in both cases. The difference in the adsorbed amounts is only 7%, while the fluorescence intensity is almost five times lower in the presence of HA than in its absence. It is obvious that HA decreases the measured fluorescence intensity of the samples. This points out to differences in surface speciation in both compared systems.

**Tab. 10.7:** Comparison of the relative fluorescence intensity and the amount of U(VI) adsorbed onto kaolinite of the samples prepared at pH ~ 7 in the absence and presence of HA.

| pH ~ 7 | U(VI)adsorb. (%) | RFI[a] |
|---|---|---|
| **HA absence** | 91 | 12000 |
| **HA presence** | 98 | 2500 |

[a] Relative fluorescence intensity

Table 10.8 shows the comparison of the mean values of the fluorescence lifetimes of both species obtained in the presence and absence of HA. In the presence of HA, the fluorescence lifetimes of both species are significantly shorter. Shorter fluorescence lifetimes indicate HA in the coordination environment of the adsorbed U(VI) surface species, because HA quenches the fluorescence lifetime. This means that in the presence of HA the hydrate shell of uranyl ions is partly displaced with HA.

**Tab. 10.8:** Comparison of fluorescence lifetimes in the absence and presence of HA.

| pH 5 - 8 | $\tau_1$ (ns) | $\tau_2$ (ns) |
|---|---|---|
| **HA absence** | **5900** ± 700 | **42500** ± 1700 |
| **HA presence** | **4400** ± 600 | **30900** ± 3600 |

In Fig. 10.15 the obtained lifetimes of the surface species identified in the presence and absence of HA as a function of pH values are depicted. It becomes evident that pH values have no significant influence on the fluorescence lifetimes of U(VI) surface species in the binary as well as in the ternary system.

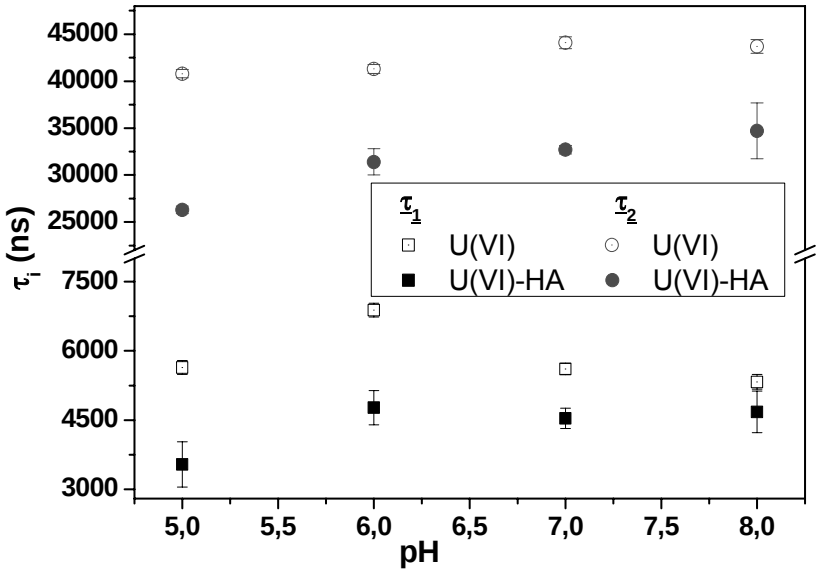


**Fig. 10.15:** Fluorescence lifetimes as a function of pH values.

Six fluorescence emission bands were obtained for the fluorescence spectra of all measured samples of U(VI) adsorbed onto kaolinite in the absence of HA. In the presence of HA, only five peaks were found due to the lower quality of the spectra. The comparison of the mean values of identified peak positions for the samples in the absence and presence of HA is given in Tab. 10.9. No differences in peak positions were observed. Therefore, it can be concluded that HA does not influence the peak positions of both surface species.

**Tab. 10.9:** Comparison of absorption peak positions in the absence and presence of HA.

| pH 5 – 8 | 1st peak | 2nd peak | 3rd peak | 4th peak | 5th peak | 6th peak |
|---|---|---|---|---|---|---|
| **HA absence** | 486.9 ± 0.9 | 501.8 ± 0.6 | 520.6 ± 0.9 | 541.7 ± 0.7 | 567.8 ± 1.5 | 583.3 |
| **HA presence** | 486.6 ± 1.1 | 501.1 ± 2.2 | 520.5 ± 1.5 | 542.2 ± 2.6 | 566.7 ± 3.6 | - |

### 10.3.5 Comparison with model systems

Spectroscopic techniques were used to obtain detailed information about the U(VI) interaction with kaolinite. They should help to identify, on which of possible binding sites of kaolinite (silanol, aluminol groups) U(VI) prefers to adsorb. Unfortunately, in EXAFS it is not possible to distinguish between Al and Si atoms. To decide between aluminol and silanol groups, TRLFS measurements of the system U(VI)-kaolinite were compared with U(VI)-gibbsite

(Křepelová et al. 2006c) and U(VI)-silica gel (Trepte, 2006) systems. Gibbsite, $Al(OH)_3$, was chosen as a model mineral for aluminol sites and silica gel, $SiO_2$, represents silanol binding groups. Tab. 10.10 shows the comparison of mean values of fluorescence lifetimes obtained for the U(VI)-kaolinite system and for both model systems. In all systems, at least two fluorescence lifetimes were identified.

**Tab. 10.10:** Comparison of mean values of fluorescence lifetimes obtained for the systems studied in this work with those of the model systems $UO_2$-gibbsite and $UO_2$-silica gel.

| System | $\tau_1$ (ns) | $\tau_2$ (ns) | Reference |
|---|---|---|---|
| **$UO_2$-gibbsite** | 2360 ± 220 | 13200 ± 2500 | Křepelová et al. 2006c |
| **$UO_2$-silica gel** | 138400 ± 52900 | 361800 ± 103200 | Trepte, 2006 |
| **$UO_2$-kaolinite** | 5900 ± 700 | 42500 ± 1700 | this work |
| **$UO_2$-HA-kaolinite** | 4400 ± 600 | 30900 ± 3600 | this work |

It becomes evident that the values of fluorescence lifetimes of both fluorescence species on kaolinite lie in the range between values obtained for gibbsite and for silica gel, however, the fluorescence lifetimes of species on kaolinite are closer to those on gibbsite than on silica gel. It seems that U(VI) adsorbs on both kinds of available sites but not equal. It is not easy to identify, in which ratio they are represented or which binding sites are more occupied by U(VI). Aluminol binding sites are assumed to control the sorption of U(VI). In untreated kaolinite, the excess of $Al_2O_3$ was found by chemical analysis (cf. Tab. 2.1). From electron scanning microscopy of kaolinite particles, the ratio between planes and edges of kaolinite particles was calculated to be about 0.72, which indicates a higher amount of edges relative to basal planes. Similarly, Brady et al. (1998) reported higher percentage of edges relative to basal plane of the kaolinite KGa-1 resulting from scanning force microscopy. They also reported elevated reactivity of Al edge sites, relative to Si, and the weak sorption on basal planes resulting from their molecular modeling.

In conclusion, two adsorbed U(VI) species on kaolinite were identified in the binary (U(VI)-kaolinite) as well as in the ternary (U(VI)-HA-kaolinte) system. Both surface species can be attributed to adsorbed bidentate mononuclear surface complexes, in which two equatorial oxygen atoms of the uranyl ion are bound to two Al and/or Si (preferentially to Al) atoms of aluminol octahedra and/or silicon tetrahedra. Both surface species differ likely in the amount of water molecules in their coordination environment. In the ternary system, U(VI) prefers direct binding to the kaolinite than via HA, which is distributed between kaolinite particles. The hydrate shell of U(VI) is partly displaced with complexed HA.

# 11 Uranium(VI) sorption onto synthetic humic substance-kaolinite sorbates

Batch experiments in the ternary system U(VI)-HA-kaolinite showed that HA affects the U(VI) sorption onto kaolinite (chapter 10.1). However, natural clays are closely associated with a mélange of natural organic matter. Therefore, a more complex interaction is expected in contrast to the ternary system. The synthetic humic substance-kaolinite sorbates developed within this project contain a mixture of humic-like materials, especially humic substances that are assumed to be more hydrophobic than synthetic HA-like substances that were extracted from these sorbates directly after their syntheses (chapter 5). These sorbates can be used as model compounds for natural organic rich clays. They offer the possibility to approach natural conditions.

Within the project the U(VI) sorption onto two different types of synthetic humic substance-kaolinite-sorbates was studied. The results were compared to those of the ternary system U(VI)-HA-kaolinite and the binary system U(VI)-kaolinite.

During the syntheses of humic substance-kaolinite-sorbates, kaolinite is heated at 80 °C for 90 h in aqueous solution and is subjected to an alkaline and acidic treatment during the isolation of the sorbates. In order to study the influence of these treatments on the sorption properties of kaolinite, a pure kaolinite sample underwent the whole synthesis procedure described in chapter 5, however, without addition of further precursor substances. The U(VI) sorption behavior of the resulting product was measured in comparison to that of original kaolinite KGa-1b.

## 11.1 Experimental

The batch experiments described in this report were performed with synthetic humic-substance-kaolinite sorbates type M1-KS(B) and M42-KS (see chapter 5.3). The sorption experiments were carried out under ambient atmosphere according to the sorption experiments described in chapter 10. However, slightly changed experimental conditions were applied.

***U(VI) sorption onto synthetic humic substance-kaolinite-sorbates***

Humic-substance-kaolinite sorbates M1-KS(B) (batch M189KS, TOC: 3.9 mg/g) and M42-KS (batch R11/04KS, TOC: 4.9 mg/g) were pre-equilibrated with 0.01 M $NaClO_4$ solution for 96 h between pH 3 and pH 10. The solid-to-liquid ratio (S/L) was 4 g/L. The resulting TOC content in the samples amounts to about 16 and 20 mg/L for M1-KS(B) and M42-KS, respectively. For the studies at pH >7, a calculated amount of $NaHCO_3$ was added to the suspensions to accelerate the equilibration with atmospheric $CO_2$. After pre-equilibration, a $UO_2(ClO_4)_2$ stock solution was added to the suspensions with a final U(VI) concentration of $1 \cdot 10^{-6}$ M. The pH values of the samples were readjusted immediately and the samples were shaken for 72 h. After shaking, the final pH values were measured and the samples were centrifuged for phases separation (30 min at 4000 rpm; model Megafuge 1.0, Heraeus Sepatech). The supernatants were removed from the solids and the U(VI) concentrations of the solutions were measured without further filtration by ICP-MS (ELAN 6000, Perkin Elmer). As humic substances were extracted from the humic substance-kaolinite-sorbates, the dissolved humic material was digested with $HNO_3$ in a microwave oven (model mls 1200 mega, MLS) before ICP-MS analyses. The U(VI) sorption onto the vial walls was investigated. For that, the vials were washed with water and dried. Then, 7 mL 1 M $HNO_3$ were added, the vials were shaken for 2 days and the U(VI) concentration in the $HNO_3$ solution was measured by ICP-MS. The amount of uranium adsorbed on the surface of the humic substance-kaolinite sorbates was calculated as the difference between the initial uranium concentration in solution and the sum of the amounts of uranium remaining in solution and adsorbed onto the vial walls.

In order to assess the amount of humic material released from the sorbates after the end of the experiments, UV-vis measurements (CARY-5G, Varian) were performed. The amount of humic substances in solution was estimated from the absorption intensities at 254 nm. Calibration curves were used from experiments where the pH dependent TOC release from synthetic humic-substance-kaolinite sorbates was studied.

***U(VI) sorption onto original and treated kaolinite in absence of humic acid***

The U(VI) sorption onto the original kaolinite and the kaolinite sample that was subjected to the synthesis procedure for humic substance-kaolinite-sorbates (see above) was studied under comparable experimental conditions: S/L: 4 g/L, pH 3-10, I: 0.01 M $NaClO_4$, [U(VI)]: $1 \cdot 10^{-6}$ M. After the contact time of 72 h, the sample phases were separated by centrifugation (4000

rpm, 30 min) and the U(VI) concentration in the supernatants was mesured by ICP-MS without prior filtration step. The U(VI) sorption onto the vial walls was determined as described above.

***U(VI) sorption onto original kaolinite in presence of humic acid***

In order to compare the U(VI) sorption onto the humic substance-kaolinite-sorbates type M1-KS(B) and M42-KS with that of U(VI) onto kaolinite in presence of separately added HA, sorption experiments with HA type M1 or M42 were carried out applying comparable TOC contents in solution. For that the basic experimental conditions were kept constant (S/L: 4 g/L, pH 3-10, I: 0.01 M $NaClO_4$, [U(VI)]: $1 \cdot 10^{-6}$ M). HA concentrations of 29 and 35 mg/L HA type M1 and M42, respectively, were applied. These concentrations correspond to about 19 and 20 mg/L TOC. For the experiments, HA type M1 (batch M100A, Sachs et al. 2003) and type M42 (batch M145) were used. The HA solutions were spiked with $^{14}C$-labeled HA type M1 (batch M130/4, 54.8 MBq/g) and type M42 (batch M180, 17.0 MBq/g) in order to determine the HA sorption onto kaolinite.

After pre-equilibration of kaolinite KGa-1b, uranyl humate solutions equilibrated for 24 h were added to the samples resulting in final U(VI) concentrations of $1 \cdot 10^{-6}$ M and the HA concentrations given above. The pH values of the suspensions were readjusted and the samples were shaken for 72 h. Then, the final pH values were measured, solutions and solids were separated by centrifugation (4000 rpm, 30 min). The remaining U(VI) concentrations in solution were analyzed by ICP-MS after digestion of the HA (see above). The HA concentrations were measured by liquid scintillation counting (LSC; Wallac System 1414, Perkin Elmer). Finally, the vial wall sorption of U(VI) and HA was determined using 1 M $HNO_3$ and 1 M NaOH, respectively, as described above.

## 11.2 Results and discussion

### 11.2.1 U(VI) sorption onto original and synthetic treated kaolinite KGa-1b

Figure 11.1 shows the results of the U(VI) sorption onto original kaolinite KGa-1b in comparison to that of U(VI) sorbed onto kaolinite that was treated by the synthesis procedure for humic substance-kaolinite-sorbates.

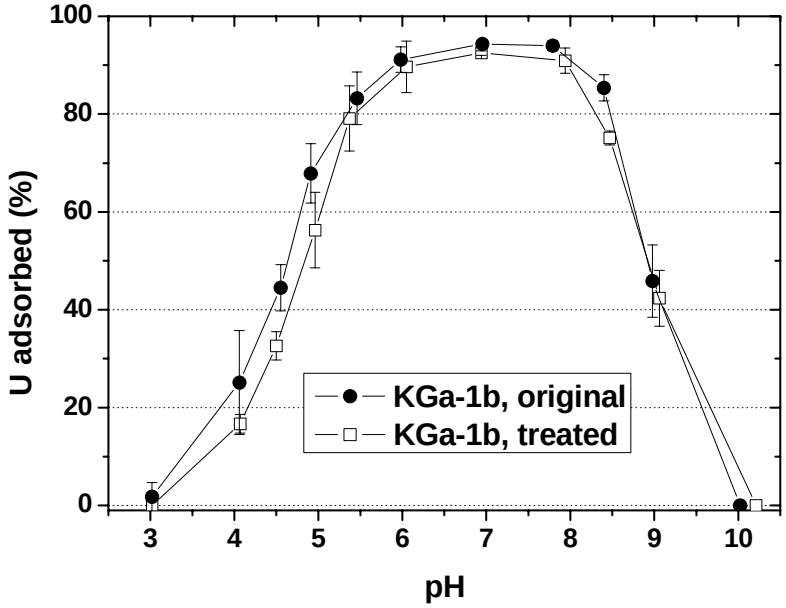


**Fig. 11.1:** U(VI) sorption onto original and treated kaolinite KGa-1b ([U(VI)]: $1 \cdot 10^{-6}$ M, I: 0.01 M $NaClO_4$, S/L: 4 g/L).

The sorption data obtained for U(VI) onto original kaolinite KGa-1b are in good agreement with those depicted in Fig. 10.7, where the sample solutions were subjected to an additional filtration step. The untreated and treated kaolinite samples exhibit a comparable sorption capacity for U(VI) between pH 3 and 10 within the experimental errors. From that it can be concluded that the synthesis procedure, i.e., the heating as well as the alkaline and acidic treatment of kaolinite, during the preparation of humic substance-kaolinite-sorbates has no significant influence on the sorption properties of KGa-1b.

### 11.2.2 U(VI) sorption onto synthetic humic substance-kaolinite-sorbates in comparison to that of U(VI) onto kaolinite in presence of humic acid

Figure 11.2 illustrates the results of the U(VI) sorption onto the synthetic humic substance-kaolinite-sorbate type M1-KS(B) in comparison to that of U(VI) onto kaolinite in absence and presence of HA. The sorbed/bound amounts of humic matter in the studied systems as a function of pH are plotted in Fig. 11.3.

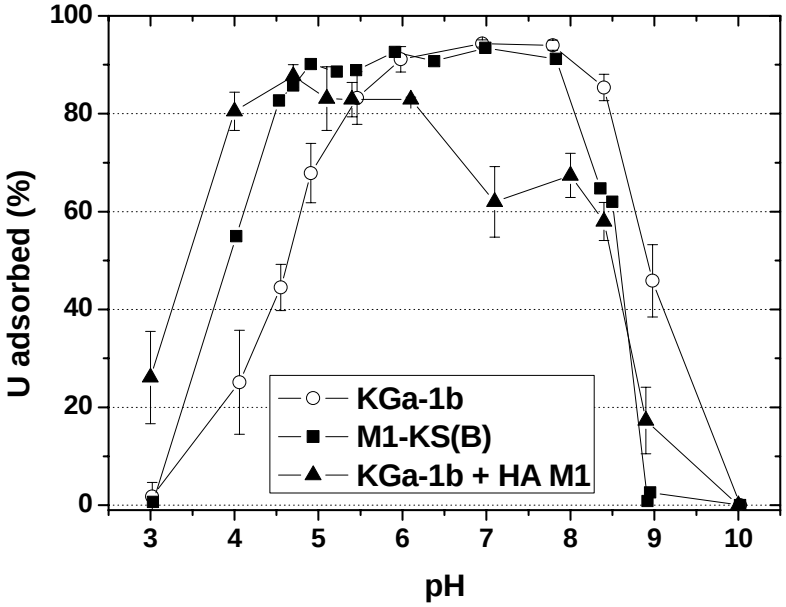


**Fig. 11.2:** U(VI) sorption onto M1-KS(B) in comparison to the U(VI) sorption onto KGa-1b in absence and presence of 29 mg/L HA type M1 ([U(VI)]: $1 \cdot 10^{-6}$ M, I: 0.01 M $NaClO_4$, S/L: 4 g/L, TOC: 16 mg/L (M1-KS(B)) and 19 mg/L (HA M1)).

As already discussed in chapter 10.1, it can be concluded from Fig. 11.2 that humic substances influence the U(VI) sorption onto kaolinite. Compared to the HA-free system, the U(VI) sorption onto kaolinite is increased in the acidic pH range between pH 3 and 5, whereas it is decreased in the ternary system (U(VI)-HA M1-KGa-1b) between pH 6 and 8. The increase is attributed to the sorption/association of humic substances onto/with kaolinite which provides additional binding sites for U(VI). The amount of sorbed humic matter onto kaolinite is decreased with increasing pH value (see Fig. 11.3). As a result of this release, soluble binary and ternary uranyl humate complexes can be formed resulting in the decrease of the sorbed amount of U(VI). However, despite of similar initial TOC concentrations, the effect of humic material on the U(VI) sorption onto M1-KS(B) differs significantly from that

onto KGa-1b in presence of HA type M1. In presence of 28 mg/L HA type M1, significantly less U(VI) is sorbed onto KGa-1b than in the system M1-KS(B).

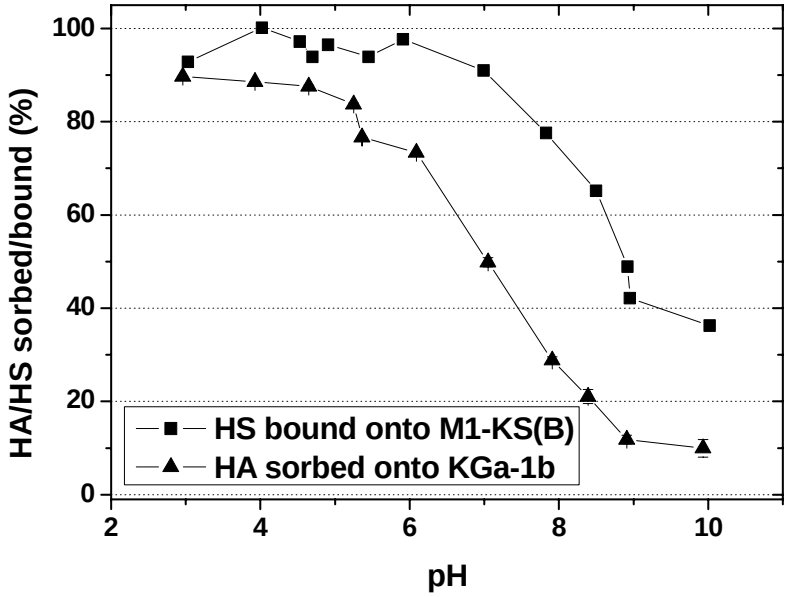


**Fig. 11.3:** Estimated amount of humic substances (HS) sorbed onto M1-KS(B) in comparison to the amount of HA type M1 sorbed onto KGa-1b.

The amount of sorbed/bound humic substances is decreased with increasing pH value in both systems (see Fig. 11.3). However, the HA in the ternary system is more mobile than the organic matter in the humic substance-kaolinite-sorbate. It is not clear if the material liberated from M1-KS(B) represents HA slowly released from the sorbate and not extracted during the isolation of the sorbate or if this material is produced by chemical transformations of non-HA-like substances during the batch experiments. Balcke et al. (2002) reported that the adsorption affinity of humic substances onto clays correlates directly with their aromaticity and inversely with their polarity. Based on that it is supposed that the humic matter associated with M1-KS(B) represents more hydrophobic humic substances with a higher aromaticity and a lower polarity than HA type M1. Probably, the humic material released from M1-KS(B) is a weaker complexing agent for U(VI) and keep less U(VI) in solution.

In all three systems, a further strong reduction of the U(VI) sorption can be observed between pH 8 and 10 (see Fig. 11.2). This behavior can be attributed to two overlapping and competing processes: (i) the formation of soluble U(VI) humate complexes and (ii) the formation of U(VI) carbonates which dominates the U(VI) sorption in the HA-free system in this pH range (see chapter 10.1).

Figure 11.4 depicts the U(VI) sorption onto M42-KS in comparison to that onto kaolinite in absence and presence of HA type M42. The amounts of sorbed humic matter onto M42-KS and kaolinite are shown in Fig. 11.5.

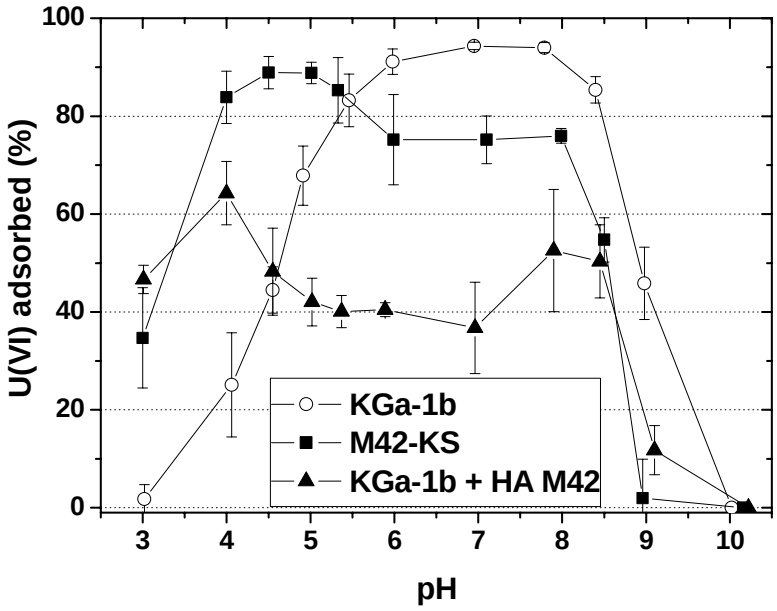


**Fig. 11.4:** U(VI) sorption onto M42-KS in comparison to the U(VI) sorption onto KGa-1b in absence and presence of 35 mg/L HA type M42 ([U(VI)]: $1 \cdot 10^{-6}$ M, I: 0.01 M $NaClO_4$, S/L: 4 g/L, TOC: 20 mg/L (M42-KS) and 20 mg/L (HA M42)).

In general, the humic matter bound in M42-KS as well as HA type M42 influences the U(VI) sorption in a similar way as discussed in the systems with M1-KS(B) and HA type M1. However, the mobilizing effect in the neutral pH range is stronger pronounced. In the acidic pH range (pH 3-5: M42-KS; pH 3-4.5: KGa-1b + HA M42) the U(VI) sorption in presence of humic materials is increased. At higher pH values (pH ≥5-8) the U(VI) sorption is significantly reduced. Again, both systems differ significantly in their mobilizing properties on U(VI) which is attributed to their different release behavior of humic matter in the solutions (see Fig. 11.5). The reasons for that are the same as described above, namely differences in the aromaticity and the polarity of the humic materials.

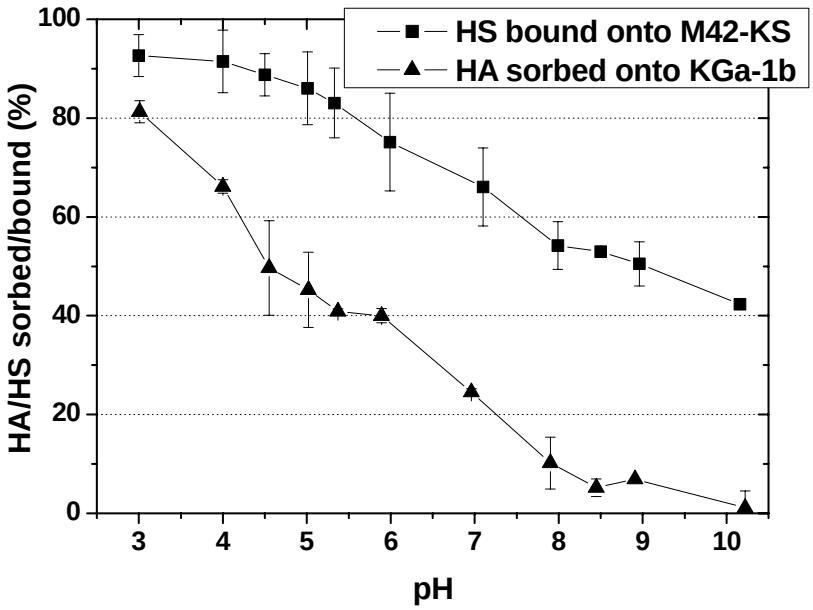


**Fig. 11.5:** Estimated amount of humic substances (HS) bound onto M42-KS in comparison to the amount of HA type M42 sorbed onto KGa-1b.

Comparing the sorption data shown in Fig. 11.2 and 11.4 it becomes obvious that the humic substances released from M42-KS as well as desorbed HA type M42 exhibits a stronger mobilizing effect on U(VI) than those released from M1-KS(B) and HA type M1. One possible reason for that is found in the slightly higher TOC concentrations in the system U(VI)-M42(KS) and U(VI)-HA M42-KGa-1b. This results in higher humate concentrations in solution and consequently in an increased uranyl humate complex formation. Nevertheless, differences in the aromaticity and the polarity influencing the sorption properties of the humic matter can also cause the observed dissimilarities. Previously, in own NMR studies it was found that HA type M1 is characterized by a higher aromaticity than HA type M42.

Compared to the studies of Křepelova et al. (2006b) differences in the sorption behavior of U(VI) in the ternary system with HA type M42 were found in the basic pH range. Křepelova et al. (2006b) found a higher U(VI) sorption due to a possible interaction of uranyl carbonato humate complexes with the kaolinite surface. This behavior cannot be confirmed by these studies. Differences in the sample preparation (analysis of the supernatant solutions after centrifugation without filtration) could be the reason. Probably, the applied centrifugation is not able to remove U(VI)-HA-kaolinite colloids at such high HA concentrations from the solutions. Hence, the amount of U(VI) in solution was slightly overestimated, resulting in lower sorption rates.

The formation of humic matter-kaolinite colloids will be subject of future studies. Additionally, the structural and functional properties of humic matter released from the sorbates will be studied in more detail and compared to those of HA.

Humic substances associated with clay minerals can influence the migration behavior of U(VI). On the one hand, immobilization of U(VI) can occur due to humic matter associated with the clay. On the other hand, the release of humic substances from the clay and the formation of U(VI) humate complexes in solution can mobilize U(VI). The impact of humic substances on the migration behavior of U(VI) is controlled by the pH value and the structural and functional properties of the humic matter in the clay and in the aquifer systems. It was shown that HA separately added to the system can cause a stronger immobilizing effect on U(VI) than humic matter associated with clay.
These experiments show that synthetic humic-substance-kaolinite sorbates can be used as model compounds for organic matter-containing natural clay minerals. Processes influencing the migration behavior of actinide ions in clay formations can be identified by the use of these materials.

# 12 Neptunium(V) sorption onto kaolinite in the absence and presence of humic acid

In this work, the sorption of Np(V) onto kaolinite is studied under aerobic conditions as a function of pH, ionic strength and Np concentration in a series of batch equilibrium experiments. Furthermore, the effect of HA on the Np sorption is studied in order to determine whether humic material is likely to significantly influence Np sorption on kaolinite.

## 12.1 Experimental

### *Materials*

For the sorption experiments the kaolinite standard KGa-1b from the Clay Minerals Society Source Clays Repository (Washington County, Georgia) was applied. The material is described in detail in chapter 2.

For preparation of a Np(V) stock solution, solid $^{237}NpO_2$ was dissolved in $HNO_3$. The Np solution was purified by anion exchange (Dowex 1X8) according to the procedure described in (Seibert, 1999). The effluent was evaporated repeatedly to dryness with addition of $HClO_4$ and redissolved in 1 M $HClO_4$. The hexavalent Np thus obtained was reduced electrolytically to Np(V).

As HA the $^{14}C$-labeled synthetic HA type M42 (charge M180, specific activity: 17 MBq/g) and the inactive HA type M42 (charge M145) (see chapter 3) were used for the experiments.

***Sorption experiments***

40 mg kaolinite were weighed into 15 mL centrifuge tubes (PP, Nalgene). For sorption experiments in the absence and presence of HA, 10 mL and 9 mL 0.01/0.1 M $NaClO_4$ solution, respectively, were added. Then, the desired pH values (pH 6 to pH 10.5) were adjusted by addition of diluted $HClO_4$ or NaOH. For studies at pH values higher than 7, a calculated amount of $NaHCO_3$ was added to accelerate the equilibrium process with atmospheric $CO_2$. During pre-equilibration of the samples (60 h), the samples were shaken continuously and the pH values were readjusted.

The HA stock solutions were prepared by dissolving 2.5 mg $^{14}C$-labeled synthetic HA type M42 (charge M180) and 10 mg inactive HA type M42 (charge M145/00) in 25 mL 0.01/0.1 M $NaClO_4$. The Np(V) stock solutions were prepared prior to each sorption run by passing the solutions through Dowex-50 to separate the $^{233}Pa$ daughter from $^{237}Np$, so that the determination of the β-active nuclide $^{14}C$ of the $^{14}C$-labeled HA by liquid scintillation (LS) counting was not interfered from the beta decay of $^{233}Pa$. The oxidation state of Np in the stock solutions was spectroscopically confirmed to be pentavalent. Different dilutions of the Np(V) stock solutions were prepared.

The sorption experiments in the absence of HA were started by adding about 60 µL Np(V) stock solution to the preconditioned kaolinite. The sorption experiments in the presence of HA were started by adding 1 mL HA stock solution and instantly after this about 60 µL Np(V) stock solution to the preconditioned kaolinite. The initial Np and HA concentrations in the sample solutions were $1 \cdot 10^{-5}$ M or $1 \cdot 10^{-6}$ M and 50 mg/L, respectively. The solid solution ratio was 4 g/L. The pH values were readjusted immediately after addition of the stock solutions. Then, the samples were shaken at room temperature for about 72 h during which the Np and HA sorption onto the solids reached equilibrium. After centrifugation of the samples (4000 rpm, 30 min), the equilibrium pH values were measured. The final Np and HA concen-

tration was determined by analyzing the LS spectra recorded with an LS counter (Wallac system 1414, Perkin Elmer) using α-β discrimination. For this, 1 mL of the sample supernatant was mixed with 15 mL of a Ultima Gold$^{TM}$ scintillation cocktail (Packard BioScience Company). The amount of Np and HA adsorbed to the mineral surface was calculated as the difference between the initial Np and HA concentration and the sum of the final Np and HA concentration in the sample solutions and the amount of Np and HA adsorbed onto the vial walls.

## 12.2 Results and discussion

The Np speciation, calculated for the experimental conditions applied in this study, is shown in Fig. 12.1. It was calculated with the geochemical computer code EQ3/6 (Wolery, 1992) applying the Np(V) complexation constants compiled in the NEA data base (Guillaumont et al., 2003), the Np(V) humate complexation constant log$\beta$ = 3.6 and the pH function of the loading capacity (LC) with LC = -0.589 + 0.101 · pH (Sachs et al., 2004). The results show that the free neptunyl ion predominates the Np speciation in aqueous solution up to pH 8.3 both in the absence and in the presence of HA. Starting at about pH 7.3, the neptunyl carbonate species are formed increasingly in solution and dominate the Np speciation above pH 8.3. In the presence of HA, $NpO_2HA(I)$ is formed between pH 6 and pH 9 with a maximum of 11.2% near pH 8. For the higher pH region, the formation of the mixed ternary neptunyl carbonate humate complex is expected. Presently, however, this complex cannot be quantified thermodynamically. The Np speciation calculated for the lower initial Np concentration applied in this study ($1 \cdot 10^{-6}$ M) is not shown because it differs only slightly.

In Fig. 12.2, the pH-dependency of the Np sorption onto kaolinite in the absence of HA is shown as a function of the initial Np concentration. The results obtained for sorption experiments applying $1 \cdot 10^{-5}$ M Np show that the Np sorption increases with pH up to pH 9 and decreases again at higher pH values. At pH 9, $NpO_2CO_3^-$ dominates the Np speciation in solution (cf. Fig. 12.1). Between pH 9 and pH 10, neptunyl carbonate complexes with a higher negative charge are formed in solution ($NpO_2(CO_3)_2^{3-}$, $NpO_2(CO_3)_2(OH)^{4-}$ and $NpO_2(CO_3)_3^{5}$). The surface charge of kaolinite in the considered pH range is also negative (p.z.c. = 6.0 (Redden et al., 1998), p.z.n.p.c. = 5.1±0.2 (Sutheimer et al., 1999), 4.99±0.03 (Schroth and Sposito, 1997)). Thus, the electrostatic repulsion between these neptunyl carbonate complexes and kaolinite decreases the Np sorption onto kaolinite above pH 9.

The decrease of the initial Np concentration from $1 \cdot 10^{-5}$ M to $1 \cdot 10^{-6}$ M leads to a shift of the Np adsorption edge to lower pH values by a half pH unit.

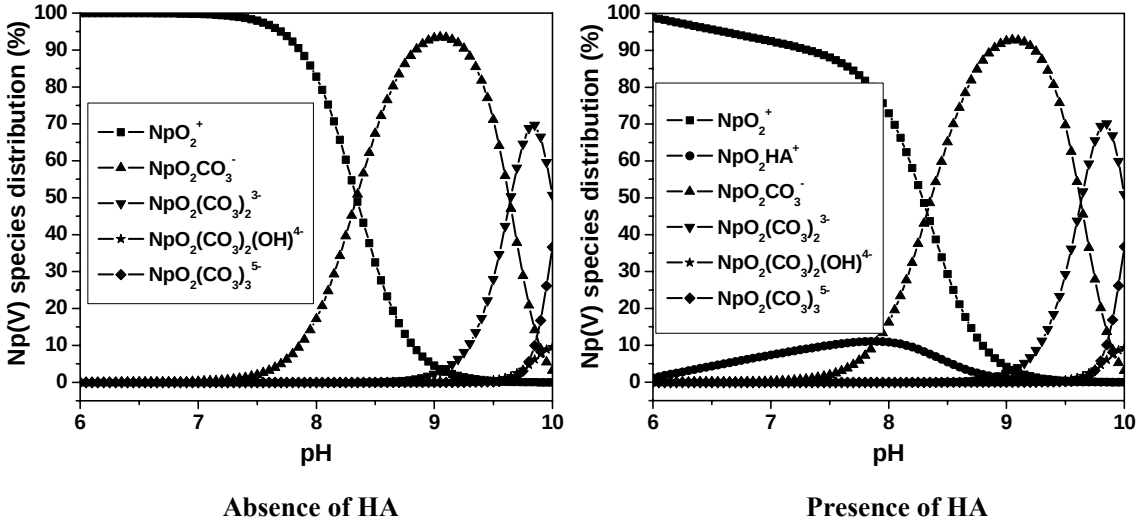


**Fig. 12.1:** Np speciation in solution in the absence and presence of HA ($[NpO_2^+]$: $1 \cdot 10^{-5}$ M; [HA]: 0 or 50 mg/L; I: 0.01 M $NaClO_4$; $pCO_2$: $10^{-3.5}$ atm).

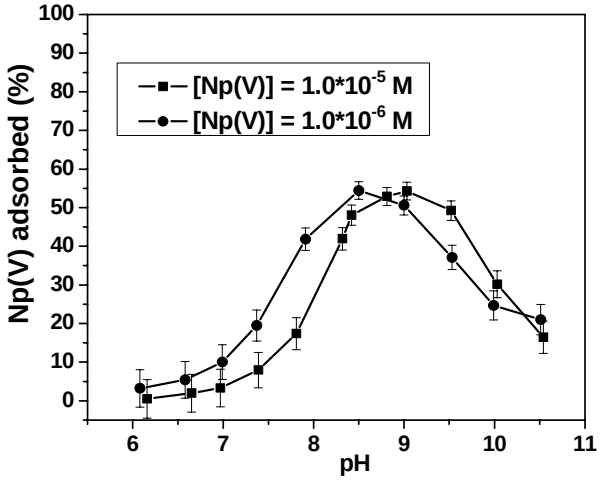


**Fig. 12.2:** Np sorption onto kaolinite in the absence of HA ($[NpO_2^+]$: $1 \cdot 10^{-5}$ or $1 \cdot 10^{-6}$ M; I: 0.01 M $NaClO_4$; $pCO_2$: $10^{-3.5}$ atm).

Figure 12.3 shows the influence of HA on the Np sorption onto kaolinite as a function of pH. In experiments with $1 \cdot 10^{-5}$ M Np the Np sorption is slightly enhanced by HA between pH 6 and pH 7.5. A slightly enhanced Np sorption onto kaolinite in the presence of HA and EDTA between pH 6 and pH 8 was also found by Niitsu et al. (1997) and Kohler et al. (1992), respectively. In experiments with $1 \cdot 10^{-6}$ M Np no effect of HA on the Np sorption is detectable in this pH range. At higher pH values up to pH 10.5 the amount of Np adsorbed onto kaolinite

is decreased by HA. On the one hand, this can be attributed to the formation of dissolved neptunyl humate complexes which are formed in solution between pH 6 and pH 9 with a maximum of 11.2% near pH 8 (cf. Fig. 12.1). On the other hand, the mixed ternary neptunyl carbonate humate complex (mentioned above) would explain the reduction of the Np sorption by HA at pH values higher than 9. The mobilizing effect of HA on Np is more strongly pronounced in sorption experiments with the higher initial Np concentration ($[NpO_2^+]$: $1 \cdot 10^{-5}$ M).

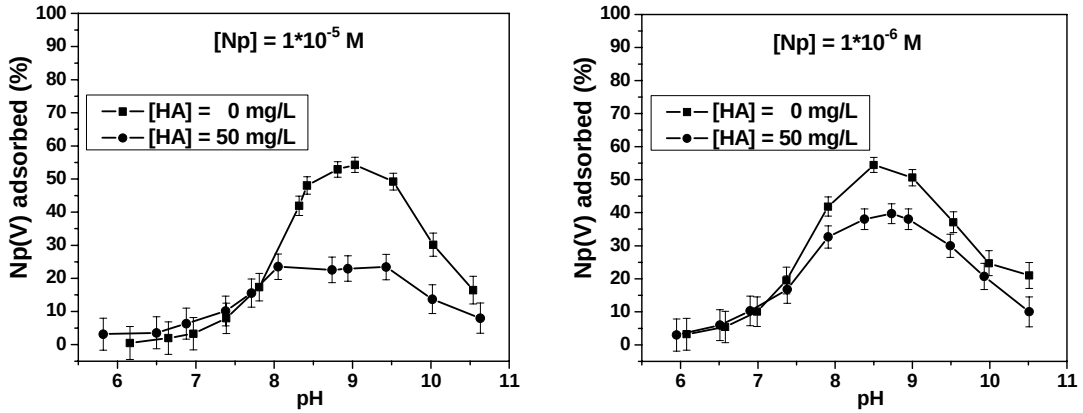


**Fig. 12.3:** Influence of HA on the Np sorption onto kaolinite ($[NpO_2^+]$: $1 \cdot 10^{-5}$ or $1 \cdot 10^{-6}$ M; [HA]: 0 or 50 mg/L, I: 0.01 M $NaClO_4$; $pCO_2$: $10^{-3.5}$ atm).

The HA sorption onto kaolinite as a function of pH in the absence and presence of Np is shown in Fig. 12.4. The HA sorption decreases with increasing pH. This can be attributed to electrostatic repulsion between negatively charged carboxyl groups of HA and the negative surface charge of kaolinite in the considered pH range. The influence of Np on the HA sorption is small for both initial Np concentrations.

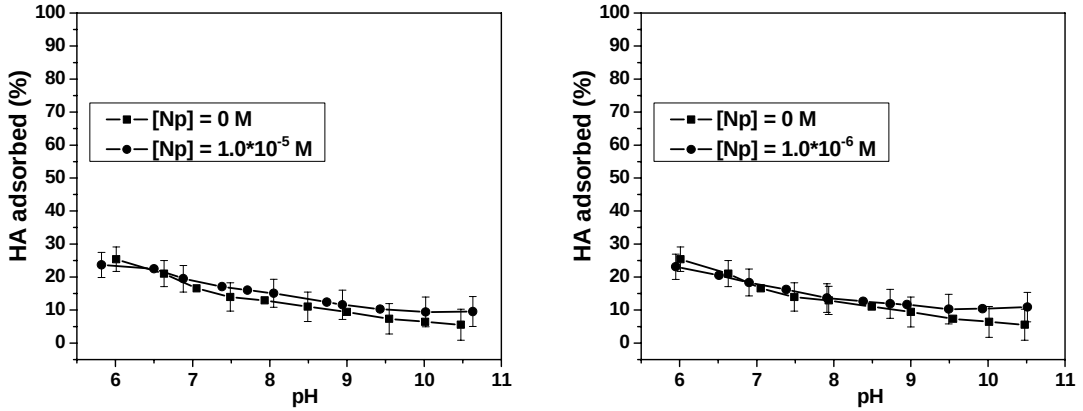


**Fig. 12.4:** HA sorption onto kaolinite in the absence and presence of Np ($[NpO_2^+]$: $1 \cdot 10^{-5}$ or $1 \cdot 10^{-6}$ M; [HA]: 50 mg/L, I: 0.01 M $NaClO_4$; $pCO_2$: $10^{-3.5}$ atm).

The influence of the ionic strength on the Np sorption onto kaolinite in the absence of HA is shown in Fig. 12.5. Compared to the sorption experiments performed with an ionic strength of 0.01 M ($NaClO_4$) the Np sorption is increased between pH 7.4 and pH 10 when a higher ionic strength of 0.1 M ($NaClO_4$) is applied. This result is consistent with the results obtained by Amayri (2006). The effect of the ionic strength on the Np sorption onto kaolinite in the presence of HA is relatively small (not shown here).

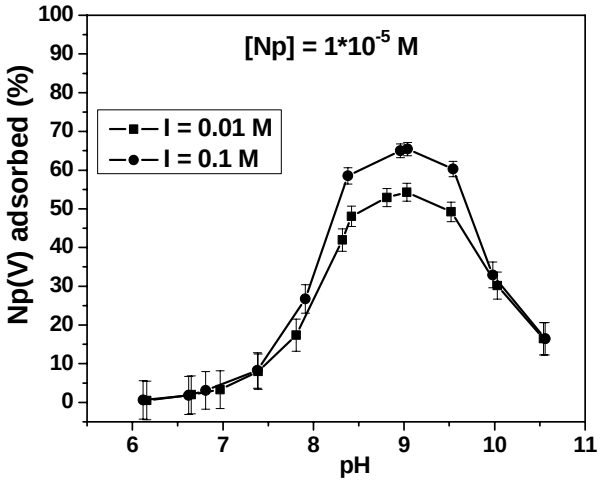


**Fig. 12.5:** Influence of ionic strength on the Np sorption onto kaolinite ([$NpO_2^+$]: $1 \cdot 10^{-5}$ M; I: 0.01 or 0.1 M $NaClO_4$; $pCO_2$: $10^{-3.5}$ atm).

The study showed that the Np(V) sorption on kaolinite under aerobic conditions is effected by pH, ionic strength, Np concentration and the presence of HA. HA influences significantly the Np sorption onto kaolinite. Between pH 7.5 and pH 10.5 the mobility of Np(V) is increased due to HA. This is attributed to formation of dissolved neptunyl humate complexes and/or neptunyl carbonate humate complexes.

# 13 Studies of the migration behavior of humic acids in compacted clay and of the influence of humic acids on the uranium(VI) transport

Little is known on the migration behavior of humic substances in clay formations which is supposed to be governed by diffusion processes. Since HA show a strong ability for complex formation, they can influence the migration of radioactive and non-radioactive toxic metal ions in clayey environments.

The results of former studies on the migration of HA in clay systems and their influence on radionuclide migration are discussed controversially. Wold and Eriksen (2005) found that humic colloids are able to diffuse through compacted bentonite without strong physical hindrance and to mobilize metal ions such as Co(II). Likewise, a nearly unhindered diffusion of lignosulfonate has already been reported by Wold and Eriksen (2003). Wang et al. (2005), however, found a significant immobilization of Eu(III) by humic substances in compacted bentonite.

Maes et al. (2006) studied the migration of radionuclides in Boom Clay and gave information that the bulk of Am(III) dissociates nearly instantaneously from complexes with mobile organic matter and is bound to the clay and immobile organic matter. Only a small part of Am(III) has been transported over short distances. The reversibility of the interaction between radionuclide, organic matter and clay governs the migration of actinides in the organic-rich Boom Clay.

Field studies from Hendry et al. (2003 and 2005) substantiate a diffusive transport through a clay-rich till aquitard. Only the smallest molecular fraction of the dissolved organic matter proved mobile in the field and laboratory tests.

In the present study, we investigated the diffusion behavior of humic colloids in compacted clay as a function of the dry bulk density and of the pH. Furthermore, the impact of HA on the uranium transport was studied at pH 5 and 7. The U(VI) diffusion was measured in absence and presence of HA type M42. Additionally, the diffusion behavior of U(VI) was studied in a synthetic humic substance-kaolinite-sorbate (see chapter 5), representing a model substance for clays containing organic matter.

## 13.1 Experimental

The diffusion of humic colloids and its impact on the U(VI) migration was studied in a laboratory model system at room temperature and ambient air. The schematic set-up of the experiments is shown in Fig. 13.1.

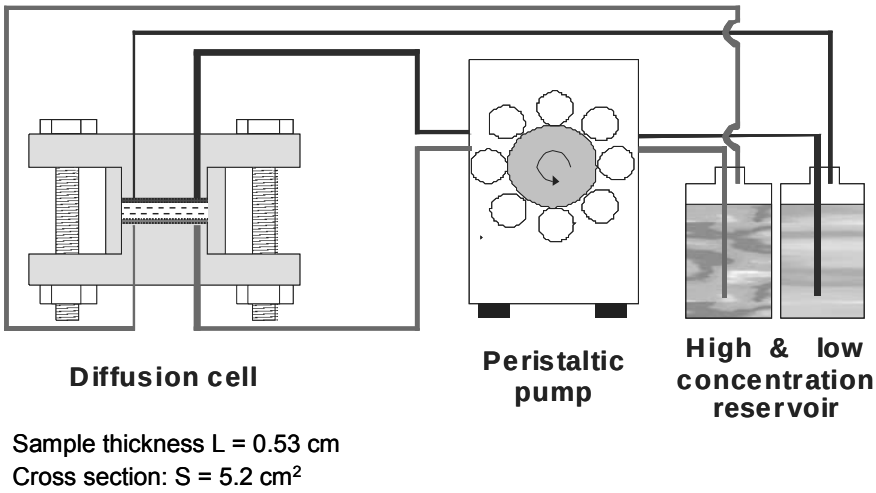


**Fig. 13.1:** Schematic set-up of the diffusion experiments (Van Loon and Soler, 2004).

In order to study the HA diffusion as a function of the porosity, kaolinite KGa-1b was compacted to bulk dry densities of 1.32, 1.56 and 1.67 g/cm$^3$ and fixed between two filter plates in the diffusion cell. For the experiments with U(VI), the kaolinite as well as the synthetic humic substance-kaolinite-sorbate (batch R1/06KS, see chapter 5.3) were compacted to bulk dry densities of 1.56 g/cm$^3$. Subsequently, the clay plugs were equilibrated for 3 to 4 weeks with 0.01 M $NaClO_4$ solution (1 mM $NaN_3$) at pH 5 and pH 7 in case of the experiments with kaolinite and at pH 7 for the study with the synthetic humic substance-kaolinite-sorbate.

The effective porosity of the clay plugs and the effective diffusion coefficient for the non-retarded transport through the cell were measured using tritiated water (HTO) as a conservative tracer. The HA diffusion was studied using $^{14}$C-labeled synthetic HA type M42 (batch M180; see chapter 3) at a concentration of about 12 mg/L. For the experiments involving U(VI), the $UO_2^{2+}$ concentration was $1 \cdot 10^{-6}$ M ($^{238}$U). $^{234}$U was used as tracer in the experiments with humic substances. A steady state through-diffusion technique (Shackelford, 1991; Van Loon and Soler, 2004) with constant concentration gradient was applied. For that, the tracer concentrations at the boundaries ($^{14}$C and/or $^{234}$U, $^{238}$U) have been kept constant. The tracer activities in the high (x = 0) and low (x = L) concentration reservoirs were periodically analyzed by liquid scintillation counting (LSC; Wallac System 1414, Perkin Elmer) with α-β-

separation ($^{14}C$, $^{234}U$) and by ICP-MS ($^{238}U$; Elan 6000, Perkin Elmer). In case of $^{234}U$, the α-LSC spectra were deconvoluted to determine the activity contribution of $^{232}U$ (contamination of $^{234}U$) and its daughter nuclides (Nebelung, 2002).

To give an example, Fig. 13.2 shows the $^{14}C$ and $^{234}U$ tracer concentration at the high concentration boundary for a diffusion experiment with HA and U(VI) as a function of time.

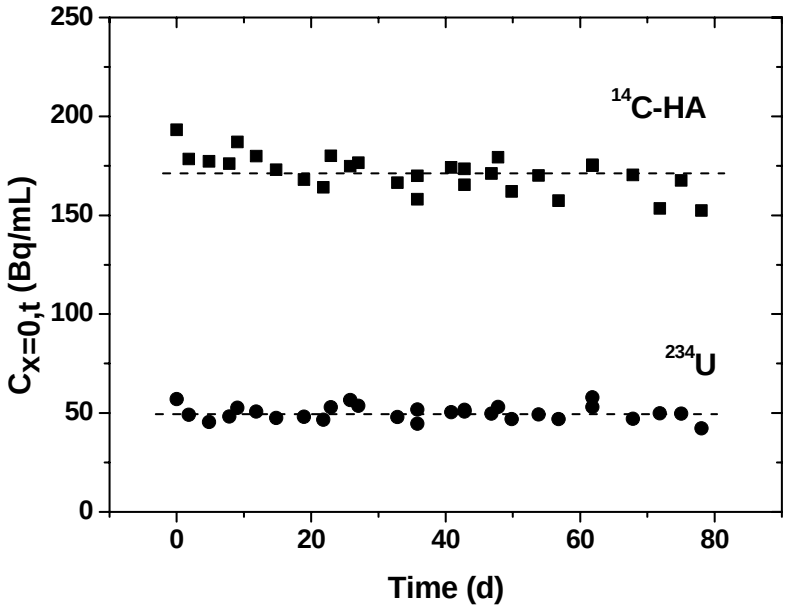


**Fig 13.2:** $^{14}C$ and $^{234}U$ tracer concentration at the high concentration boundary $C_{x=0,t}$ ($\rho_{bulk:}$ 1.56 g/cm$^3$, pH 5).

In one experiment (HA diffusion, pH 5, $\rho_{bulk}$ = 1.56 g/cm$^3$), the high-concentration reservoir has been exchanged with a tracer-free solution after completing the through-diffusion experiment and out-diffusion has been started. The amount of tracer released from the clay to the external reservoirs has been monitored as a function of time.

To determine the tracer concentration within the clay plug, the cells were opened and the clay was cut into slices of 0.5 or 1 mm. After drying, HA and U were extracted from the clay by 1 M NaOH and 1 M $HNO_3$, respectively, and analyzed as described above.

The HA particle size distribution in the high and low concentration reservoir was measured by ultra centrifugation using filters of pore width of 1 to 1000 kD (Microsep Centrifugal Devices, Pall).

## 13.2 Data processing

The data evaluation of the through-diffusion experiments is based on Fick's second law (cf. Shackelford, 1991):

$$\frac{\partial C}{dt} = D_a \frac{\partial^2 C}{\partial x^2} \tag{13.1}$$

with

$$D_a = \frac{D_e}{\alpha} \tag{13.2}.$$

$C$ represents the activity (Bq/m$^3$), $t$ is the time (s), $D_a$ is the apparent diffusion coefficient (m$^2$/s), $x$ is the distance (m), $D_e$ is the effective diffusion coefficient (m$^2$/s), and $\alpha$ is the rock capacity factor (-) according to Eq. (13.3).

$$\alpha = \varepsilon + \rho K_d \tag{13.3}$$

In Eq. (13.3), $\varepsilon$ represents the effective porosity (-), $\rho$ is the bulk dry density (g/m$^3$) and $K_d$ is the distribution coefficient (m$^3$/g). For a non-sorbing tracer, e.g., HTO, $K_d = 0$, thus, $\alpha$ is equal to $\varepsilon$, the porosity accessible for diffusion.

The results of the steady state part of the experiments were fitted to an analytical solution of the diffusion equation (Van Loon et al., 2003). Once steady state is reached, the accumulated activity $A$ (Bq) becomes a linear function of $t$:

$$A(t) = \frac{-SLC_0\alpha}{6} + \frac{SC_0D_e}{L}t \tag{13.4}$$

with $S$ the cross sectional area (m$^2$), $L$ the layer thickness (m), and $C_0$ the initial tracer concentration at the high concentration boundary (Bq/m$^3$). According to Eq. (13.4), $D_e$ and $\alpha$ can be obtained by linear regression. The out-diffusion process can be modeled by a nonlinear equation presented in Van Loon and Soler (2004) not shown here.

In order to describe the transient diffusion profiles, the tracer concentrations in the clay plug were interpreted by Eq. (13.5) according to Crank (1975):

$$\frac{C_{S(x,t=t_{end})}}{C_{B(x=0,t=t_{end})}} = erfc\left(\frac{x}{2\sqrt{D_a t}}\right) \tag{13.5}$$

where $C_{S\,(x,\,t=tend)}$ is the resident concentration in the solid (mol/g) normalized to the concentration at the high concentration boundary $C_{B\,(x=0,t=tend)}$ (mol/g).

## 13.3 Results and discussion

### 13.3.1 Diffusion of HTO

In all experiments, the diffusion of HTO was studied to determine the effective porosity $\varepsilon$ of the kaolinite and the effective diffusion coefficient $D_e$ for the non-reactive tracer diffusion through kaolinite. Figure 13.3 illustrates the diffused activity ($A_{HTO}$) and the diffusive flux in a through-diffusion experiment with HTO.

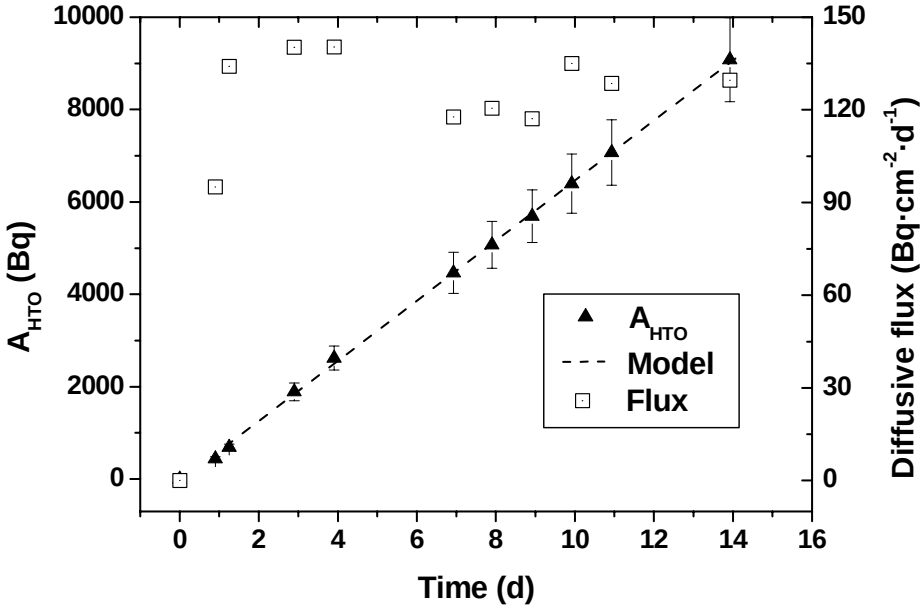


**Fig. 13.3:** Diffused activity and diffusive flux of HTO vs. time ($\rho_{bulk}$: 1.56 g/cm$^3$).

The effective porosities and the effective diffusion coefficients of the conservative tracer of all experiments are summarized in Fig. 13.9 and Tab. 13.1.

### 13.3.2 Humic acid diffusion in compacted clay

Figure 13.4 depicts the amount of HA diffused through the clay and the diffusive flux as a function of time in an experiment at a dry bulk density of 1.56 g/cm$^3$ and pH 5.

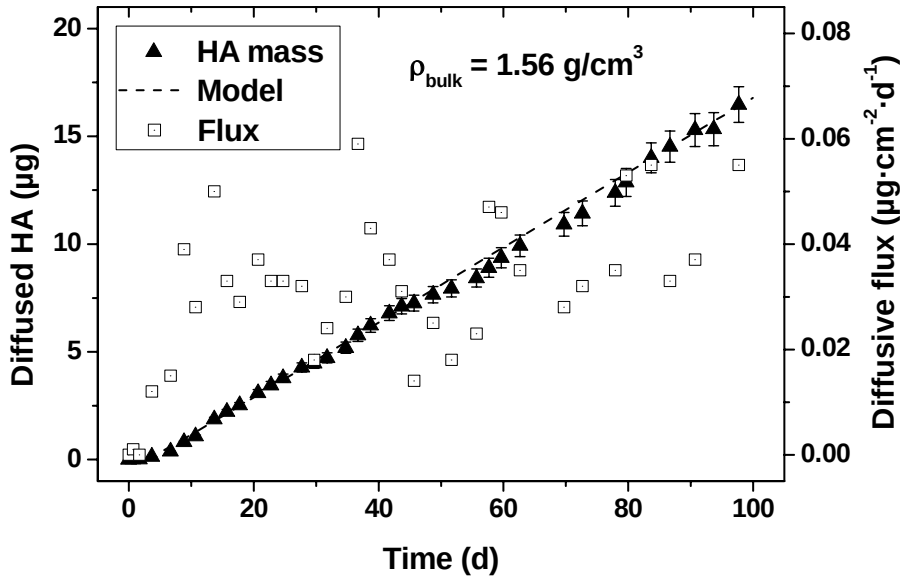


**Fig. 13.4:** Cumulative mass and diffusive flux of HA as a function of time (ρ: 1.56 g/cm$^3$, pH 5, [HA]: 12.6 mg/L, I: 0.01 M $NaClO_4$, 1 mM $NaN_3$).

The flux steadily increases over a transient period of 20 d. Then it achieves values scattering between 0.02 and 0.06 µg·cm$^{-2}$·d$^{-1}$. In steady-state, the amount of diffused HA increases linearly with time.

Figure 13.5 illustrates the particle size distribution of HA in the high and low concentration reservoir of the same experiment. In the high concentration reservoir, the HA shows a particle size distribution with a mean particle size of about 50 kD. The mean particle size of HA shifts to less than 1 kD in the low concentration reservoir. From the filtration results, it can be concluded that only small HA particles are able to pass the narrow pores indicating a fractionation of colloidal particles in the clay system. Comparable results were found in all diffusion experiments with HA also in presence of U(VI).

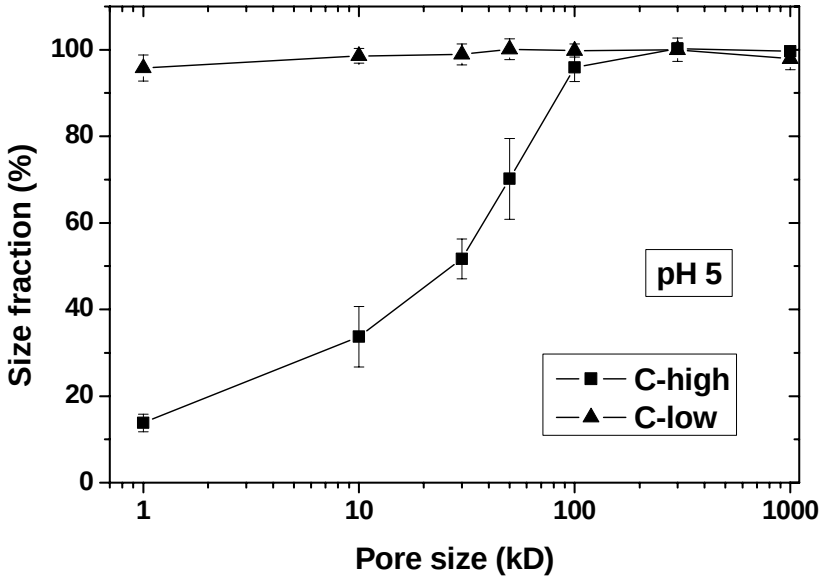


**Fig. 13.5:** Size distribution of humic colloids in the high and low concentration reservoir.

The out-diffusion of HA from the clay plug (pH 5, $\rho = 1.56$ g/cm$^3$) is demonstrated in Fig. 13.6. The accumulated tracer amounts in the external reservoirs of the high and low concentration side are plotted as a function of time. At the low concentration side, the tracer amount reaches a plateau after about 30 d. This behavior is describable by the model equation in Van Loon and Soler (2004) and the parameter set $D_e = 6 \cdot 10^{-12}$ m$^2$/s and $\alpha = 1.15$ could be estimated. This is comparable with the parameter from the corresponding through-diffusion experiment ($D_e = 1.2 \cdot 10^{-11}$ m$^2$/s and $\alpha = 0.78$) within a deviation of 50% of the higher value. In contrast to the expected behavior, the high concentration side continuously released HA, not reaching a plateau in the accumulated concentration diagram over the experimental duration. The model assumes a linear tracer distribution within the clay plug when reaching the steady-state through-diffusion. Probably the distribution was non-linear. This was checked after terminating the out-diffusion by analyzing the residual profile. Figure 13.7 presents a view to the high concentration side after opening the cell. The dark areas indicate the accumulation of HA at the boundary between clay and external solution (filterplate).

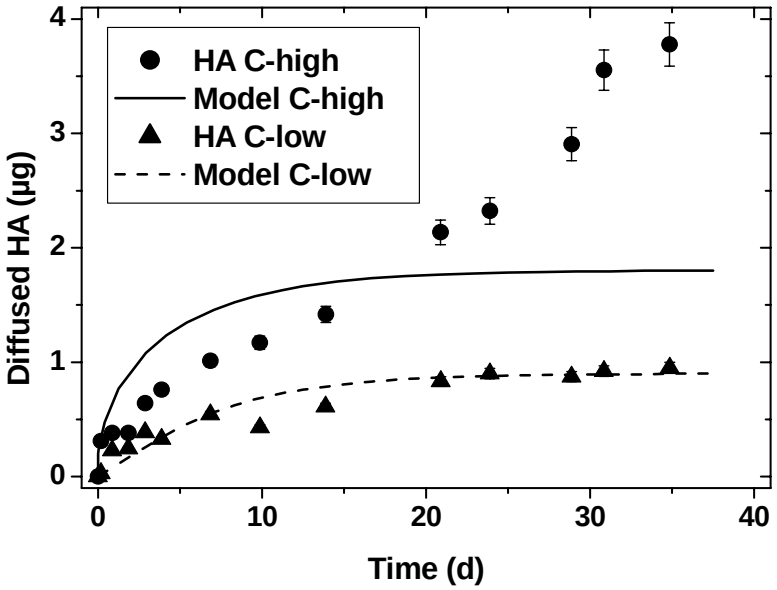


**Fig. 13.6:** Out-diffusion: cumulative mass vs. time (ρ: 1.56 g/cm$^3$, pH 5), model parameters ($D_e = 6 \cdot 10^{-12}$ m$^2$/s and $\alpha = 1.15$) estimated from the low concentration side.

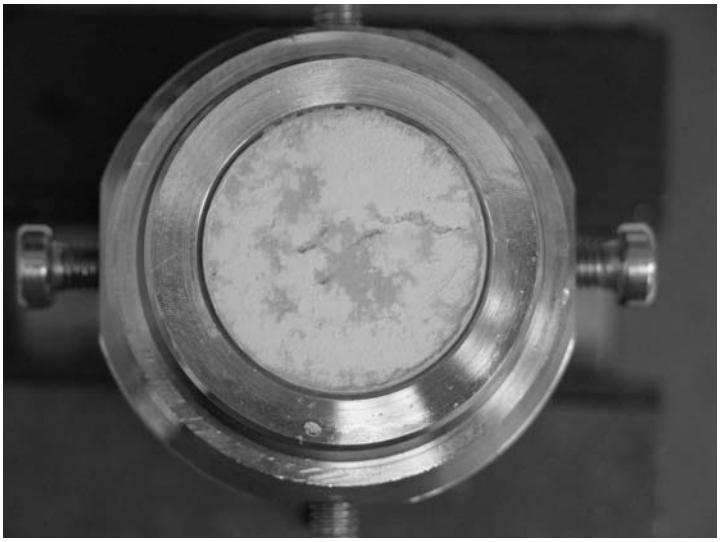

**Fig. 13.7:** Front view to an opened diffusion cell (ρ: 1.56 g/cm$^3$, pH 5), diameter of the clay plug 25.7 mm.

The HA distribution as a function of the distance is shown in Fig. 13.8. The bulk of HA has been accumulated near the high concentration boundary entering the clay to a depth of ca. 1 mm. This accumulation is in accordance with the strong size fractionation.

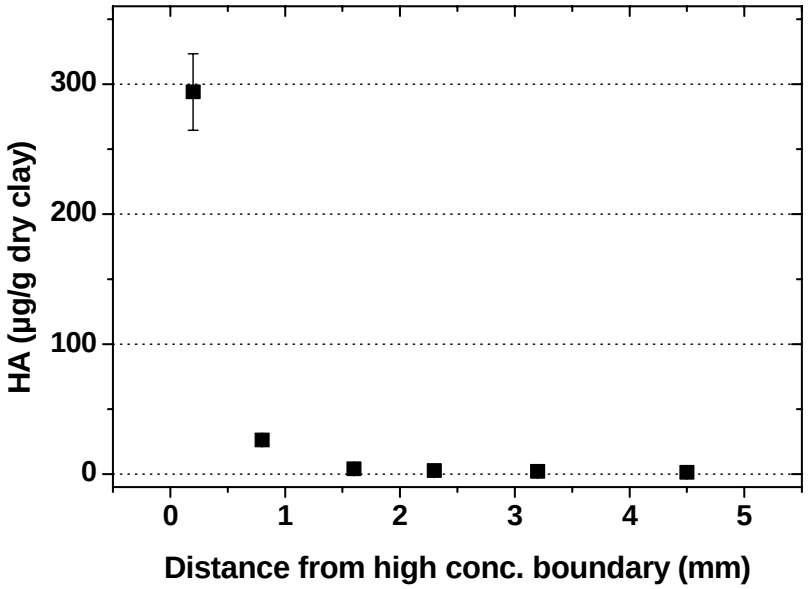


**Fig. 13.8:** Residual mass of HA in the clay plug after out-diffusion (t: 35 d, ρ: 1.56 g/cm$^3$, pH 5).

Based on Eq. (13.4), the effective diffusion coefficients $D_e$ and the rock capacity factors α of HA were deduced from the steady-state periods of the experiments. Figure 13.9 illustrates the obtained data as a function of the bulk dry density in comparison to those of HTO. Furthermore, the data are summarized in Tab. 13.1.

**Tab. 13.1:** $D_e$, and $\alpha$ for HTO and HA as a function of the bulk dry density.

| Parameter | Bulk dry density (g/cm$^3$) | | |
|---|---|---|---|
| | **1.32** | **1.56** | **1.67** |
| | | **pH 5** | |
| **α, HTO (-)** | 0.45 ± 0.14 | 0.37 ± 0.11 | 0.39 ± 0.12 |
| **$D_{e, HTO}$ (m$^2$/s)** | (2.70 ± 0.27) · 10$^{-10}$ | (1.80 ± 0.18) · 10$^{-10}$ | (1.57 ± 0.16) · 10$^{-10}$ |
| **α, HA (-)** | 31.96 ± 9.59 | 0.78 ± 0.23 | 0.35 ± 0.10 |
| **$D_{e, HA}$ (m$^2$/s)** | (1.23 ± 0.12) · 10$^{-10}$ | (1.20 ± 0.12) · 10$^{-11}$ | (5.13 ± 0.51) · 10$^{-12}$ |
| | | **pH 7** | |
| **α, HTO (-)** | n.m. [a] | 0.26 ± 0.08 | (0.910 ± 0.27) |
| **$D_{e, HTO}$ (m$^2$/s)** | n.m. | (2.68 ± 0.27) · 10$^{-10}$ | (1.95 ± 0.20) · 10$^{-10}$ |
| **α, HA (-)** | n.m. | 11.56 ± 3.47 | 13.59 ± 4.08 |
| **$D_{e, HA}$ (m$^2$/s)** | n.m. | (4.08 ± 0.41) · 10$^{-11}$ | (3.01 ± 0.30) · 10$^{-11}$ |

[a] n.m.: not measured.

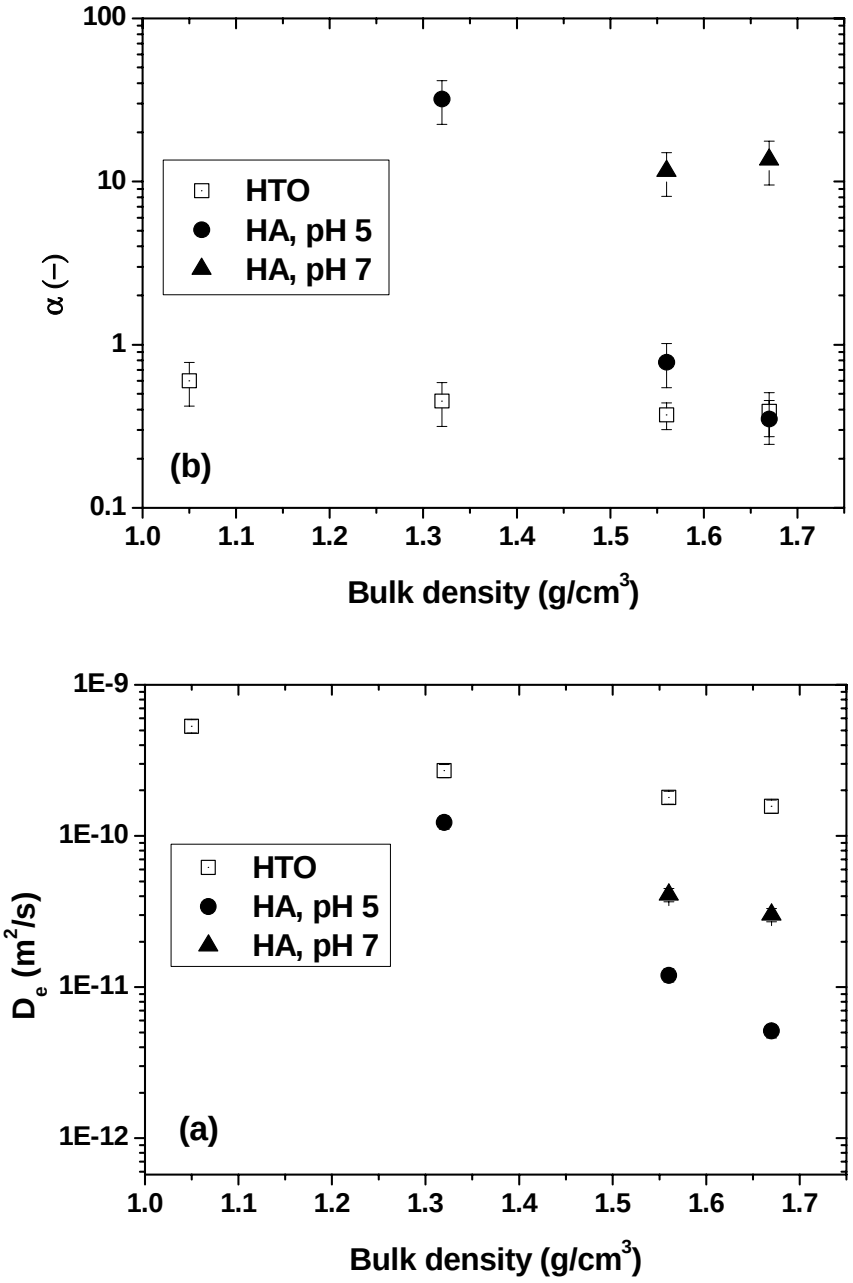


**Fig. 13.9:** Diffusion parameters $D_e$ (a) and rock capacity factors $\alpha$ (b) for HTO and HA as a function of the bulk dry density.

At pH 5 and pH 7, HTO and HA show decreasing $D_e$ values with increasing density. The $D_e$ values of HA are always smaller than the corresponding values of HTO. This effect becomes stronger with increasing density and points to an increased steric hindrance of the colloidal HA transport in the narrow pore space of kaolinite. This result is in agreement with the size distribution shown in Fig. 13.5, from which a fractionation of HA molecules in the clay plug could be concluded. The effective diffusion coefficients of HA were found to be higher at pH 7 compared to pH 5 (see Tab. 13.1). As the effective diffusion coefficients apply for the steady state, differences in the equilibrium interaction between HA and clay due to changes in the protonation state of the functional groups are not expected. Rather, variations in the free diffusion coefficients $D_0$ of the macro molecules are assumed. Lead et al. (2000) observed an increase in the $D_0$ of Suwannee river HA by a factor of about 1.2 when increasing the pH from 5 to 7. This effect has been attributed to an aggregation of humic colloids at pH <7.

The effective porosity $\varepsilon$ of the system is represented by $\alpha_{HTO}$. With the exception of the obtained value at $\rho = 1.67$ g/cm$^3$ (pH 7), it decreases slightly with increasing bulk density. The rock capacity factor $\alpha$ for HA depends stronger on the bulk density. At pH 5 an increase of $\alpha$ was observed with decreasing density. At pH 7 similar results were found at both studied densities. Based on the applied diffusion model, $\alpha_{HA}$ describes the sum of the accessible pore space for the HA diffusion as well as the sorption ($K_d$) of the HA in the system. From the data at pH 5 it can be concluded that sorption processes seem to be less effective at high densities. However, at low densities, these processes obviously become more important, which can be concluded from the increased $\alpha_{HA}$ values. The capacities obtained at pH 7 are not consistent with that. The observed trend at pH 7 is opposite to that at pH 5. Unfortunately, there exist data at only two different bulk densities and pH 7 not enabling a confirmation of the trend.

The rock capacity factors of HA at pH 5 are significantly lower than those at pH 7, pointing to a stronger sorption at pH 7. This is in contrast to the results of the batch sorption experiments with HA (cf. chapter 10.1) where a lower amount of sorbed HA was found at pH 7. The batch experiments were performed with the entire non-fractionated size spectrum of the HA and the data set represents the sorption behavior of the whole HA. In contrast to that, the rock capacity factor $\alpha$ applies only for the diffused part of HA, i.e., only for the low-molecular HA fraction that is able to pass the pore system. It might be possible that this HA fraction shows a different sorption behavior than the entire HA, resulting in the different diffusion behavior. Furthermore, the used $K_d$ approach is possibly not able to describe the interaction sufficiently. Former studies on HA transport in quartz sand (Mibus et al., 2007) suggested a kinetic interaction of HA with the quartz surface which were definitely not describable by $K_d$.

### 13.3.3 Influence of humic acid on the uranium(VI) migration

#### 13.3.3.1 Uranium(VI) diffusion in absence of humic acid

The U(VI) diffusion in absence of HA was studied at pH 5 and 7 at U(VI) concentrations of $1 \cdot 10^{-6}$ M. By the termination of the experiment (70 d at pH 5, 64 d at pH 7), no U(VI) breakthrough was observed. Because of that the cells were opened and the kaolinite plugs were cut into slices, which were analyzed on their U(VI) content. Figure 13.10 shows the U(VI) distribution in the kaolinite after the experiments.

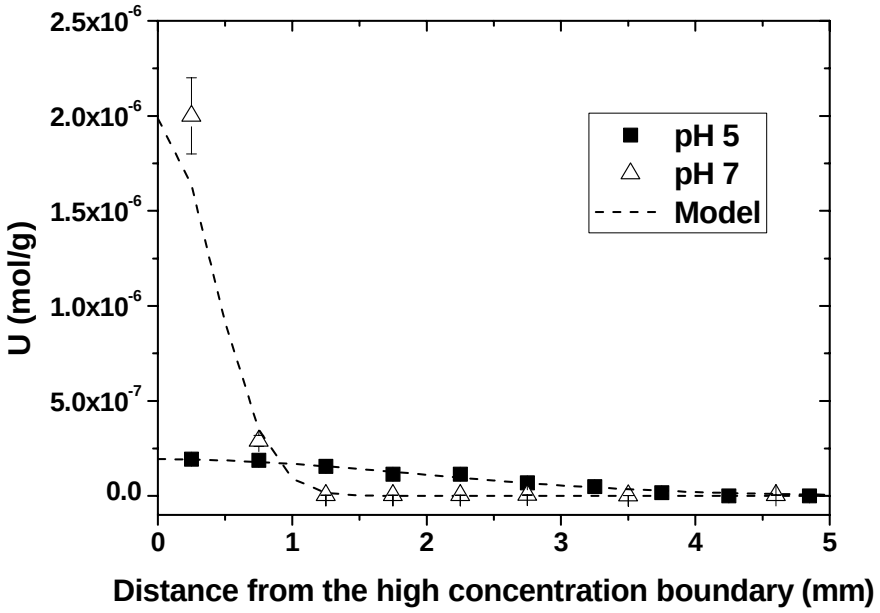


**Fig. 13.10:** U tracer concentration in the clay plug after 70 d (pH 5) and 64 d (pH 7).

At pH 5 and 7, U(VI) shows the typical behavior of a strong sorbing tracer. However, there are differences in the diffusion behavior at pH 5 and 7. At pH 5 the diffusion profile of U(VI) stretches across the clay plug. The U(VI) concentration decreases with increasing distance from the high concentration boundary. At pH 7, in contrast, U(VI) is accumulated at the high concentration boundary. Only a small part of U(VI) is able to enter the first layer of the clay plug. This behavior is attributed to the stronger U(VI) sorption onto KGa-1b at pH 7 (Křepelová et al., 2006b) preventing a deeper penetration of U(VI) into the clay compared to pH 5. This diffusion behavior is reflected in the apparent diffusion coefficients $D_a$ of U(VI) at both pH values which amount to $1.5 \cdot 10^{-13}$ and $6.0 \cdot 10^{-15}$ $m^2/s$ at pH 5 and 7, respectively.

#### 13.3.3.2 Uranium(VI) diffusion in presence of humic acid

The low molecular fraction of HA diffusing through the clay plug was not found to convey uranium within the experimental duration. Possibly the uranyl humate complexes formed in solution dissociates in the pore system due to competition between humate and surface complexes. Alternatively, the mobile low molecular HA fraction is not able to complex U(VI) due to structural and functional dissimilarities.

The in-diffusion profiles of both tracers are illustrated in Fig. 13.11. As in the experiments on HA diffusion, HA is immobilized at the high concentration boundary. In presence of HA, the U(VI) concentration is permanently lower compared to the HA-free system. The bulk of U(VI) is immobilized associated with HA at the solution clay boundary. Comparing pH 5 and pH 7, a deeper penetration of U(VI) was observed at pH 5. This is in concordance with the penetration depth of HA, the complexing agent, and U(VI) in absence of HA. From the diffusion profiles of U(VI) in presence of HA it becomes clear that HA penetrates the clay deeper than U(VI) (see Fig. 13.11). This is in agreement with the observed through-diffusion behavior of the low molecular HA fraction.

In general, HA has a clearly immobilizing effect on the migration of uranium in the studied system.

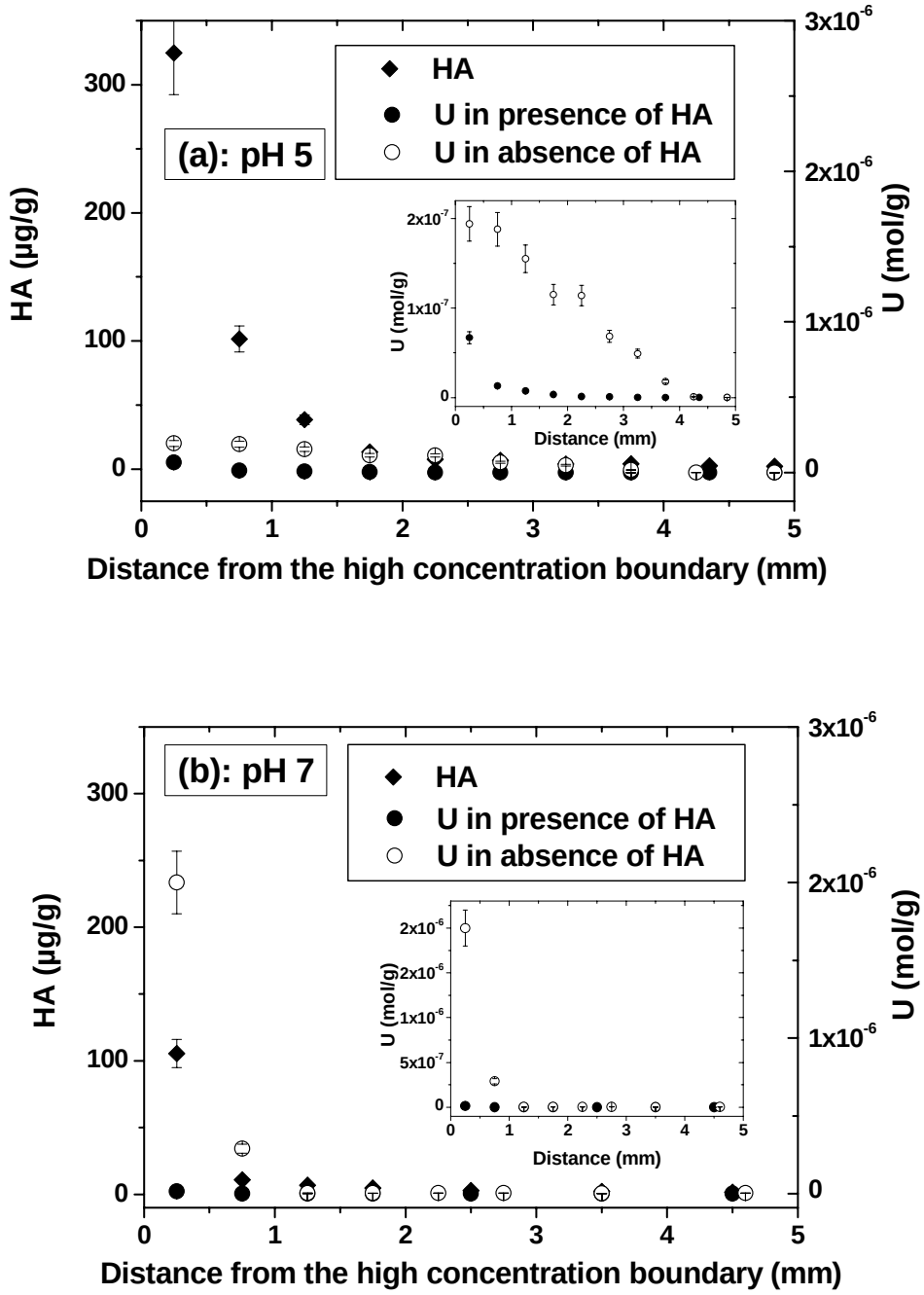


**Fig. 13.11:** U and HA distribution in the clay plug at pH 5 (a) and pH (7) (b). Reaction time in absence of HA: 70 d (pH 5), 64 d (pH 7), in presence of HA: 78 d (pH 5 and 7)

#### 13.3.3.3 Uranium(VI) diffusion in a synthetic humic substance-kaolinite-sorbate

Figure 13.12 presents the U(VI) distribution in the synthetic humic substances-kaolinite-sorbate after 79 d in comparison to that of U(VI) in kaolinite in absence of HA. From Fig. 13.12 it becomes clear that U(VI) is not able to migrate deep into the humic substance-kaolinite sorbate. It is immobilized at the solution clay boundary most likely in association with humic substances. However, the comparison of the results of this experiment with those of the experiment with kaolinite and HA in solution (Fig. 13.13.) shows that U(VI) penetrates slightly more into the humic substance-kaolinite-sorbate. There are different processes that can effect these differences in the migration behavior.

At the start of the experiment with the synthetic humic substance-kaolinite-sorbate, U(VI) exists in a HA-free solution. With access to the sorbate, U(VI) can interact with the immobilized humic material as well as with the kaolinite surface. From XPS measurements it is known that the surface of the kaolinite particles is not covered by a homogeneous humic substance layer (see chapter 5.3 and Reich et al, 2006a). Simultaneously, HA-like substances diffuse from the clay layer into the high and low concentration reservoir solutions, whose total organic carbon (TOC) concentrations steadily increase during the experiment. After the end of the experiment, the TOC content in the high and low concentration reservoir amounted to about 1.8 and 0.8 mg C respectively, representing about 3.2 and 1.5 mg of mobilized HA-like substances. These HA-like substances are able to complex increasing amounts of U(VI) in form of the ternary uranyl mono hydroxo humate complex. Thus, the diffusion of U(VI) is increasingly influenced by this complex and U(VI) is probably immobilized at the solution clay boundary in association with HA.

The deeper penetration of U(VI) into the kaolinite-humic substance-sorbate (see Fig. 13.13.) may be attributed to the first stage of the experiment, when no HA-like substances were present in solution and U(VI) was allowed to diffuse as non-HA-complexed species (see Fig. 13.10).

As many natural sediments and soils contain considerable amounts of organic matter, this model system is expected to reflect migration processes in the environment more realistically than the pure clay system originally free of organic matter.

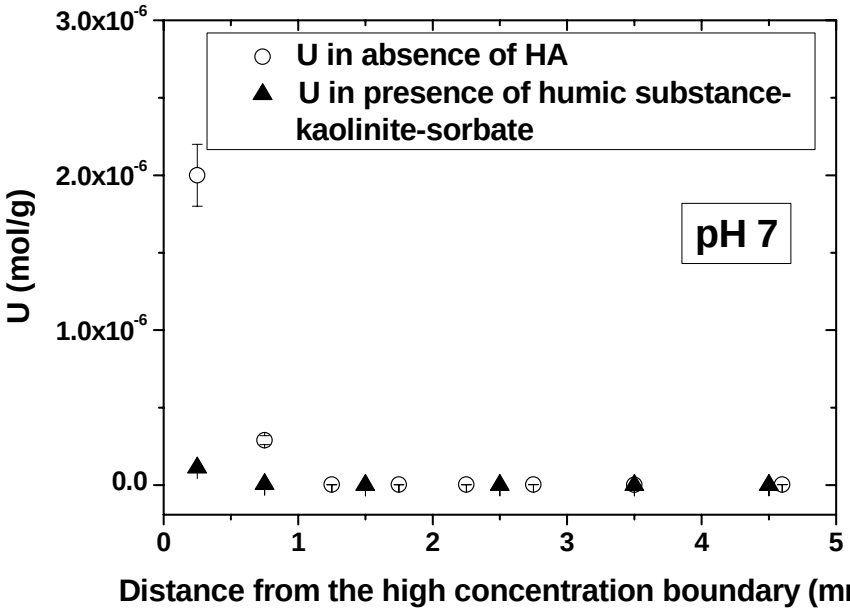


**Fig. 13.12:** U distribution in the kaolinite-humic substance-sorbate after 79 d in comparison to the U distribution in absence of HA ($\rho_{bulk}$: 1.56 g/cm$^3$).

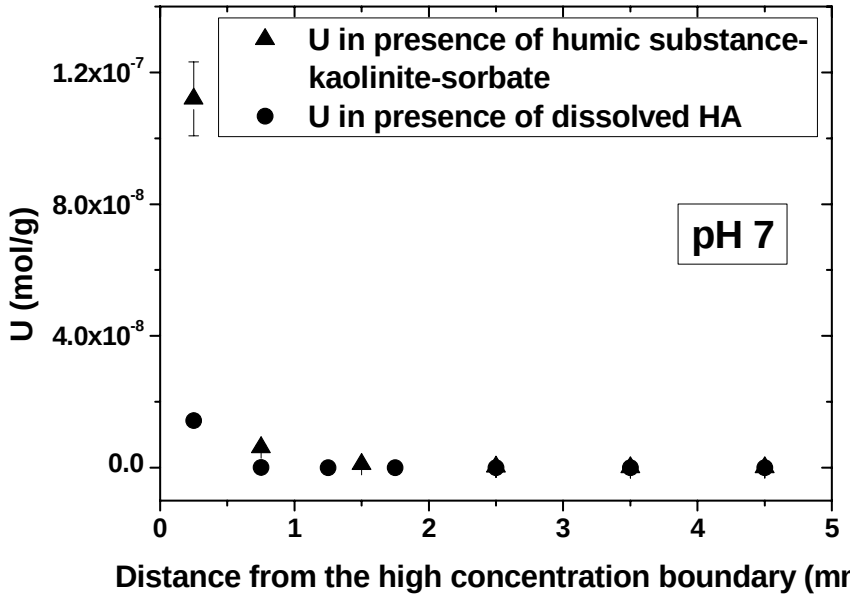


**Fig. 13.13:** U distribution in the clay plug after the experiment with the kaolinite-humic substance-sorbate and with kaolinite and HA in solution (pH 7, $\rho_{bulk}$: 1.56 g/cm$^3$).

The migration of HA in clay is governed by diffusion. It is influenced by the colloidal behavior of HA. At higher clay bulk densities, size fractionation affects the diffusion parameters. In presence of HA colloids U(VI) is immobilized in association with HA near the high concentration boundary.
In the advective quartz sand system, HA exhibits an ambivalent influence on the uranium transport (Mibus et al., 2007). Depending on the environmental conditions, an accelerating or a retarding moment could become effective. In the clay system, the retarding moment, i.e., the settlement of colloids and associated U(VI), clearly dominates, whereas the acceleration (humic colloid borne transport of U) could not be demonstrated.

# 14 Summary and outlook

The aim of this project was the study of basic interaction processes in the system clay-humic substance-aquifer to obtain a better process understanding, to improve the knowledge of the interaction behavior of HA with metal ions and to amend the thermodynamic database. Within the project kaolinite KGa-1b was used as model mineral.

In order to identify nitrogen-containing functional groups in HA, a $^{15}$N-labeled HA type M1 was synthesized and characterized by $^{15}$N-NMR spectroscopy. It was concluded, that the nitrogen forms in HA type M1 can be attributed to different types of linkages (pyrrole- and/or indole-like N, primary and/or secondary amine N, N in terminal amino acid groups), which agrees with literature data for natural HA. Based on these results, first U(VI) complexation studies with organic model ligands (phenylalanine, 3-phenylpropionic acid, glycine) were carried out to get an impression on the influence of $NH_2$ groups on the metal ion complexation by HA. It was found that the amino function seems to be not involved in the uranyl complexation at pH 4. A rather destabilizing effect on the complex was observed. To elucidate the impact of nitrogen-containing functional groups on the HA-metal ion-interaction further investigations are necessary under different experimental conditions using other model ligands representing alternative nitrogen functionalities in HA.

The impact of kaolinite on the formation of humic substances and humic substance-kaolinite-sorbates was investigated. Within these studies it was found that the presence of kaolinite during the HA synthesis mainly influences the yields on HA and their elemental compositions.

Besides HA, it was possible to obtain humic-substance-kaolinite-sorbates that contain humic materials, which is assumed to be more hydrophobic than HA. The obtained sorbates are suitable model compounds for organic rich clays and were already used in batch and diffusion experiments.

To amend the thermodynamic database for the system actinide-HA-water, the U(VI) complexation by HA in the neutral pH range as well as the redox stability of Np(V) in presence of HA with different functionalities were studied. For the first time, two independent laser induced spectroscopic methods were applied to study the formation of the ternary U(VI) mono hydroxo humate complex $UO_2(OH)HA(I)$ by reaction of $UO_2OH^+$ with HA. Assuming that all proton exchanging functional groups of the HA are able to contribute to the complex formation, a mean stability constant of 6.58 ± 0.24 was derived for $UO_2(OH)HA(I)$. Alternatively, the analytical data were evaluated based on the metal ion charge neutralization model resulting in a complexation constant of 6.95 ± 0.10 (LC: 0.76 ± 0.28). An overall complexation constant of $\log\beta_{0.1M}$ = 14.89 ± 0.54 was calculated for the total reaction of U(VI) with HA starting from the non-hydrolyzed $UO_2^{2+}$ ion. Taking the $UO_2(OH)HA(I)$ complex into account, the speciation of U(VI) in presence of HA was recalculated. The calculations indicate, that the formation of $UO_2(OH)HA(I)$ can significantly influence the U(VI) speciation in the environmentally relevant pH region. As a consequence, the mobility of U(VI) in natural aquifer systems could be enhanced. The digital database for humics complexation based on the metal ion charge neutralization model was updated.

The redox properties of various natural and synthetic humic substances towards Np(V) were determined under anaerobic conditions between pH 3.5 and pH 9. In comparison to the natural humic substances (AHA, KFA), the synthetic HA (type Hyd-Glu and Cat-Gly) lead to a stronger reduction of Np(V) to Np(IV) and to a stabilization of the tetravalent oxidation state in form of Np(IV) humate complexes. The stronger reduction behavior of the synthetic HA in comparison to the natural humic substances can be attributed to their higher amount of phenolic/acidic OH groups. The influence of phenolic/acidic OH groups on the redox behavior of humic substances was verified applying a synthetic HA with blocked phenolic/acidic OH groups. By application of the synthetic HA with distinct redox properties actinides can be stabilized in lower oxidation states, e.g. in complexation and sorption studies.

Sorption experiments were performed to determine the influence of HA on the U(VI) and Np(V) sorption onto kaolinite. For comparison, the U(VI) sorption onto synthetic humic substance-kaolinite-sorbates was studied. For U(VI) a pH dependent sorption behavior onto kaolinite, which is affected by its concentration and the presence of $CO_2$ and HA, was observed. The adsorption of U(VI) closely follows the adsorption of HA. In the acidic pH range, HA enhances the U(VI) uptake compared to the HA-free system, whereas in the near-neutral pH range the formation of dissolved uranyl humate complexes reduces the U(VI) sorption, therefore, the presence of HA can enhance the U(VI) migration under environmentally relevant conditions. The structure of U(VI) kaolinite surface complexes in presence of HA was investigated applying spectroscopic methods (EXAFS, TRLFS) and compared to that in absence of HA. From EXAFS results it was concluded that HA has no effect on EXAFS structural parameters in the system U(VI)-HA-kaolinite. In presence of HA, U(VI) seems to adsorb directly onto kaolinite than via HA. Both in the absence and in the presence of HA, two adsorbed U(VI) species on kaolinite were identified by TRLFS spectroscopy. These surface complexes differ likely in their amount of coordinated water molecules. The TRLFS measurements confirmed, that in presence of HA U(VI) prefers to bind directly onto kaolinite than via HA. In the ternary system the hydrate shell of sorbed U(VI) is partly displaced by HA molecules.

From the U(VI) sorption experiments with synthetic humic substance-kaolinite-sorbates representing model substances for organic rich clays it was concluded, that humic matter associated with clay can exhibit an immobilizing as well as an mobilizing effect on U(VI). Due to structural and functional differences of the humic matter, the sorption behavior of U(VI) onto synthetic humic substance-kaolinite sorbates differs from that of U(VI) in the system U(VI)-HA-kaolinite. HA separately added to the system can cause a stronger immobilizing effect on U(VI) than humic matter associated with clay.

In case of Np(V) it was found that the sorption behavior of Np onto kaolinite is effected by pH, ionic strength, Np concentration and the presence of HA. HA exhibits a significant influence on the Np sorption onto kaolinite. Between pH 7.5 and pH 10.5 the mobility of Np(V) is increased due to HA, which is attributed to formation of dissolved neptunyl humate complexes and/or neptunyl carbonate humate complexes.

Diffusion experiments were carried out to determine processes influencing the migration of humic colloids in compacted clay and its influence on the U(VI) migration. Additionally, the U(VI) diffusion in a compacted synthetic humic substance-kaolinite sorbate was measured. It

was found that the migration of HA in clay is governed by diffusion and influenced by its colloidal behavior. Generally it was shown that in presence of humic matter U(VI) is immobilized near the high concentration boundary in association with HA. However, a deeper penetration of U(VI) into the clay layer was observed for the humic substance-kaolinite-sorbate which exhibits more hydrophobic humic matter.

The results of these studies improve the knowledge on basic interaction processes of actinides (U(VI), Np(V)) in the system clay humic substance-aquifer. Important results were obtained on the characterization of humic material and its complexation properties, the complexation of U(VI) under neutral conditions, the redox stability of Np(V), as well as on the influence of humic matter on the U(VI) and Np(V) sorption onto kaolinite and the U(VI) migration in compacted clay. Within the project data were generated that extent the thermodynamic database under environmentally relevant conditions. Furthermore, a better process understanding was obtained. In their combination the results contribute to a more realistic description of the migration behavior of actinides in clay formations and to an improved risk assessment for potential nuclear waste repositories.

Future studies should focus on interaction processes of actinides with natural clay rocks and the determination of the impact of natural organic matter present in the clay on the actinide migration. At first Opalinus clay will be investigated. Further studies on the actinide complexation by HA have to be performed. This includes model investigations on the influence of HA functional groups, other than oxygen-containing (nitrogen- and sulfur-containing), on the metal ion complexation by HA and studies on the formation of ternary actinide carbonato humate complexes. The thermodynamic database of the actinide humate complexation under near-natural conditions has to be completed. Besides tetravalent actinides (e.g. U(IV)), environmentally relevant temperature and concentration dependencies has to be considered.

# 15 References


Amayri, S. (2006). Wechselwirkung von Neptunium und Plutonium mit Huminstoffen und Kaolinit. 6. Workshop des Verbundprojektes 'Migration von Actiniden im System Ton, Huminstoff, Aquifer'. Mainz, 28.-29.03.2006.

André, C., Choppin, G.R.: Reduction of Pu(V) by Humic Acid (2000). Radiochim. Acta **88**, 613.

Ankudinov, A. L., Bouldin, C.E., Rehr, J.J., Sims, J., Hung, H. (2002). Parallel Calculation of Electron Multiple Scattering Using Lanczos Algorithms. Phys. Rev. **B 65,** 104107.

Arnold, T., Zorn, T., Bernhard, G., Nitsche, H. (1998). Sorption of Uranium(VI) onto Phyllite. Chem. Geol. **151**, 129.

Arnold, T., Utsunomiya, S., Geipel, G., Ewing, R.C., Baumann, N., Brendler, V. (2006). Adsorbed U(VI) Surface Species on Muscovite Identified by Laser Fluorescence Spectroscopy and Transmission Electron Microscopy. Environ. Sci. Technol. **40**, 4646.

Artinger, R., Marquardt, C.M., Kim, J.I., Seibert, A., Trautmann, N., Kratz, J.V. (2000). Humic Colloid-borne Np Migration: Influence of the Oxidation State. Radiochim. Acta **88**, 609.

Artinger, R., Kuczewski, B., Marquardt, C.M., Schäfer, Th., Seibert, A., Fanghänel, Th. (2004). Comparison of Humic Colloid Mediated Transport of Plutonium Studied by Column Experiments with Tri- and Tetravalent Actinide Experiments. In: FZKA 6969, Wissenschaftliche Berichte (G. Buckau, ed.). Forschungszentrum Karlsruhe, Karlsruhe, p. 47.

Babanov, Yu.A., Vasin, V.V., Ageev, Al.L, Ershov, N.V. (1981). A New Interpretation of EXAFS Spectra in Real Space . 1. General Formalism. Physica Status Solidi B-Basic Research **105,** 747.

Balcke, G.U., Kulikova, N.A., Hesse, S., Kopinke, F.-D., Perminova, I., Frimmel, F. (2002). Adsorption of Humic Substances onto Kaolin Clay Related to Their Structural Features. Soil Sci. Soc. Am. J. **66**, 1085.

Baumann, N., Brendler, V., Arnold, T., Geipel, G., Bernhard, G. (2005). Uranyl Sorption onto Gibbsite Studied by Time-resolved Laser-induced Fluorescence Spectroscopy (TRLFS). J. Coll. Interf. Sci. **290,** 318.

Bell, J.T., Biggers, R.E. (1968). Absorption Spectrum of the Uranyl Ion in Perchlorate Media. III. Resolution of the Ultraviolet Band Structure; Some Conclusions Concerning the Excited State of $UO_2^{2+}$. J. Mol. Spectr. **25**, 312.

Benzing-Purdie, L.M., Ratcliffe, C.I. (1986). A Study of the Maillard Reaction by $^{13}C$ and $^{15}N$ CP-MAS NMR: Influence of Time, Temperature, and Reactants on Major Products. Developments in Food Science **13**, 193.

Berger, S., Braun, S., Kalinowski, H.-O. (1992). *NMR-Spektroskopie von Nichtmetallen. Band 2: $^{15}N$-NMR-Spektroskopie.* Thieme Verlag, Stuttgart.

Bertrand, P.A., Choppin, G.R. (1982). Separation of Actinides in Different Oxidation States by Solvent Extraction. Radiochim. Acta **31**, 135.

Borden, D., Giese, R.F. (2001). Baseline Studies of the Clay Minerals Society Source Clays: Cation Exchange Capacity Measurements by the Ammonia-Electrode Method. Clays Clay Miner. **49**, 444.

Bortiatynski, J.M., Hatcher, P.G., Knicker, H. (1996). NMR Techniques (C, N, and H) in Studies of Humic Substances. In: *ACS Symposium Series 651 (Humic and Fulvic Acids)*, American Chemical Society, p. 57.

Brady, P.V., Cygan, R.T., Nagy, K.L. (1998). Surface Charge and Metal Sorption to Kaolinite. In: *Adsorption of Metals by Geomedia: Variables, Mechanisms, and Model Applications* (Jenne, E.A., ed.). Academic Press, San Diego, p. 371.

Brendler, V., Brachmann, A., Geipel, G. (1997). Software to Compute Lifetimes from Time-Resolved Laser-Induced Fluorescence Spectroscopy (TRLFS) Studies, Exploiting the Full Spectrum. In: *Institute of Radiochemistry, Annual Report 1996*. Wissenschaftlich-Technische Berichte, FZR-180 (H. Nitsche, ed.), Forschungszentrum Rossendorf, Dresden, p. 13.

Brendler, V., Sachs, S. (2006). Aqueous Uranium(VI) Hydrolysis Species Characterised by TRLFS. Spectrochim. Acta, in preparation.

Bubner, M., Heise, K.H. (1994). Characterization of Humic Acids. II Characterization by Radioreagent-derivatization with [$^{14}$C]Diazomethane. In: *Institute of Radiochemistry, Annual Report 1993*. Wissenschaftlich-Technische Berichte, FZR-43 (H. Nitsche and G. Bernhard, eds.), Forschungszentrum Rossendorf, Dresden, p. 22.

Chen, Y.Z., Tan, B.M., Lin, Z.J. (1993). A Kinetic Study of the Reduction of Np(VI) with Humic Acid. Radiochim. Acta **62**, 199.

Chipera, S.J., Bish, D.L. (2001). Baseline Studies of the Clay Minerals Society Source Clays: Powder X-ray Diffraction Analyses. Clays Clay Miner. **49**, 398.

Choppin, G.R.: Humics and Radionuclide Migration (1988). Radiochim. Acta **44/45**, 23.

Claret, F., Schäfer, T., Bauer, A., Buckau, G. (2003). Generation of Humic and Fulvic Acid from Callovo-Oxfordian Clay Under High Alkaline Conditions. Sci. Tot. Environm. **317**, 189.

Costanzo, P.A., Guggenheim, S., guest editors (2001). Baseline Study of the Clay Minerals Society Source Clays. Clays Clay Miner. **49**, 371-453.

Cox, J.D., Wagman, D.D., Medvedev, V.A. (1989). *CODATA Key Values for Thermodynamics*, Hemisphere, New York.

Crank, J. (1975). *The Mathematics of Diffusion*, 2nd ed., Pergamon Press Oxford.

Czerwinski, K.R., Buckau, G., Scherbaum, F., Kim, J.I. (1994). Complexation of the Uranyl Ion with Aquatic Humic Acid. Radiochim. Acta **65**, 111.

Fernandez-Botello, A., Gomez-Coca, R.B., Holy, A., Moreno, V., Sigel, H. (2002). Metal-ion Binding Properties of O-phosphonatomethylcholine (PMCh-). Effect of the Positive Charge of a Distant Trimethylammonium Group on the Coordinating Qualities of a Phosph(on)ate Group. Inorg. Chim. Acta **331**, 109.

Geipel, G., Bernhard, G., Rutsch, M., Brendler, V., Nitsche, H. (2000). Spectroscopic Properties of Uranium(VI) Minerals Studied by Time-resolved Laser-induced Fluorescence Spectroscopy (TRLFS). Radiochim. Acta **88**, 757.

Geipel, G., Acker, M., Vulpius, D., Bernhard, G., Nitsche, H., Fanghänel, Th. (2004). An Ultrafast Time-resolved Fluorescence Spectroscopy System for Metal Ion Complexation Studies with Organic Ligands. Spectrochim. Acta Part A **60**, 417.

George, G.N., Pickering, I.J. (1995). EXAFSPAK: *A Suite of Computer Programs for Analysis of X-ray Absorption Spectra*. Stanford Synchrotron Radiation Laboratory, Stanford, CA, USA.

Glaus, M.A., Hummel, W., Van Loon, L.R. (1995). Stability of Mixed-Ligand Complexes of Metal Ions with Humic Substances and Low Molecular Weight Ligands. Environ. Sci. Technol. **29**, 2150.

Guillaumont, R., Fanghänel, T., Fuger, J., Grenthe, I., Neck, V., Palmer, D.A., Rand M.H. (2003). *Update on the Chemical Thermodynamics of Uranium, Neptunium, Plutonium, Americium and Technetium*. *Chemical Thermodynamics Vol. 5* (OECD Nuclear Energy Agency, ed.), Elsevier, Amsterdam.

Günther, A., Geipel, G., Bernhard, G. (2007). Complex Formation of Uranium(VI) with the Amino Acids L-glycine and L-cysteine: A Fluorescence Emission and UV-vis Absorption Study. Polyhedron **26**, 59.

Hasegawa, Y., Yamazaki, N., Usui, S., Choppin, G.R. (1990). Effects of Phenyl Groups on Thermodynamic Parameters of Lanthanoid(III) Complexation with Aromatic Carboxylic Acids. Bull. Chem. Soc. Jpn. **63**, 2169.

Hendry, M.J., Ranville, J.R., Boldt-Leppin, B.E.J., Wassenaar, L.I. (2003). Geochemical and Transport Properties of Dissolved Organic Carbon in a Clay-rich Aquitard. Water Resour. Res. **39**, 1194.

Hendry, M.J., Wassenaar, L.I. (2005). Origin and Migration of Dissolved Organic Carbon Fractions in a Clay-rich Aquitard: C-14 and Delta C-13 Evidence. Water Resour. Res. **41**, 2021.

Ishimitsu, T., Hirose, S., Sakurai, H. (1977). Microscopic Acid Dissociation Constants of 3,4-Dihydroxyphenylpropionic Acid and Related Compounds, and 3,4-dihydroxyphenylalanine (DOPA). Talanta **24**, 555.

Kakihana, M., Nagumo, T., Okamoto, M., Kakihana, H. (1987). Coordination Structures for Uranyl Carboxylate Complexes in Aqueous Solution Studied by IR and $^{13}C$ NMR Spectra. J. Phys. Chem. **91**, 6128.

Keller, C. (1971). The Chemistry of the Transuranium Elements (K.H. Lieser, ed.). Verlag Chemie GmbH, Weinheim, p. 294.

Kilislioglu, A., Bilgin, B. (2002). Adsorption of Uranium on Halloysite. Radiochim. Acta **90**, 155.

Kim, J.I., Czerwinski, K.R. (1996). Complexation of Metal Ions with Humic Acids: Metal Ion Charge Neutralization Model. Radiochim. Acta **73**, 5.

Kim, J.I., Buckau, G. (1998). *Characterization of Reference and Site Specific Humic Acids.* RCM-Report 02188, TU München.

Koban, A., Geipel, G., Bernhard, G. (2003). Complex Formation Between Uranium(VI) and α-D-glucose 1-phosphate. Radiochim. Acta **91**, 393.

Koban, A., Bernhard, G. (2006). Uranium Complexes with Phospholipid Model Compounds – A Laser Spectroscopic Study. J. Inorg. Biochem., submitted.

Kogel, J.E., Lewis, S.A. (2001). Baseline Studies of the Clay Minerals Society Source Clays: Chemical Analysis by Inductively Coupled Plasma-mass Spectroscopy (ICP-MS). Clays Clay Miner. **49**, 387.

Kohler, M., Wieland, E., Leckie, J.O. (1992). Metal-ligand-surface Interactions During Sorption of Uranyl and Neptunyl on Oxides and Silicates. Water-Rock Interaction. Kharaka & Maest, eds., Balkema, Rotterdam, 51.

Křepelová, A. (2006a). *Influence of Humic Acid on the Sorption of Uranium(VI) and Americium(III) onto Kaolinite.* PhD Thesis, TU Dresden, in preparation.

Křepelová, A., Sachs, S., Bernhard, G. (2006b). Uranium(VI) Sorption onto Kaolinite in the Presence and Absence of Humic Acid. Radiochim. Acta **94**, 825.

Křepelová, A., Brendler, V., Sachs, S., Baumann, N., Bernhard, G. (2006c). New TRLFS Measurements of U(VI) Sorption onto Gibbsite. Annual Report 2006, in preparation.

Kretzschmar, R., Hesterberg, D., Sticher, H. (1997). Effects of Adsorbed Humic Acid on Surface Charge and Flocculation of Kaolinite. Soil Sci. Soc. Am. J. **61**, 101.

Kumke, M.U., Tiseanu, C., Abbt-Braun, G., Frimmel, F.H. (1998). Fluorescence Decay of Natural Organic Matter (NOM)-Influence of Fractionation, Oxidation, and Metal Ion Complexation. J. Fluorescence **8**, 309.

Kumke, M.U., Zwiener, C., Abbt-Braun, G., Frimmel, F.H. (1999). Spectroscopic Characterization of Fulvic Acid Fractions of a Contaminated Groundwater. Acta Hydrochim. Hydrobiol. **27**, 409.

Lagaly, G. (1993). Reaktionen der Tonminerale. In: *Tonminerale und Tone. Struktur, Eigenschaften, Anwendung und Einsatz in Industrie und Umwelt* (K. Jasmund, G. Lagaly, eds.), Steinkopff, Darmstadt, chapter 3.

Lead, J.R., Wilkinson, K.J., Starchev, K., Canonica, S., Buffle, J. (2000). Determination of Diffusion Coefficients of Humic Substances by Fluorescence Correlation Spectroscopy: Role of Solution Conditions. Environ. Sci. Technol. **34**, 1365-1369.

Madejová, J., Komadel, P. (2001). Baseline Studies of the Clay Minerals Society Source Clays: Infrared Methods. Clays Clay Miner. **49**, 410.

Maes, N., Wang, L., Hicks, T., Bennett, D., Warwick, P., Hall, T., Walker, G., Dierckx, A. (2006). The Role of Natural Organic Matter in the Migration Behaviour of Americium in the Boom Clay-Part I: Migration Experiments. Physics and Chemistry of the Earth **31**, 541.

Marquardt, C., Herrmann, G., Trautmann, N. (1996). Complexation of Neptunium(V) with Humic Acids at Very Low Metal Concentrations. Radiochim. Acta **73**, 119.

Marquardt, C., Kim, J.I. (1998). Complexation of Np(V) with Humic Acid: Intercomparison of Results from Different Laboratories. Radiochim. Acta **80**, 129.

Marquardt, C., Artinger, R., Zeh, P., Kim, J.I. (1999). Redoxchemistry of Neptunium in a Humic Rich Groundwater. In: FZKA 6324, Wissenschaftliche Berichte (G. Buckau, ed.). Forschungszentrum Karlsruhe, Karlsruhe, p. 21.

Marquardt, C.M., Pirlet, V., Kim, J.I. (2000). Initial Studies on the Complexation of Tetravalent Neptunium with Fulvic Acid. In: FZKA 6524, Wissenschaftliche Berichte (G. Buckau, ed.). Forschungszentrum Karlsruhe, Karlsruhe, p. 45.

Marquardt, C.M., Seibert, A., Artinger, R., Denecke, M.A., Kuczewski, B., Schild, D., Fanghänel, Th. (2004). The Redox Behaviour of Plutonium in Humic Rich Groundwater. Radiochim. Acta **92**, 617.

Mibus, J., Sachs, S., Pfingsten, W., Nebelung, C., Bernhard, G. (2007). Migration of Uranium (IV)/(VI) in the Presence of Humic Acids in Quartz Sand: A Laboratory Column Study. J. Contam. Hydr. **89**, 199.

Moll, H., Geipel, G., Reich, T., Bernhard, G., Fanghänel, T., Grenthe, I. (2003). *Uranyl(VI) Complexes with Alpha-substituted Carboxylic Acids in Aqueous Solution.* Radiochim. Acta **91**, 11.

Montavon, G., Mansel, A., Seibert, A., Keller, H., Kratz, J.V., Trautmann, N. (2000). Complexation Studies of $UO_2^{2+}$ with Humic Acid at Low Metal Ion Concentrations by Indirect Speciation Methods. Radiochim. Acta **88**, 17.

Morgenstern, M., Klenze, R., Kim, J.I. (2000). The Formation of Mixed-Hydroxo Complexes of Cm(III) and Am(III) with Humic Acid in the Neutral pH Range. Radiochim. Acta **88**, 7.

Moulin, V., Moulin, C. (1995). Fate of Actinides in the Presence of Humic Substances under Conditions Relevant to Nuclear Waste Disposal. Appl. Geochem. **10**, 573.

Moulin, C., Laszak, I., Moulin, V., Tondre, C. (1998). Time-Resolved Laser-Induced Fluorescence as a Unique Tool for Low-Level Uranium Speciation. Appl. Spectroscopy **52**, 528.

Murphy, E.M., Zachara, J.M., Smith, S.C., Phillips, J.L. (1992). The Sorption of Humic Acids to Mineral Surfaces and their Role in Contaminant Binding. Sci. Tot. Environ. **117/118**, 413.

Nash, K., Fried, S., Friedman, A.M., Sullivan, J.C. (1981). Redox Behavior, Complexing, and Adsorption of Hexavalent Actinides by Humic Acid and Selected Clays. Environ. Sci. Technol. **15**, 834.

Nebelung, C. (2002). Correction of Sorption Data of $^{234}U$ Contaminated with $^{232}U$. In: Institute of Radiochemistry, Annual Report 2001. Wissenschaftlich-Technische Berichte, FZR-343 (Th. Fanghänel, ed.), Forschungszentrum Rossendorf, Dresden, p. 32.

Niitsu, Y., Sato, S., Ohashi, H., Sakamoto, Y., Nagao, S., Ohnuki, T., Muraoka, S. (1997). Effects of Humic Acid on the Sorption of Neptunium(V) on Kaolinite. J. Nuclear Materials **248**, 328.

Panak, P., Klenze, R., Kim, J.I. (1996). A Study of Ternary Complexes of Cm(III) with Humic Acid and Hydroxide or Carbonate in Neutral pH Range by Time-Resolved Laser Fluorescence Spectroscopy. Radiochim.Acta **74**, 141.

Pashalidis, I., Czerwinsky, K., R., Fanghänel, Th., Kim, J.I. (1997). Solid-Liquid Phase Equilibria of Pu(VI) and U(VI) in Aqueous Carbonate Systems. Determination of Stability Constants. Radiochim. Acta **76**, 55.

Pashalidis, I., Kim, J.I., Buckau, G. (2006). U(VI) Mono-Hydroxo Humate Complexation. J. Radioanal. Nucl. Chem., accepted.

Payne, T.E., Davis, J.A., Lumpkin, G.R., Chisari, R., Waite, T.D. (2004). Surface Complexation of Uranyl Sorption on Georgia Kaolinite. Appl. Clay Sci. **26**, 151.

Pompe, S., Bubner, M., Denecke, M.A., Reich, T., Brachmann, A., Geipel, G., Nicolai, R., Heise, K.H., Nitsche, H. (1996). A Comparison of Natural Humic Acids with Synthetic Humic Acid Model Substances: Characterization and Interaction with Uranium(VI). Radiochim. Acta **74**, 135.

Pompe, S., Brachmann, A., Bubner, M., Geipel, G., Heise, K.H., Bernhard, G., Nitsche, H. (1998). Determination and Comparison of Uranyl Complexation Constants with Natural and Model Humic Acids, Radiochim. Acta **82**, 89.

Pompe, S., Bubner, M., Schmeide, K., Heise, K.H., Bernhard, G., Nitsche, H. (2000a). *Influence of Humic Acids on the Migration Behavior of Radioactive and Non-Radioactive Substances under Conditions Close to Nature. Synthesis, Radiometric Determination of Functional Groups, Complexation.* Wissenschaftlich-Technische Berichte, FZR-290, Forschungszentrum Rossendorf, Dresden.

Pompe, S., Schmeide, K., Bubner, M., Geipel, G., Heise, K.H., Bernhard, G. Nitsche, H. (2000b). Investigation of Humic Acid Complexation Behavior with Uranyl Ions Using Modified Synthetic and Natural Humic Acids. Radiochim. Acta **88**, 553.

Pruett, R.J., Webb, H.L. (1993). Sampling and Analysis of KGa-1b Well-crystallized Kaolin Source Clay. Clays Clay Miner. **41**, p. 514.

Redden**,** G.D., Jinhe, L., Leckie, J. (1998). Adsorption of U(VI) and Citric Acid on Goethite, Gibbsite, and Kaolinite. Comparing Results for Binary and Ternary Systems. In: *Adsorption of Metals by Geomedia*. *Variables Mechanisms Model Appl.* (Jenne, E. A, ed.). Academic Press, San Diego, p. 291.

Reich, T., Drebert, J., Křepelová, A., Sachs, S. (2006a). XPS Study of Humic Acid/Kaolinite Interaction. In: *Institute of Radiochemistry, Annual Report 2005.* Wissenschaftlich-Technische Berichte, FZR-443 (G. Bernhard, ed.), Forschungszentrum Rossendorf, Dresden, p. 46.

Reich, T. Ye., Kokrshunov, M.E., Antonova, T. V., Ageev, A.L., Moll, H., Reich, T. (2006b). New Regularizaton Method for EXAFS Analysis. AIP Proceedings XAFS13, in press.

Sachs, S., Heise, K.H., Bernhard, G. (2003). Synthetic Humic Acid Model Substances with Specific Functional Properties for the Use in Complexation and Sorption Experiments with Actinides. In: FZKA 6800, Wissenschaftliche Berichte (G. Buckau, ed.). Forschungszentrum Karlsruhe, Karlsruhe, p. 51.

Sachs, S., Schmeide, K., Brendler, V., Křepelová, A., Mibus, J., Geipel, G., Heise, K.H., Bernhard, G. (2004). *Investigation of the Complexation and the Migration of Actinides and Non-radioactive Substances with Humic Acids under Geogenic Conditions.* Wissenschaftlich-Technische Berichte, FZR-399, Forschungszentrum Rossendorf, Dresden.

Sachs, S., Bernhard, G. (2005a). NIR Spectroscopic Study of the Complexation of Neptunium(V) with Humic Acids: Influence of Phenolic OH Groups on the Complex Formation. Radiochim. Acta **93**, 141.

Sachs, S., Geipel, G., Bernhard, G. (2005b). Study of the Redox Stability of Uranium(VI) in Presence of Humic Substances. In: FZKA 7070, Wissenschaftliche Berichte (G. Buckau, ed.). Forschungszentrum Karlsruhe, Karlsruhe, p. 11.

Sachs, S., Brendler, V., Geipel, G. (2006). Uranium(VI) Complexation by Humic Acid under Neutral pH Conditions Studied by Laser-induced Fluorescence Spectroscopy. Radiochim. Acta, in press.

Samadfam, M., Jintoku, T., Sato, S., Ohashi, H., Mitsugashira, T., Hara, M., Suzuki, Y. (2000). Effects of Humic Acid on the Sorption of Am(III) and Cm(III) on Kaolinite. Radiochim. Acta **88**, 717.

Schmeide, K., Zänker, H., Heise, K.H., Nitsche, H. (1998). Isolation and Characterization of Aquatic Humic Substances from the Bog 'Kleiner Kranichsee'. In: FZKA 6124, Wissenschaftliche Berichte (G. Buckau, ed.). Forschungszentrum Karlsruhe, Karlsruhe p. 161.

Schmeide, K., Pompe, S., Bubner, M., Heise, K.-H., Bernhard, G., Nitsche, H. (2000). Uranium(VI) Sorption onto Phyllite and Selected Minerals in the Presence of Humic Acid. Radiochim. Acta **88**, 723.

Schmeide, K., Sachs, S., Bubner, M., Reich, T., Heise, K.H., Bernhard, G. (2003). Interaction of Uranium(VI) with Various Modified and Unmodified Natural and Synthetic Humic Substances Studied by EXAFS and FTIR Spectroscopy. Inorg. Chim. Acta **351**, 133.

Schmeide, K., Reich, T., Sachs, S., Brendler, V., Heise, K.H., Bernhard, G. (2005). Neptunium(IV) Complexation by Humic Substances Studied by X-ray Absorption Fine Structure Spectroscopy. Radiochim. Acta **93**, 187.

Schnitzer, M., Khan, S.U. (1972). *Humic Substances in the Environment* (A.D. McLaren, ed.). Marcel Dekker, Inc. New York.

Schroth, B.K., Sposito, G. (1997). Surface Charge Properties of Kaolinite. Clays Clay Miner. **45**, 85.

Seibert, U.A. (1999). Wechselwirkung von neptunium mit Huminstoffen unter naturnahen Bedingungen. PhD Thesis, Johannes Gutenberg-Universität Mainz.

Seibert, A., Mansel, A., Marquardt, C.M., Keller, H., Kratz, J.V., Trautmann, N. (2001). Complexation Behaviour of Neptunium with Humic Acid. Radiochim. Acta **89**, 505.

Shackelford, C.D. (1991). Laboratory Diffusion Testing for Waste Disposal-A Review. J. Contam. Hydrol. 7, 177.

Shanbhag, P.M., Choppin, G.R. (1981). Binding of Uranyl by Humic Acid. J. Inorg. Nucl. Chem. **43**, 3369.

Shin, H.-S., Hong, K.-H., Lee, M.-H., Cho, Y.-H., Lee, C.-W. (2001). Fluorescence Quenching of Three Molecular Weight Fractions of a Soil Fulvic Acid by $UO_2$(II). Talanta **53**, 791.

Silva, R.J., Bidoglio, G., Rand, M.H., Robouch, P.B., Wanner, H., Puigdomenech, I. (1995). *Chemical Thermodynamics, Volume 2: Chemical Thermodynamics of Americium.* North-Holland, Amsterdam.

Stevenson, F.J. (1994). *Humus Chemistry. Genesis, Composition, Reactions.* 2nd ed., J. Wiley, New York.

Sumner, M.E., Miller, W.P. (1996). Cation Exchange Capacity and Exchange Coefficients. In: *Methods of Soil Analysis*. *Part 3: Chemical Methods.* Soil Science Society of America, Inc., USA, p. 1201.

Sutheimer, S.H., Maurice, P.A., Zhou, Q. (1999). Dissolution of Well and Poorly Crystallized Kaolinites: Al Speciation and Effects of Surface Characteristics. Am. Mineral. **84**, 620.

Taguchi, K., Sampei, Y. (1986). The Formation, and Clay Mineral and $CaCO_3$ Association Reactions of Melanoidins. Org. Geochem. **10**, 1081.

Tan, J.X., Chen, Y.Z., Lin, Z.J. (1993). A Kinetic Study of the Reduction of Plutonium with Humic Acid. Radiochim. Acta **61**, 73.

Thompson, H.A., Parks, G.A., Brown, Jr., G.E. (1998). Structure and Composition of Uranium(VI) Complexes at the Kaolinite-Water Interface. In: *Adsorption of Metals by Geomedia*. *Variables Mechanisms Model Appl*. (Jenne, E. A, ed.). Academic Press, San Diego, 349.

Trepte, P. (2006). Sorption von Radionukliden an Tongestein: Spektroskopische Referenzdaten. Diplomarbeit, HTW Dresden.

Van Loon, L.R., Soler, J.M., Bradbury, M.H. (2003). Diffusion of HTO, $^{36}Cl^-$ and $^{125}I^-$ in Opalinus Clay Samples from Mont Terri. Effect of Confined Pressure. J. Contam. Hydrol. **61**, 73.

Van Loon, L. R., Soler, J. M. (2004). Diffusion of HTO, $^{36}Cl^-$, $^{125}I^-$ and $^{22}Na^+$ in Opalinus Clay: Effect of Confining Pressure, Sample Orientation, Sample Depth and Temperature. PSI Report 04-03, Villigen.

Vulpius, D. (2005). Zur Komplexbildung von Actiniden (U, Np) mit Hydroxybenzoesäuren. PhD Thesis, TU Dresden.

Wang, X., Chen, C., Yu, S., Zhou, X., Xu, D., Ren, A. (2005). Effect of pH and Fulvic Acid on the Sorption and Diffusion of Europium Ions in Compacted Bentonite as Studied by the Capillary Method. Ads. Sci. Technol. **23**, 801.

Wimmer, H., Klenze, R., Kim, J.I. (1992). A Study of Hydrolysis Reaction of Curium(III) by Time Resolved Laser Fluorescence Spectroscopy. Radiochim. Acta **56**, 79.

Wold, S., Eriksen, T.E. (2003). Diffusion of Lignosulfonate Colloids in Compacted Bentonite. Appl. Clay Sci. **23**, 43.

Wold, S., Eriksen, T.E. (2005). Diffusion of Humic Colloids in Compacted Bentonite. Proceedings of the 2nd International Symposium "Clays in natural and engineered barriers for radioactive waste confinement", Tours, France, 14-18 March 2005, p. 547.

Wolery, T.J. (1992). *EQ3/6, a Software Package for the Geochemical Modeling of Aqueous Systems.* UCRL-MA-110662, Part 1, Lawrence Livermore National Laboratory.

Wu, W. (2001). Baseline Studies of the Clay Minerals Society Source Clays: Colloid and Surface Phenomena. Clays Clay Miner. **49**, 446.

Zeh, P., Czerwinski, K.R., Kim, J.I. (1997). Speciation of Uranium in Gorleben Groundwaters. Radiochim. Acta **76**, 37.

Zeh, P., Kim, J.I., Marquardt, C.M., Artinger, R. (1999). The Reduction of Np(V) in Groundwater Rich in Humic Substances. Radiochim. Acta **87**, 23.

Ziechmann, W. (1994). *Humic Substances*. BI Wissenschaftsverlag, Mannheim.

# 16 Acknowledgements

The authors thank R. Ruske, M. Meyer and H. Heller for their valuable help with synthesis and characterization of humic materials, performance of batch experiments and sample preparation. We thank Dr. H. Foerstendorf and K. Heim for recording of FTIR and ATR FTIR spectra and for their help in the spectra interpretation. For technical support we thank C. Eckardt (BET and TOC analyses), K. Muschter (FTIR measurements), U. Schaefer and M. Leckelt (ICP-MS analyses), H. Görner (elemental analyses) and A. Scholz (XRD measurements). Thanks are given to Dr. N. Baumann for the performance of TRLFS measurements with kaolinite samples. We thank Ch. Müller for their technical assistance in the performance of diffusion experiments and C. Nebelung for evaluation of LSC spectra.

We thank Dr. E. Brendler (Institute of Analytical Chemistry, Faculty for Chemistry and Physics, TU Bergakademie Freiberg) for recording of $^{15}$N-NMR spectra and for her support in the interpretation of these spectra.

We gratefully acknowledge Prof. Dr. T. Reich (Institut für Kernchemie, Johannes-Gutenberg University Mainz) for his support and the very good cooperation in the analysis and discussion of EXAFS spectra and for the performance and evaluation of XPS measurements.

EXAFS measurements were performed at BM20 at the European Synchrotron Radiation Facility in Grenoble (France). Thanks are given to Dr. A. Scheinost, Dr. H. Funke, Dr. H. Hennig, and Dr. A. Roßberg for their support during the EXAFS measurements.

The studies of the Np(V) reduction were partly supported by the EC Commission under contract No. FIKW-CT-2001-00128.

We would like to thank all colleagues who contributed to the success of this work.